Dynamics of Bacterial Biofilm Predation

Dissertation

zur

Erlangung des Doktorgrades der Naturwissenschaften

(Dr. rer. nat.)

dem Fachbereich Biologie
der Philipps-Universität Marburg

vorgelegt von

Lucia Vidakovic

aus Groß-Gerau

Marburg, März 2019

Erstgutachter: Prof. Dr. Knut Drescher
Zweitgutachter: Prof. Dr. Victor Sourjik

Ehrenwörtliche Erklärung

Hiermit versichere ich, Lucia Vidakovic, die vorliegende Dissertation mit dem Titel:

Dynamics of Bacterial Biofilm Predation

ohne Hilfe Dritter und nur mit den angegebenen Quellen und Hilfsmitteln angefertigt zu haben. Alle Stellen, die Quellen entnommen wurden, sind als solche kenntlich gemacht worden. Diese Arbeit hat in gleicher oder ähnlicher Form noch keiner Prüfungsbehörde vorgelegen.

Datum: Unterschrift:

Summary

This thesis focused on two bacterial interactions with naturally-occurring predators.

The first project examined viral infection dynamics of *Escherichia coli* biofilms with the lytic bacteriophage T7. By combining fluorescence confocal microscopy, automated image analysis and molecular biology, this investigation provided new mechanistic insights into biofilm matrix-mediated bacteriophage protection of entire bacterial communities. Bacteria infected by bactriophages were reliably detected with the use of genetically modified T7 bacteriophages, which resulted in the production of a fluorescent protein by bacteriophage-infected bacteria. Exposure of biofilms of varying ages to T7 bacteriophages revealed a biofilm development-specific bacteriophage protection: Biofilms grown for up to 48 h in microfluidic channels were susceptible to phage-mediated killing, but in contrast, biofilms that were more than 60 h old survived during the constant influx of bacteriophages. Bacteriophage protection of *E. coli* biofilms solely depends on the presence of one component in the biofilm matrix, i.e., amyloid curli fibers. Moreover, the development of protection temporally coincides with the production of curli fibers during late stages of biofilm formation. To uncover this curli fiber-mediated protection mechanism, the biofilm architecture was analyzed and bacteriophage virions were visualized spatiotemporally in living bacterial and *in vitro* constructed artificial biofilms. Together, the results demonstrate that curli fibers provide a close cell-cell arrangement, filling space between the cells, so that bacteriophages cannot invade the bacterial community. In addition, curli fibers are necessary and sufficient to protect single cells from bacteriophage-mediated killing if bacteria are completely encapsulated by matrix. In conclusion, community and single-cell studies comprehensively showed how amyloid curli fibers confer collective, as well as, individual protection to biofilm-dwelling cells against bacteriophage infection.

The second part of the thesis investigated the interaction of *Vibrio cholerae* with human macrophages (cells of the innate immune system responsible for clearance of bacteria during invasion of human tissues). *V. cholerae*, traditionally known to colonize the small intestine and cause the diarrheal cholera disease, was able to attach to the surface of macrophages *in vitro*. Once attached, bacterial biofilms were formed on the macrophage, followed by biofilm dispersal. Comprehensive examination of the interaction dynamics showed that colonization is a flagella and

type IV pili-driven process. The polar flagellum, together with mannose-sensitive hemagglutinin type IV pili, facilitates bacterial attachment to the macrophage surface. During biofilm growth, *V. cholerae* initiates the production of toxin-coregulated type IV pili, which enhances cohesion between biofilm-dwelling bacteria and prevents complete dispersal of biofilms. Co-incubation studies revealed that production of one type of pili, mannose-sensitive hemagglutinin pili or toxin-coregulated pili, by motile *V. cholerae* cells is necessary and sufficient for attachment and biofilm formation. Major biofilm matrix components described for *V. cholerae* biofilms (RbmA, RbmC, Bap1, and VPS) are dispensable for colonization of human macrophages *in vitro*. These observations demonstrate an inversion of the classical predator-prey concept, by which bacteria act collectively via biofilm formation to evade phagocytosis.

Zusammenfassung

Die vorliegende Arbeit befasste sich mit der Interaktion zwischen Bakterien und zwei, natüurlich in der Umwelt, vorkommenden Präadatoren.

Das erste Projekt befasste sich mit den Dynamiken der Infektion von *Escherichia coli* AR3110 Biofilmen mit T7 Bakteriophagen (vereinfacht: Phagen). Konfokale Fluoreszenzmikroskopie mit anschließender Bildanalyse ermöglichte eine genaue Aufklärung, wie bakterielle Gemeinschaften durch die Produktion von Biofilm-Matrix vor einer Infektion durch Bakteriophagen geschützt werden. Der Einsatz von genetisch modifizierten T7 Phagen und die darin resultierende Produktion von sfGFP durch infizierte Bakterien ermöglichte eine präzise Detektion von infizierten Wirtszellen. Als Biofilme verschiedenen Alters T7 Phagen ausgesetzt wurden, konnte in Abhängigkeit des Entwicklungsstadiums der Biofilme ein Schutz vor einer Phageninfektion beobachtet werden. Bakterien innerhalb von Biofilmen bis zu einem Alter von 48 h konnten erfolgreich von T7 Phagen infiziert werden. Demgegenüber konnten Biofilme ab einem Alter von 60 h nicht von T7 Phagen infiziert werden. Der Schutz von *E.coli* Biofilmen vor einer Phageninfekton hängt einzig und allein mit der Anwesenheit von sogenannten amyloiden Curli Fibern innerhalb der Biofilm-Matrix zusammen. Das Ausbleiben der Phageninfektion ist zudem zeitlich geknüupft mit der Produktion von Curli Fibern. Der Mechanismus, wie Curli Fibers die Phageninfektion verhindern, konnte anhand der Analyse der Biofilm-Architektur sowie der raumzeitlichen Visualisierung von Phagen-Partikeln während der Co-Inkubation mit bakteriellen Biofilmen oder *in vitro* hergestellten künstlichen Biofilmen aufgeschlüsselt werden. Curli Fibers sorgen für einen engen Zusammenhalt der Bakterien untereinander und füllen den Freiraum zwischen benachbarten Zellen, sodass die Invasion der bakteriellen Gemeinschaft durch Phagen blockiert wird. Zudem ist die Produktion von Curli Fibers notwendig als auch ausreichend, um einzelnen Zellen Schutz vor Phageninfektion zu gewähren. Zusammenfassend konnte in Untersuchungen auf Populations- sowie Einzelzellebene gezeigt werden, dass Curli Fibers Biofilme im kollektiv, aber auch individuelle Curli Fibers produzierende Zellen vor einer Infektion durch Phagen schützen.

Im zweiten Projekt wurde die Interaktion zwischen *Vibrio cholerae* und humanen Makrophagen untersucht. *V. cholerae* besiedelt üblicherweise den Dünndarm und löst die Durchfallerkrankung Cholera aus. Makrophagen sind Teil des angeborenen

Immunsystems und verantwortlich für die Beseitigung von eingedrungenen Bakterien in Geweben. Untersuchungen konnten zeigen, dass *V. cholerae* in der Lage ist, sich *in vitro* an Makrophagen anzuheften. Im Anschluss folgte die Biofilmbildung auf der Oberfläche der Makrophagen, sowie darauffolgend das Auflösen der bakteriellen Gemeinschaft. Unteruchungen zur Interaktionsdynamik konnten zeigen, dass die Besiedlung der Makrophagenoberfläche von Flagellen sowie Pili abhängig ist. Das polare Flagellum zusammen mit MSHA Pili ermöglicht die Adhäsion der Bakterien an die Oberfläche der Makrophagen. Während der Biofilmbildung produziert *V. cholerae* toxin-coregulierte Pili (TCP), welche für einen festen Zusammenhalt zwischen Zellen sorgen und zur unvollständigen Auflösung des Biofilms beitragen. Weitere Interaktionsstudien haben gezeigt, dass *V. cholerae* im Besitz eines polaren Flagellums auf die Produktion von nur einer Sorte von Pili, MSHA Pili oder TCP, angewiesen ist, um Biofilme auf der Oberfläche von Makrophagen auszubilden. Hauptkomponenten der Matrix beschrieben für *V. cholerae* Biofilme (RbmA, RbmC, Bap1 und VPS) sind nicht essentiell für die Besiedlung von Makrophagen *in vitro*. Zusammenfassend zeigen diese Beobachtungen diese Beobachtungen eine neue Art von Zell-Zell-Interaktion, welche bisher noch nicht für *V. cholerae* beschrieben wurde.

Table of Contents

1 Introduction

Bacteria are the most abundant organisms on earth. Despite their size of a few micrometers, their existence is crucial for life on our planet. Bacteria are involved in various biogeochemical cycles and colonization of higher organisms by bacteria is indispensable [1–6].

1.1 Bacterial Biofilms in the Environment

In nature, bacteria exist in two distinct modes of life: planktonic cells and biofilms. Biofilms, defined as mirobial communities attached to a surface, constitute the predominant bacterial lifestyle [7]. In these cellular consortia, bacteria are embedded in a self-produced matrix of extracellular polymeric substances (EPS) [8].

Among bacteria, biofilm formation follows a regulated developmental process [9]. First, planktonic cells attach irreversibly to a surface, which is facilitated by proteins or structures present on the bacterial cell surface (e.g. pili, flagella). Once bacteria adhered, microcolony formation as well as biofilm maturation follows, during which, growing cells surround themselves with matrix. Production of biofilm matrix proceeds in a controlled manner, takes place in discrete regions inside the community and is responsible for shaping the biofilm architecture. The establishment of multicellular bacterial assemblies can be severely impaired by attenuation in surface attachment or deficiency in biofilm matrix production. Biofilm dispersal comprises the final stage in the developmental program, which is either an active or passive process. Various environmental as well as bacterial-associated signals are known to trigger release of cells from biofilms. Bacteria are then capable to colonise new habitats and another cycle of biofilm formation can be initiated [10–15].

Biofilm-dwelling bacteria are characterized by differential gene expression patterns. These can arise from chemical concentration gradients (e.g nutrients, oxygen) that prevail inside the three-dimensional structure, but also from stochastic gene expression [16]. As a result, subpopulations emerge in respect to biofilm matrix production, antibiotic tolerance and also metabolic activity [16–18] . Heterogeneity leads to cooperative as well as competitive interactions between bacteria and these shape the behaviour of biofilms as a whole [19, 20].

Compared to the existence as an individual cell, being part of multicellular communities provides various benefits for bacteria, making biofilms a fundamental mode of bacterial life. Biofilm growth promotes the acquisition of genetic material by horizontal gene transfer, thereby contributing to the bacterial diversity [21]. Another important feature related to biofilms is the protection of matrix-embedded bacteria against environmental changes. Compared to single bacteria, biofim-dwelling cells are capable to withstand environmental stress. The most common example is the increased tolerance of biofilms towards antimicrobial agents making biofilms a pervasive threat to human health. Bacterial survival can be attributed to the failure of biocidal agents to penetrate the microbial community. In addition, decreasing metabolic activity of cells towards deeper regions of the community and the existence of a transiently antibiotic-tolerant bacterial subpopulation, called persister cells, contributes to insufficient eradication of biofilm-embedded bacteria. Re-growth of surviving cells will then for example lead to chronic bacterial infections in the human body [22–25]. In addition to diminishing the antimicrobial effect, biofilm formation greatly influences the outcome of predation by protozoans. While planktonic cells are eliminated, matrix-embedded bacteria have been shown to survive protozoan grazing [26, 27]. Other naturally occurring threats to bacterial life are bacteriophages as well as macrophages. Bacteriophages are viruses, that use bacteria as their host for self-replication. Which strategies do bacteria utilize to prevent infection by phages and whether biofilm formation is one of them, is discussed in chapter 2. Macrophages are a type of immune cells, capable to carry out elimination of bacterial cells by the uptake and ingestion of bacterial biomass. Bacterial interactions with macrophages are discusses in detail in chapter 3.

1.2 Aims of the Thesis

Life in communities, termed biofilms, has been recognized as a beneficial and successful mode of life, as bacteria are more protected against environmental stress compared to their individual counterparts [7]. How bacteria interact with naturally occurring predators should be investigated with two examples. The aim was to understand, how bacteria and their predators can co-exist in the environment.

Specifically, in the first project the interaction between *E. coli* biofilms and the bacteriophage T7 was studied. Several questions were addressed in order to understand the mechanism of biofilm-bacteriophage (simply: phages) interactions:

1) Do biofilms intrinsically tolerate the presence of phages or does the survival of bacterial communities depend on the developmental stage of the biofilm?

2) What is the mechanism of phage protection and is it associated to specific matrix components?

The second part of the thesis involved studying the interaction between *V. cholerae* and macrophages with respect to following questions:

1) Do macrophages phagocyte *V. cholerae*?

2) Can *V. cholerae* use the biotic surface of macrophages for biofilm formation?

3) What type of surface structures facilitate bacterial attachment to the surface of macrophages?

4) How are bacteria held together in biofilms formed on the macrophage surface? What are the components of the biofilm matrix?

2 Biofilm architecture confers protection against viral infection

2.1 Introduction

2.1.1 *Escherichia coli* biofilms

Escherichia coli is a gram-negative bacterium belonging to the family of Enterobacteriaceae, present as a commensal in the human gut. However, pathogenic strains of *E. coli* evolved, causing urinary tract infections or diarrhea [28, 29]. Surface colonization of *E. coli* is facilitated by proteins present on the bacterial surface, e.g flagella or type I fimbriae [30, 31]. Once attached, bacteria are able to form biofilms, where they encapsulate themselves in matrix. The composition of the biofilm matrix is variable, depending on the bacterial strain and growth condition. The polysaccharides cellulose, poly-N-1,6-acetylglucosamine and colanic acids have been identified as matrix constituents. Proteinacious components can involve Ag43, flagella and curli fibers [12].

Studies with *E. coli* W3110 and *E. coli* AR3110 macrocolonies grown on agar at temperatures below 30 °C revealed a spatial distribution of individual components of the biofilm matrix in the bacterial communities. Such an organization of the biofilm matrix could be further observed for submerged biofilms grown on a glass surface. In those bacterial communities, bacteria present near the surface surround themselves with flagellar filaments. In contrast, cells located in the upper area are encapsulated in a mesh made out of curli fibers, which represent the major protein component of the *E. coli* biofilm matrix [12, 17, 32]. In *E. coli* AR3110 biofilms, cellulose constitutes an additional component of the biofilm matrix, as cellulose synthesis has been restored in *E. coli* AR3110. Since cellulose and curli fiber production depends on the biofilm master regulator CsgD, both matrix components share the same spatial distribution in *E. coli* AR3110 biofilms [33]. Flagella, cellulose and curli fibers together are equally important for the architecture of biofilms.

Loss of one matrix constituent is sufficient to induce architectural differences to the biofilms [32, 33]. Production of flagella, curli fibers and cellulose in discrete areas of the bacterial community arise from diversification in gene expression and the inverse regulation of flagella and curli fibers in *E. coli* [17, 34, 35].

2.1.2 Inverse regulation of flagella and curli fibers in *E. coli*

In *E. coli*, production of curli and flagella is facilitated by two regulatory cascades. They are inversely regulated, with one master regulator present on top of each cascade [32, 35].

Genes involved in flagella assembly are organized in several operons. Temporal expression of these operons follows a highly regulated process, which ensures timed production of proteins required during the steps of flagella assembly. Flagellar promoters are divided into three classes: class I, II and III [36–38]. The class I promoter corresponds to a single operon *flhDC*, encoding the flagella master regulator. The proteins FlhD and FlhC form a complex, which is a transcriptional activator needed together with σ^{70} for the transcription from class II promoters [39]. Class II promoters belong to operons that encode proteins involved in assembly of the basal body and the hook of the flagellum. Furthermore, FlhDC-dependent transcription leads to the production of the σ-factor FliA (σ^{28}) and its anti-σ-factor FlgM [36]. The interplay between FliA and FlgM ensures transcription from class III, once the basal body and the hook have been assembled [40–42]. Class III promoters initiate for example transcription of genes encoding the flagella subunit or chemotaxis proteins [36].

Curli fiber biogenesis requires the master biofilm regulator CsgD , whose expression depends on several proteins, including the sigma factor RpoS [43–45]. CsgD in turn activates transcription of the *csgBAC operon* and *yaiC*, involved in curli fiber and cellulose production, respectively [46, 47].

Both regulatory cascades consist of proteins that modulate each others expression. CsgD, for example, has been shown to inhibit transcription of *fliA* and *flgM* [48]. Moreover, modulating the intracellular ci-di-GMP concentration by the action of phosphodiesterases and diguanlyate cyclases further favors one cascade over the

other. In addition, the flagella regulatory network encodes the FliA-dependent DNA binding protein FliZ. Binding of FliZ to RpoS-dependent promoters thus interferes with RpoS-dependent gene expression, thereby inhibiting curli fiber production [35, 49, 50].

2.1.3 Amyloid curli fibers

Curli fibers are amyloid proteinacious filaments produced by enteric bacteria, such as *Escherichia coli* or *Salmonella* spp. [51]. Amyloids are characterized as ß-sheet rich proteins, where the ß-sheets are aligned parallel and each ß-strand perpendicular to the fiber axis [52, 53]. In contrast to amyloid formation by eukaryotic cells, which results from protein misfolding and is associated with several human diseases, production of amyloids by bacteria is a highly regulated process, important for bacterial colonization of biotic and abiotic surfaces [54]. Curli fibers, designated as functional amyloids, are highly stable and their function in providing a structural scaffold to bacterial communities underlines their crucial role in biofilm development [33, 55]. Proteins required for curli fiber biogenesis in *E. coli* are encoded by two divergently transcribed operons: *csgBAC* and *csgDEFG* [43]. The *csgBAC* operon encodes the major (CsgA) and the minor (CsgB) structural subunit of the curli fiber. Transcription of the *csgBAC* operon is positively regulated by the transcriptinal regulator CsgD [43, 46]. CsgB is the nucleator for CsgA and crucial for fiber assembly on the bacterial surface. CsgB localizes to the bacterial surface, where it rapidly assembles into aggregates with ß-sheet structures, which then alter aggregation of CsgA. After initiation, the growing fiber serves as the template for polymerization of secreted CsgA [56, 57]. In the absence of CsgB, secreted CsgA remains unpolymerized and diffuses away from the bacterial surface [56]. However, *in vitro*, after prolonged incubation, CsgA alone is able to form curli fibers, that are indistinguishable from the ones formed *in vivo* [51]. To prevent premature amyloid protein formation inside bacterial cells, the periplasmic protein CsgC is produced, that acts as an inhibitor of amyloid formation [58]. Secretion of CsgA and CsgB through the outer membrane is facilitated by the secretion complex made out of CsgG, CsgE and CsgF [59, 60]. The periplasmic protein CsgE is responsible for substrate specificity of the oligomeric outermembrane CsgG pore [61]. CsgF is a surface-exposed component of the secretion machinery, that interacts with CsgB and ensures its localization to the bacterial surface, which is a prerequisite for curli fiber assembly [62]. For *E. coli* K-12 strains, production of curli fibers has been shown to be optimal at temperatures below 30 °C. However,

due to mutations in the promoter region of *csgD* or when grown in biofilms, bacteria are able to form curli fibers at 37 °C as well [63, 64]. Furthermore, clinical isolates have been shown to produce curli fibers at 37 °C [65, 66]. Adaptation in curli fiber production demonstrates their importance in colonization of various bacteria. Curli fibers are just one type; bacteria have evolved numerous functional amyloids that participate in biofilm formation as well as persistence in the host [67–69].

2.1.4 Bacteriophages

Bacteriophages, or phages, are viruses, that use bacteria as their host for self-replication. Phages are considered as the most abundant entities on Earth; in natural environments they outnumber bacteria by a factor of ten [70, 71]. Phages are either lytic or temperate. Infection by lytic phages is characterized by adsorption of phage virions to the bacteria cell surface and injection of the phage DNA into the bacteria cell. Once inside, the phage shuts down the production of bacterial proteins in favour of the expression of phage-encoded proteins. Progeny phages will be assembled intracellular and released in the environment after causing bacterial cell lysis. In contrast, temperate phages can either enter the lytic life cycle or their DNA will be replicated along with bacterial DNA, without the production of progeny phages [72, 73].

The lytic bacteriophage T7 belongs to the *Podoviridae* and their bacterial host is *E. coli*. The icosahedral capsid (head) of T7 phages is approximately 60 nm in diameter and made out of 415 copies of the protein Gp10. T7 phages are characterized by a noncontractile tail [74–76]. Upon binding of the phage tail fibers to the bacterial LPS, the phage ejects its double-stranded DNA into the bacterial cell [77–79]. During one infection cylce, approximately 200 progeny phages are released [78].

2.1.5 Bacterial anti-phage defense systems

Since bacteria and phages are able to co-exist, it is not surprising, that bacteria have evolved numerous strategies to resist phage infection. Bacteria can modify or block phage receptors, so that phages can not bind and inject their DNA into the bacterial cell. In case phage DNA entered the cell, it can be subjected to degradation due to bacterial restriction-modification systems or the adaptive

immunity system CRISPR-Cas. The infection process can also be interfered by abortive infection, that is accompanied by bacterial cell death. Cell death of a phage infected cell can prevent the spread of phages and ensure survival of the bacterial population. Simultaneously to the development of bacterial anti-phage defense systems, phages on the other hand evolved strategies to counteract bacterial resistance mechanisms. There is a constant arms race between bacteria and phages in order to ensure persistence in the environment [80–86].

2.1.6 Interactions of phages with bacterial biofilms

Co-existance of bacteria and phages is not only associated with the continuous adaptation of single bacteria and their corresponding viral parasites. Taking into account that bacteria mostly exist in matrix-embedded communities, such biofilms are likely to encounter phage attack. Thus, the biofilm mode of bacteria itself might contribute to co-existance [87–89]. Indeed, bacteria residing in biofilms have a higher survival rate in the presence of phages compared to planktonic bacteria [90, 91]. Biofilms have been shown to act as a physical barrier, thereby limiting the diffusion of phages into the bacterial community [91–94]. The emergence of phages with biofilm matrix degrading properties further suggests that the production of biofilm matrix very likely impedes phage infection and contributes to stable co-existance [95–97]. Despite the numerous studies demonstrating that biofilms represent a protective environment against phage-mediated killing, the protection mechanisms achieved by biofilm-associated factors still remains elusive.

2.2 Results

During their lifecycle, bacteria often reside in microbial communities, called biofilms, in which the cells are encapsulated in a self-produced matrix [7, 8]. In the environment, biofilm-resident bacteria encounter a number of stresses and predation by phages is one common example [94, 98]. To understand how bacterial communities and phages are able to coexist, phage predation in biofilms was investigated using the lytic phage T7 and the biofilm-forming bacterial strain *Escherichia coli* AR3110 as a model system. Genetic engineering in combination with time-resolved microscopy uncovered how a single component of the biofilm matrix - amyloid curli fibers - protects *E. coli* biofilms collectively, as well as single cells individually, from phage infection.

The results described in this chapter have been published in *Nature Microbiology* in January 2018 (L. Vidakovic, P.K. Singh, R. Hartmann, C.D. Nadell, K. Drescher). Bacterial strain construction, fluorescent labelling of T7 phages, isolation of the curli monomer CsgA and all phage-interaction assays were carried out by myself. P.K. Singh was involved in construction of the T7 phage harbouring the fluorescent reporter system to visualize phage-infected bacteria. R. Hartmann created custom scripts for image analysis in MATLAB. C.D Nadell and K. Drescher initiated the project.

2.2.1 Construction of a reporter system to visualize phage-infected bacteria

In order to study the interaction between biofilms and phages in real-time, a reliable method was required to distinguish phage-infected from non-infected bacteria. Therefore, a fluorescent reporter system was developed which enabled the spatiotemporal visualization of phage-infected cells within a bacterial population at the single-cell level (Figure 2.1 b). To detect phage-infected bacteria, lytic T7 phages were genetically modified by using the T7® 415-1 Cloning Kit (Merck). Here, two codon-optimized *sfgfp* (encoding superfolder green fluorescent protein), under the control of the native T7 phi10 promoter, were introduced downstream of *gp10* (encoding the capsid protein Gp10) in the genome of phage T7 (Figure 2.1 a). Infection of bacteria by these engineered T7 phages would result in bacterial synthesis of sfGFP during the process of phage replication. Thus, sfGFP produced by phage-infected bacteria serves as a fluorescent reporter for T7 phage infection.

Successful modification of wild-type (WT) T7 phages was verified by sequencing and fluorescence microscopy. Introduction of engineered T7 phages in close vicinity to *E. coli*, constitutively expressing mRuby2, resulted in bacterial expression of sfGFP (Figure 2.1 b). After bacterial cell lysis occurred, the progeny phages were able to propagate to other viable cells as surrounding bacteria subsequently started to produce sfGFP and lysed afterwards (Figure 2.1 c). In addition to fluorescence microscopy, phage infection and sfGFP synthesis was validated in liquid culture using a plate reader. Exposing exponentially growing *E. coli* cells to genetically modified T7 phages resulted in reduction in $OD_{600\,nm}$ confirming lysis of bacterial cells (Figure 2.1 d). Simultaneously, fluorescence intensity measurements confirmed the production of sfGFP during the continuous infection by progeny phages.

Together, the results indicate that the fluorescent reporter system can be applied to detect and track phage propagation throughout a bacterial population. These engineered T7 phages were used as the viral agent in the following interaction studies with biofilms.

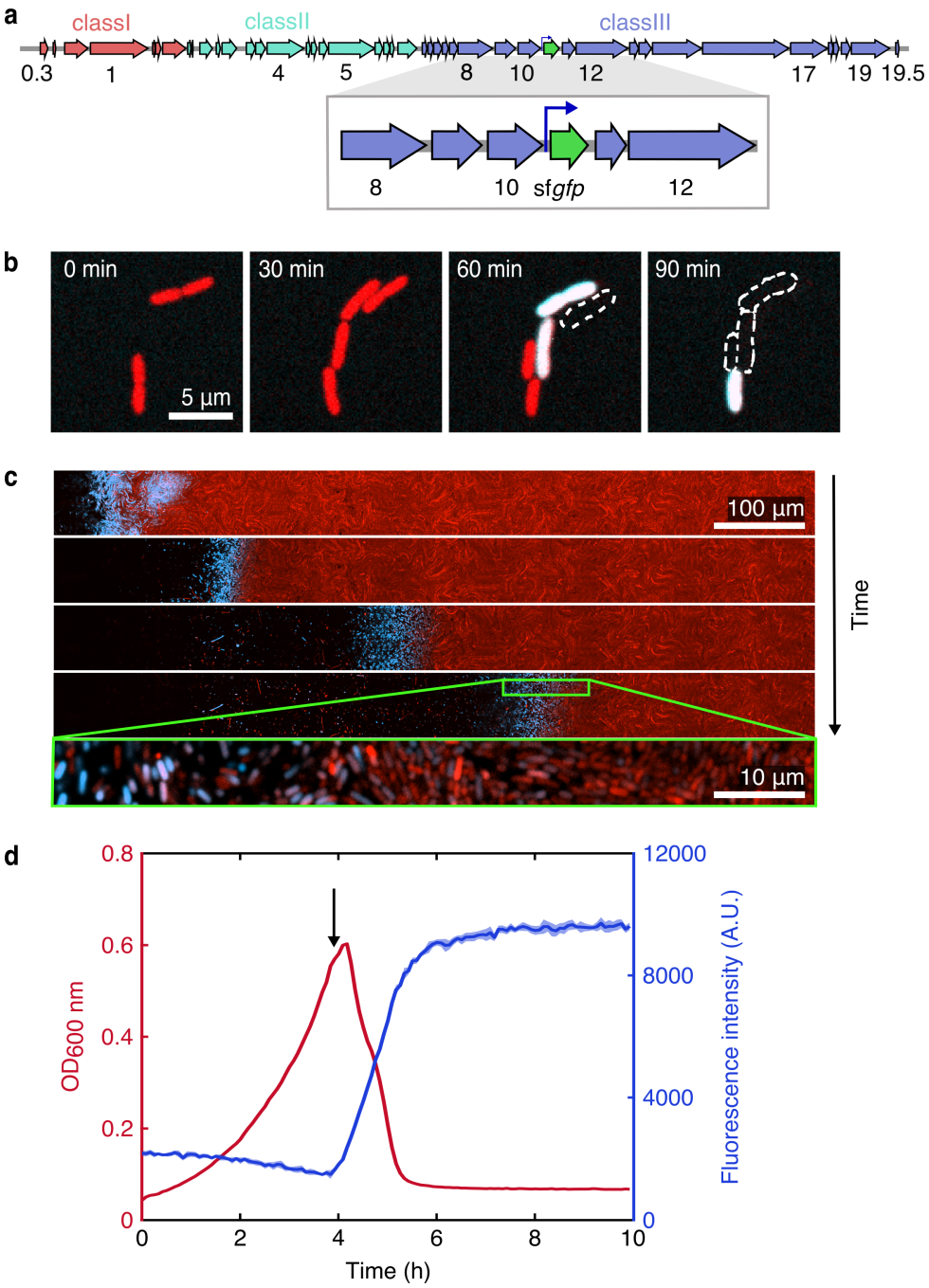

Figure 2.1: Construction of a fluorescent reporter system to visualize T7 phage-infected bacteria (a) A schematic view of the T7 phage genome showing the corresponding gene number for selected genes. *sfgfp* fused to the T7 phi10 promoter was inserted downstream of *gp10* in the T7 phage genome. (b) Exposing *E. coli* cells (constitutively expressing the fluorescent protein mRuby2, shown in red) to engineered T7 phages resulted in production of sfGFP (shown in white). (c) Propagating waves of phage infection were observed in a dense bacterial population, spread on LB agar. Cells expressing sfGFP are shown in blue. (d) Phage infection of exponentially growing cells at 37 °C in liquid culture was monitored by measuring the optical density ($OD_{600\,nm}$) and fluorescence intensity (for sfGFP production). Addition of engineered T7 phages to growing bacteria is indicated by the arrow (n=4).

2.2.2 *E. coli* biofilms and the development of phage protection

To study the interaction between biofilms and phages, *E. coli* biofilms were grown in microfluidic channels for 72 h, during which three distinct developmental stages were observed. First, cells formed separated microcolonies which later grew into a continuous flat layer of cells and then finally, into three-dimensional tower-like structures (Figure 2.2). To assess if susceptibility to phage infection was dependent on the developmental stage of the biofilms, *E. coli* biofilms of varying ages were subjected to T7 phage exposure.

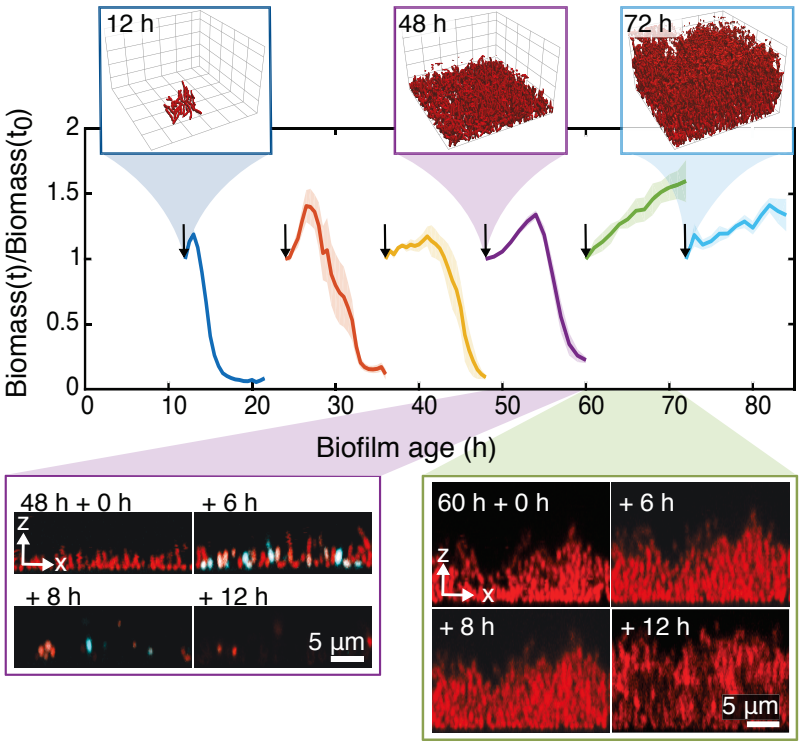

Figure 2.2: Temporal dynamics of *E. coli* biofilms exposed to T7 phages. Biofilms of varying ages were exposed to engineered T7 phages for 12 h under constant flow. Arrows indicate the time point when phages were added to the growing biofilms. For bacterial communities up to an age of 48 h, bacteria were susceptible to T7 phage infection. During co-incubation with phages, bacteria (in red) produced the fluorescent infection reporter protein sfGFP (in cyan) until cell lysis (bottom left panel). In contrast, biofilms grown for 60 h or more continued to grow in the presence of T7 phages (bottom right panel). Plotted lines represent the mean bacterial biomass normalized to the initial biomass at the beginning of phage exposure. Shaded areas represent the standard error of the mean ($n_{t=12}$=8, $n_{t=24}$=10, $n_{t=36}$=3, $n_{t=48}$=4, $n_{t=60}$=4, $n_{t=72}$=7).

Confocal fluorescence microscopy and subsequent image analysis revealed that biofilms grown for up to 48 h experienced a decrease in biomass upon the introduction of T7 phages into the mircrofluidic channels. During the continuous influx of phages for 12 h, bacteria constitutively expressing mRuby2 (shown in red) produced sfGFP (shown in cyan) until cell lysis (Figure 2.2). However, biofilms older than 60 h showed only a few phage-infected cells and continued to grow in the presence of T7 phages (Figure 2.2). Thus, susceptibility to phage infection is inversely dependent on biofilm age.

Next, it was tested if the emergence of genetic resistance was the cause for survival of *E. coli* biofilms during phage exposure. For this, 72 h old biofilms were disrupted, bacteria re-grown and exposed to engineered T7 phages in liquid culture. The addition of phages to exponentially growing cells resulted in a decrease in $OD_{600\,nm}$ and a simultaneous increase in fluorescence intensity, indicating successful phage infection (Figure 2.3 a). As the progeny bacteria were not resistant, the development of phage protection is not due to bacterial resistance.

Phage susceptibility of slow-growing cells was also investigated, as conditions within bacterial sessile communities have been found to result in a decreased growth rate [99, 100]. T7 phages were added at two time points during stationary phase of bacteria growing in liquid culture, which led to a decrease in $OD_{600\,nm}$. This demonstrates that a decrease in growth rate does not negatively affect the process of T7 phage replication in *E. coli* (Figure 2.3 b).

To determine if the development of phage protection is solely dependent on the phage species, T5 phages, which belong to a different family [101], were used in the phage-biofilm interaction assay. During co-incubation, 48 h old biofilms experienced a decrease in biomass, whereas 72 h old biofilms were able to survive and continued to grow (Figure 2.4).

These observations indicate that *E. coli* gains a biofilm-associated protection against both T7 and T5 phages. Furthermore, biofilms transition from susceptible to protected at the same biofilm age, suggesting a common mechanism of protection against phage infection (Figure 2.2, Figure 2.4).

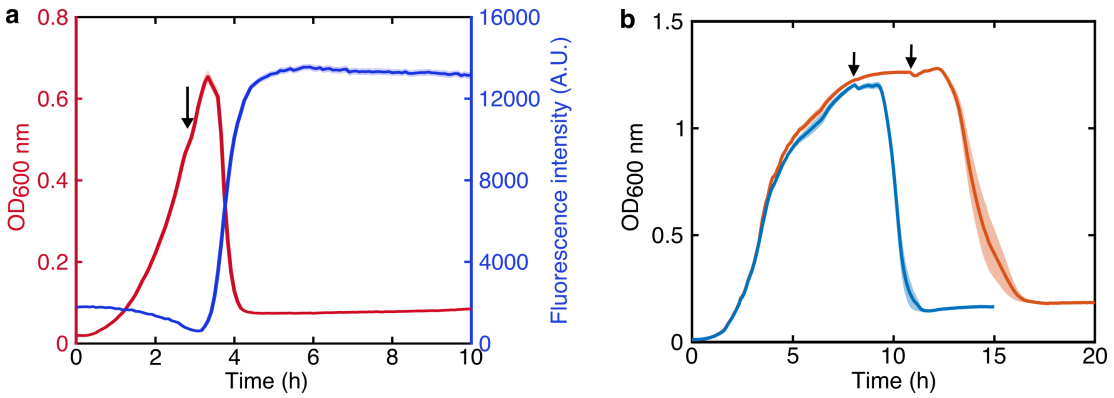

Figure 2.3: Cells from 72 h old biofilms and slow growing bacteria are susceptible to phage infection. (a) Bacteria from 72 h grown *E. coli* AR3110 biofilms were susceptible to T7 phage infection in liquid culture (incubated at 37 °C). The arrow indicates the time point of phage addition. Production of sfGFP and bacterial cell lysis as part of the phage infection process were monitored by measuring fluorescence intensity and optical density ($OD_{600\,nm}$) respectively. Plotted lines represent the mean and shaded areas the standard deviation (n=4). (b) Addition of T7 phages (indicated by arrows) at two time points during stationary growth at 37 °C revealed that slow growing bacteria were readily lysed by T7 phages. Bacterial growth was monitored by optical density ($OD_{600\,nm}$) measurements. Plotted lines represent the mean and shaded areas the standard deviation (n=8).

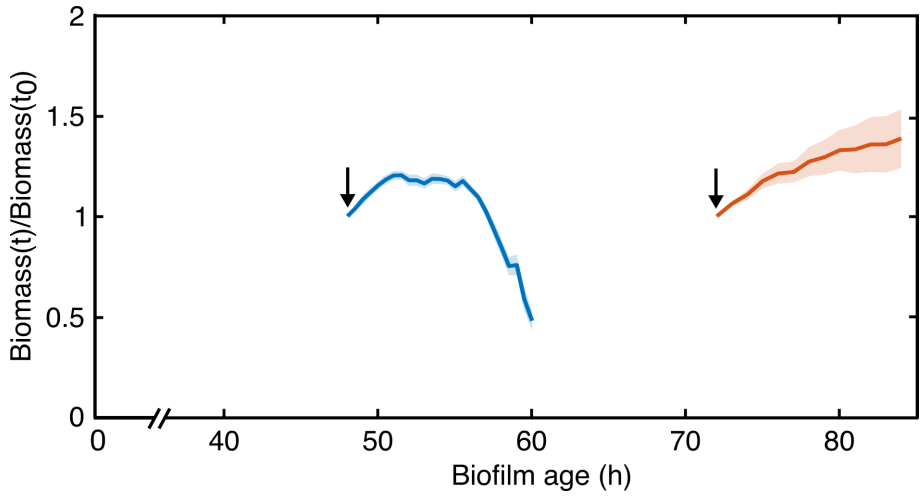

Figure 2.4: Exposure of *E. coli* AR3110 biofilms to T5 phages. Continuous influx of T5 phages (addition of phages indicated by the arrow) into microfluidic channels for 12 h resulted in phage-mediated cell lysis of 48 h old wild-type biofilms. In contrast, 72 h old biofilms continued to grow in the presence of phages. Plotted lines represent the mean bacterial biomass normalized by the initial biomass at the beginning of phage exposure. Shaded areas represent the standard error of the mean ($n_{t=48}$=12, $n_{t=72}$=9).

2.2.3 Amyloid curli fibers confer protection against phage infection

In biofilms, bacteria embed themselves in a self-produced matrix that protects bacterial communities from various exogenous stressors, including phages [90]. Hence, the biofilm matrix constituents of *E. coli* were investigated to determine the mechanism of how biofilms gain protection against phages. For this, mutants lacking different matrix components were constructed: flagella (Δ*fliC*,Δ*flhDC*), cellulose (Δ*bcsA*), poly-N-acetylglucosamine (Δ*pgaC*), colanic acid (Δ*wcaE*), type I fimbriae (Δ*fimA*) or amyloid curli fibers (Δ*csgB*). To identify the components of the biofilm matrix that contribute to phage protection, 72 h old biofilms formed by these matrix mutants were exposed to engineered T7 phages for 12 h under constant flow. Biofilms formed by bacteria deficient in amyloid curli fiber biogenesis (Δ*csgB*) were susceptible to phage infection, as the bacterial biomass decreased during co-incubation with phages (Figure 2.5 a). Ectopic expression of *csgB* in the Δ*csgB* background (Δ*csgB*, P_{csgB}-*csgB*) successfully restored the survival phenotype. For biofilms lacking any of the other matrix components, reduction in biomass could not be observed (Figure 2.5 a). Thus, the presence of curli fibers is essential for phage protection and enables biofilm survival in the presence of T7 phages.

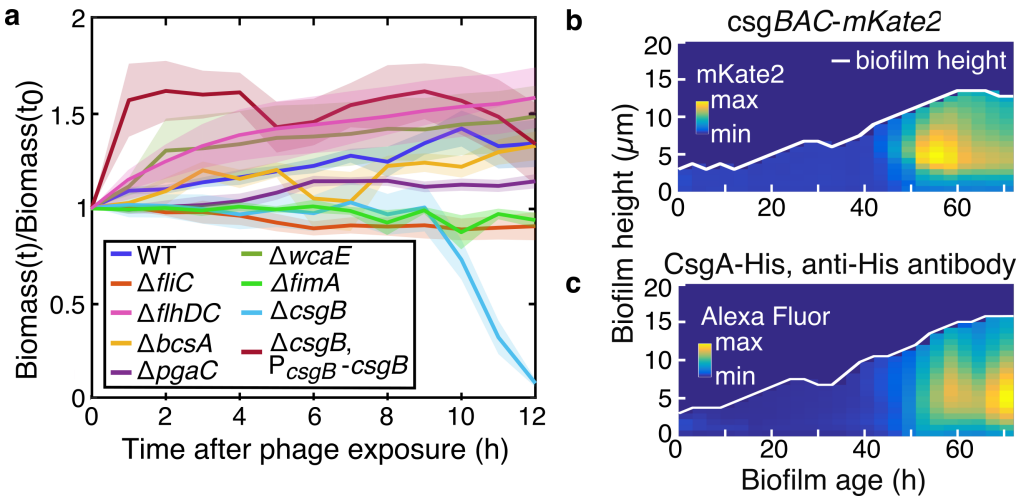

Figure 2.5: Amyloid curli fibers as part of the matrix protect *E. coli* AR3110 biofilms from phage infection. (a) Biofilms formed by matrix mutants were grown for 72 h in microfluidic channels and exposed to engineered T7 phages for 12 h under constant flow. Bacteria deficient in curli fiber assembly (Δ*csgB*) were susceptible to phage infection. Ectopic expression of *csgB* under control of the native promoter successfully restored the protection phenotype. Mutants lacking any other matrix component (flagella: Δ*fliC*, Δ*flhDC*; cellulose: Δ*bcsA*; poly-N-acetylglucosamine: Δ*pgaC*; colanic acid: Δ*wcaE*; type I fimbriae: Δ*fimA*) were protected from phage infection. Plotted lines represent the mean biomass normalized to the initial biomass and shaded areas represent the standard error of the mean ($n_{\Delta fliC}$=3, $n_{\Delta flhDC}$=5, $n_{\Delta bcsA}$=4, $n_{\Delta pgaC}$=5, $n_{\Delta wcaE}$=5, $n_{\Delta csgB}$=3, $n_{\Delta csgB,\ PcsgBAC\text{-}csgBAC}$=3). (b) Monitoring transcription of the curli operon *csgBAC* with the fluorescent reporter protein mKate2 and (c) visualization of curli fibers by immunofluorescence staining during biofilm growth revealed curli production during late stages of biofilm formation. Confocal fluorescence images were taken every three hours. For every imaging event the heatmap displays the fluorescence intensity values along the vertical axis.

To understand the curli-mediated protection mechanism found in older biofilms, the transition from being susceptible to protected was examined. Phage protection is facilitated by curli fibers as their absence in 72 h grown biofilms results in phage predation (Figure 2.5 a). Thus, susceptibility to phage infection in early stages of biofilm growth could correspond to the absence of curli fibers in the biofilm matrix. A reporter strain, with the fluorescent protein mKate2, was constructed to monitor transcriptional activity of the *csgBAC* operon every 3 h throughout biofilm growth for 72 h (Figure 2.5 b). Additionally, amyloid curli fibers were visualized by immunofluorescence staining of biofilms formed by *E. coli* expressing CsgA with a C-terminal 6x His-Tag (Figure 2.5 c). During the initial 40 h of biofilm growth, expression of the fluorescent transcriptional reporter mKate2 could not be observed (Figure 2.5 b). Consistently, fluorescent anti-6x-His antibodies

were not visualized as well (Figure 2.5 c). Hence, the *csgBAC* operon was not transcribed and curli fibers were not produced. However, between 40 h and 50 h of growth, individual cells within the continuous bacterial flat layer started to produce mKate2 and anti-6x-His antibodies were detected around them. Afterwards, as the biofilm grew in height and developed a tower-like three-dimensional structure, the amount of mKate2-producing cells increased continually. At the same time, fluorescent antibodies were detected around these cells transcribing the *csgBAC* operon. When *E. coli* biofilms grew in height, curli-producing cells predominantly localized in the upper region of the biofilms (Figure 2.6 a-e). Here, nearly all cells produced curli fibers, thereby creating a continuous mesh spanning the upper part of *E. coli* biofilms as visualized by immunofluorescence staining (Figure 2.6 d). Towards the bottom layer of the biofilm, fewer cells were surrounded by curli fibers. Monitoring curli transcription and production spatiotemporally throughout biofilm growth revealed a dynamic change in biofilm matrix composition with curli fibers being produced during late stages of biofilm formation.

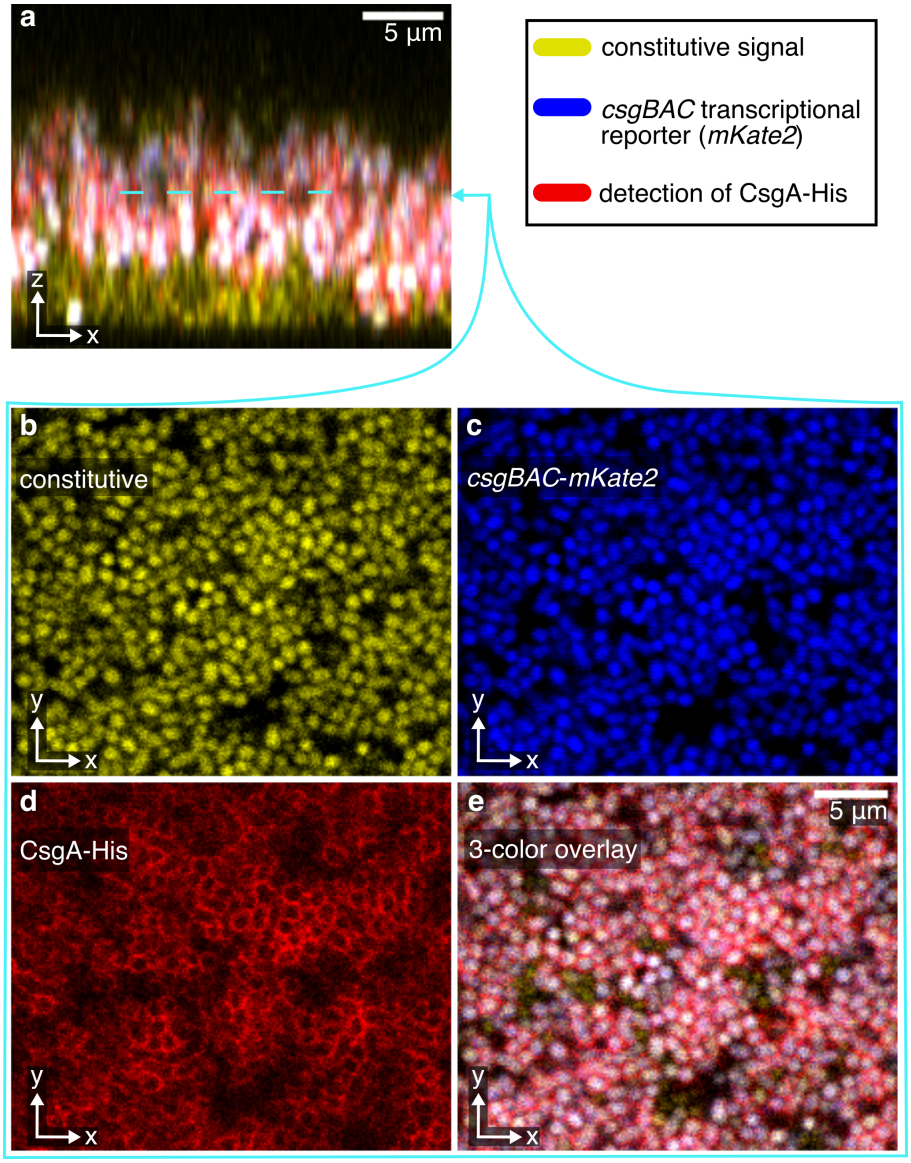

Figure 2.6: Heterogeneous transcription and production of curli fibers in wild-type *E. coli* biofilms. (a)-(e) In 72 h grown biofilms bacteria located in the upper part of the biofilm predominantly produced the curli transcriptional reporter mKate2 (blue). (b)-(e) Detailed view of one selected layer in the upper region (indicated by the dashed line and arrow in cyan) shows that mKate2-producing cells were surrounded by curli fibers, as visualized by immunofluorescence staining (red). Bacteria constitutively expressed the fluorescent protein mKOkappa (yellow) (n=3).

Curli fiber production temporally coincided with the development of phage protection. Therefor, it was tested if biofilms formed by *E. coli* overexpressing curli fibers can survive phage attack at an earlier biofilm age as compared to the wild type. By the insertion of a point mutation in the promoter of the biofilm master regulator CsgD, a constitutive expression of curli fibers was achieved [102]. These

cells showed overall faster biofilm formation. When exposed to engineered T7 phages, biofilms grown for 24 h or more were able to survive (Figure 2.7). As accelerated curli production resulted in advanced phage protection, it demonstrated that the development of phage protection is directly dependent on the presence of curli fibers in biofilms.

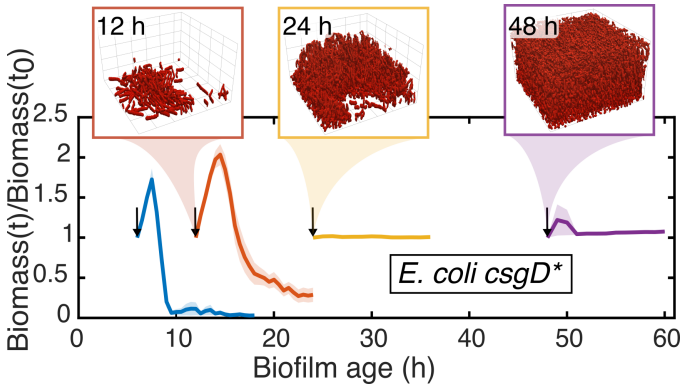

Figure 2.7: Overexpression of biofilm matrix results in phage protection at a younger biofilm age. Biofilms formed by cells overexpressing curli fibers were exposed to engineered T7 phages for 12 h and changes in bacterial biomass were monitored by fluorescence confocal microscopy. The time point of phage addition to the growing biofilms is indicated by the arrows. Biofilms up to an age of 12 h were susceptible to phage-mediated killing. However, survival could be observed at an early biofilm age of 24 h. Plotted lines represent the mean bacterial biomass normalizd to the initial biomass and shaded areas the standard error of the mean ($n_{t=6}$=4, $n_{t=12}$=8, $n_{t=24}$=8, $n_{t=48}$=6).

Together, these results reveal the crucial role of amyloid curli fiber production in the protection against infection by phages. Although the production of curli fibers is heterogeneously distributed across *E. coli* biofilms, assembly of the curli fiber mesh in the upper region of the biofilm is sufficient to confer collective protection against phage infection.

2.2.4 Monitoring the transcription of genes involved the production of biofilm matrix

Curli fiber production is temporally associated with the development of phage protection, making curli an indispensable constituent of the biofilm matrix. Other matrix components such as flagella, cellulose, colanic acid, poly-N-acetylglucosamine and type I fimbriae contribute to biofilm formation in *E. coli*. Here, these matrix components were investigated for their role in the spatiotemporal changes of the biofilm architecture during curli-mediated phage protection. As previously

described for curli fibers, the transcriptional activity of matrix-encoding genes was monitored throughout biofilm growth using the fluorescent reporter protein mKate2.

Flagella facilitate biofilm initiation as they promote surface attachment [30]. Fluorescence confocal microscopy revealed that bacteria transcribe the flagella subunit *fliC* (further referred as P_{fliC}-ON) from the initiation of biofilm formation and P_{fliC}-ON cells were present throughout growth for 72 h (Figure 2.8 a). However, the fraction of P_{fliC}-ON cells changed during biofilm development. Before curli fibers were produced, all cells transcribed *fliC* homogeneously. In contrast, when biofilms were more than 40 h old and production of curli fibers occured, *fliC* was primarily transcribed by cells located at the bottom of the biofilm (Figure 2.8 b-d). In the upper region, only a few cells appeared to be in a P_{fliC}-ON state (Figure 2.8 e-f). Hence, during late stages of biofilm development, production of the biofilm matrix components flagella and curli is limited to the cells of the lower and upper layers of the biofilm, respectively.

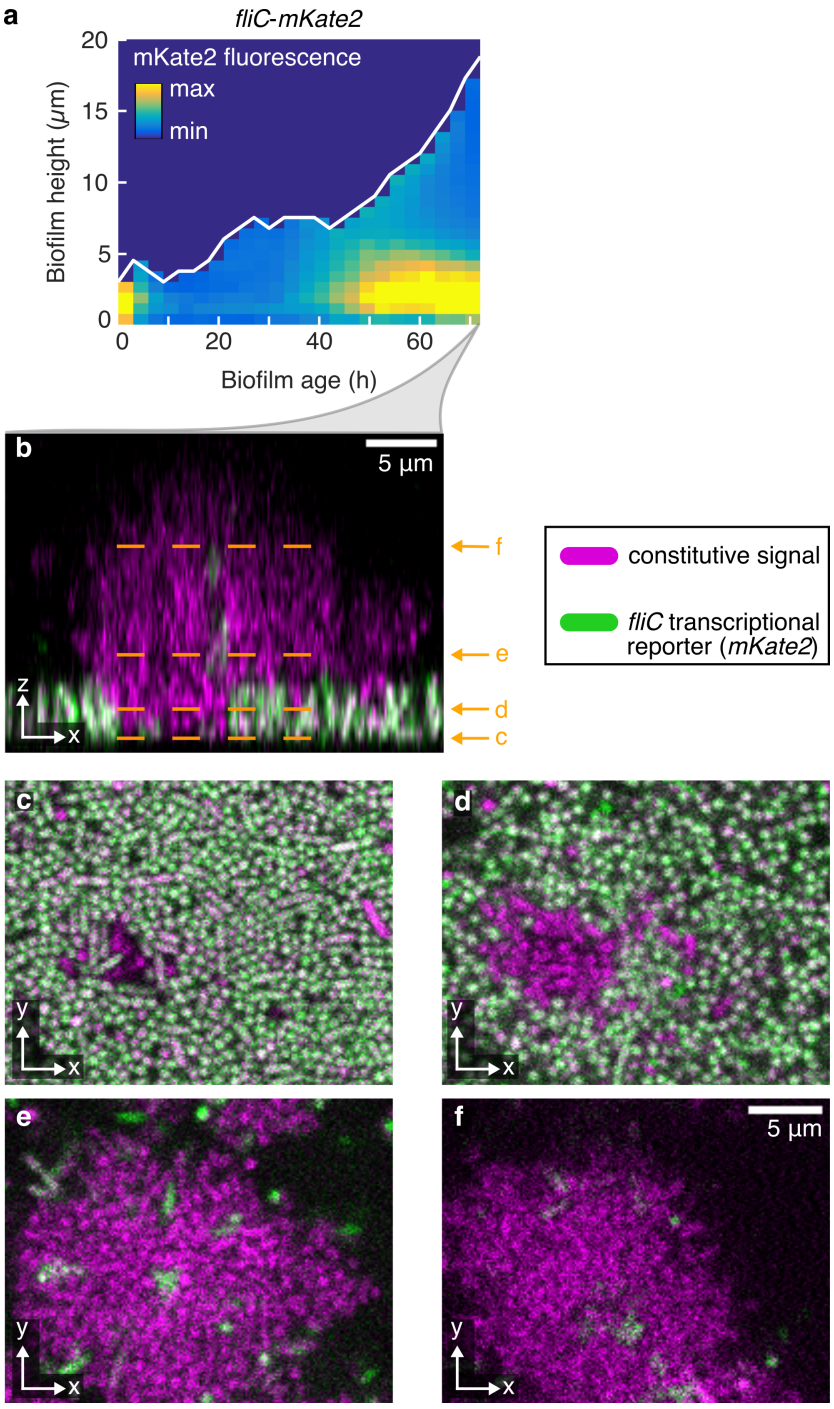

Figure 2.8: Transcription of *fliC* during growth of wild-type biofilms. (a) Monitoring the production of the fluorescent protein mKate2 as a reporter for transcription of *fliC* (encoding the flagella subunit). Fluorescence images were taken every three hours throughout biofilm growth for 72 h. For every imaging event the heatmap displays the mKate2 expression profile along the vertical axis of the biofilm. The colormap was adjusted to the minimum and maximum fluorescence intensity values of the curli transcriptional reporter (Figure 2.5) (n=3). (b)-(f) Cells transcribing *fliC* (shown in green) were heterogeneously distributed across different layers of 72 h old biofims. Bacteria were constitutively expressing mKOkappa (shown in purple) (n=3).

In *E. coli* AR3110, production of cellulose has been restored. Therefore, these bacteria are able to produce cellulose and use it as another constituent of the biofilm matrix [33]. To investigate cellulose production, the transcription of *dgcC*, encoding a diguanylate cyclase required for cellulose biosynthesis was monitored using the fluorescent protein mKate2 (Figure 2.9 a). During biofilm growth for 72 h, the mKate2 expression pattern was similar to that observed for the curli operon *csgBAC* (Figure 2.5 b). Biofilm-resident cells producing mKate2 started to appear approximately after 50 h of growth and localized in the upper region of the bacterial community. Overall, compared to *csgBAC*, lower mKate2 fluorescence intensity values were obtained in case of *dgcC*. For colanic acid (P_{wcaE}-*mKate2*), poly-N-acetylglucosamine (P_{pgaC}-*mKate2*) and type I fimbriae (P_{fimA}-*mKate2*), expression of the fluorescent transcriptional reporter mKate2 could not be detected during biofilm growth (Figure 2.9 b-d). Monitoring transcriptional promoter activity of operons involved in matrix production suggests that, in addition to curli fibers, bacteria only produce flagella and cellulose as part of their matrix.

Major changes in biofilm matrix composition involve spatiotemporal dynamics in production of curli fibers, flagella and cellulose during biofilm growth. Transcriptional activity of genes involved in colanic acid, poly-N-acetylglucosamine and type I fimbriae production did not coincide temporally with the development of phage protection.

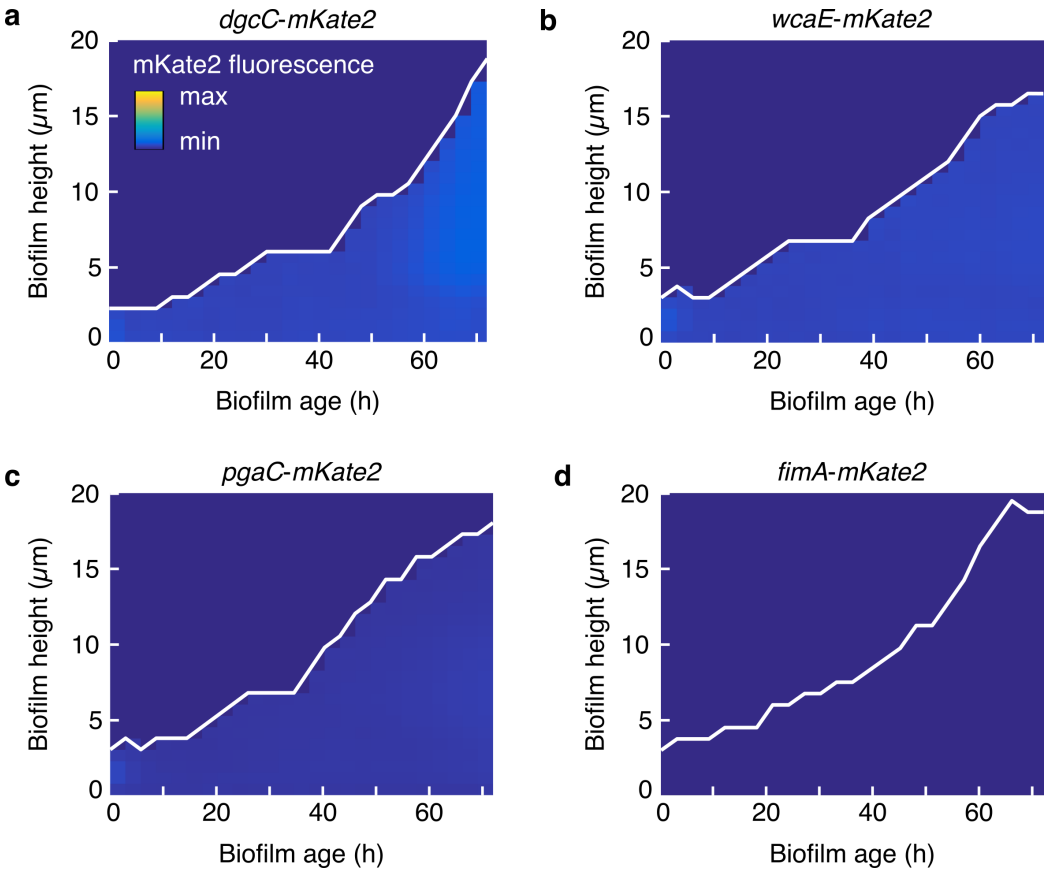

Figure 2.9: Transcription of genes involved in biofilm matrix production. Transcriptional reporter fusions using the fluorescent protein mKate2 were constructed and mKate2 expression was monitored every 3 h throughout biofilm growth for 72 h. The mKate2 fluorescence values were adjusted to the minimum and maximum obtained for the *csgBAC* operon transcriptional reporter (Figure 2.5) and displayed along the height of the biofilm for each imaging time point. Transcription was monitored for (a) *dgcC* encoding a diguanylate cyclase required for cellulose biosynthesis (n=3), (b) *wcaE* involved in colanic acid synthesis (n=3), (c) *pgaC* that codes for a poly-N-acetylglucosamine synthase (n=4) as well as (d) *fimA* encoding the type I fimbriae major subunit (n=3).

2.2.5 Biofilm architecture impacts phage mobility in biofilms

Alterations in matrix composition during the process of biofilm development contribute to the re-organization of the biofilm architecture [103]. In *E. coli*, biofilm growth is accompanied by changes in the matrix composition with increasing biofilm age. This is seen by the initiation of curli fiber production during late stages of biofilm development, which is essential for bacterial survival against phage attack. Curli fibers have been shown to promote cell-to-cell interactions [104]. Taken together, it led to the hypothesis that curli fibers induce architectural changes to

the biofilms, which protect the cells from phage infection. To test this, the cell density of 72 h grown biofilms formed by wild-type and $\Delta csgB$ cells was compared. Analysis of the biofilm architecture revealed that the cells in $\Delta csgB$ biofilms are less tightly packed compared to the wild type (Figure 2.10 a), suggesting that a wider spatial separation of bacteria in the absence of curli fibers leaves bacteria susceptible to phage attack. Further, it was hypothesized that the extent of cell packing is directly linked to phage mobility into bacterial communities. The ability of T7 phages to invade bacterial communities was investigated by using fluorescently labelled wild-type T7 phages (Alexa Fluor 488). In the presence of 72 h old wild-type biofilms, fluorescently labelled phages were exclusively found in the outer periphery of the bacterial community (Figure 2.10 b). Invasion was also tested for biofilms lacking cellulose ($\Delta bcsA$) , poly-N-acetylglucosamine ($\Delta pgaC$) and colanic acid ($\Delta wcaE$). For these biofilms, identical results were obtained. In contrast, biofilms lacking curli fibers ($\Delta csgB$) showed permissive phages invasion (Figure 2.10 f). This indicates that curli fibers protect bacteria against infection by T7 phages on the community level, by providing a close cell-to-cell arrangement which prevents the diffusion of phages into the biofilm.

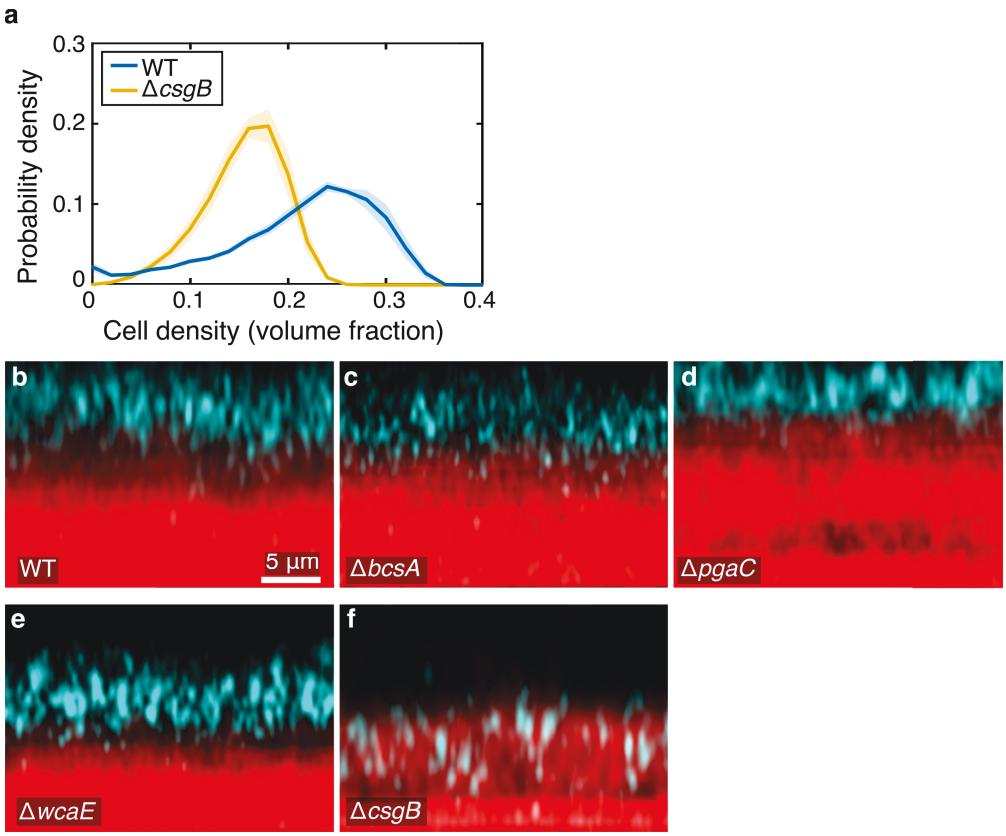

Figure 2.10: Biofilm architecture prevents invasion of biofilms by T7 phages in the presence of curli fibers. (a) Imaging of bacterial communities at single-cell resolution and biofilm reconstruction revealed a tighter cell packing in wild-type biofilms as compared to biofilms formed by Δ*csgB*. Plotted lines represent the mean and shaded areas represent the standard error of the mean (n_{WT}=9, n_{WT}=9). (b)-(f) Localization of fluorescently labelled T7 phages (cyan) after co-incubation with 72 h old biofilms (red) for 8 h displayed as maximum intensity z-projections. In case of (b) wild-type biofilms and ones lacking (c) cellulose, (d) poly-N-acetylglucosamine or (e) colanic acid, fluorescently labelled T7 phages accumulated in the outer periphery only. (f) In contrast, phages were able to penetrate bacterial communities impaired in curli fiber production.

For further verification that curli fibers prevent diffusion of phages into bacterial communities, artificial biofilms were constructed *in vitro* and exposed to fluorescently labelled T7 phages. These artificial biofilms constituted fluorescent beads, representing bacterial cells. For matrix-free artificial biofilms, invasion by phages was dependent on the diameter of the beads (Figure 2.11 d). T7 phages could not be visualized inside clusters made up of beads that were 0.5 µm in diameter. By using a larger bead size (1 µm in diameter), T7 phages were able to penetrate the clusters. As phage protection depends exclusively on curli fiber production, *in vitro* polymerized curli fibers (Figure 2.11 a) were chosen to constitute the biofilm matrix in the artificial biofilm. When beads were embedded in the curli fiber

mesh, fluorescently labelled phages could not invade artificial biofilms regardless of the bead size (Figure 2.11 d). *In vitro* polymerized curli fibers permitted fluorescently labelled T7 phages to diffuse into the three-dimensional mesh. However, the branched curli fiber network prohibited T7 phages from passing through (Figure 2.11 b). Co-localization of T7 phages with curli fibers was further confirmed by scanning electron microscopy (Figure 2.11 c). Taken together, the distribution of curli fibers around and between cells/beads (Figure 2.11 e) was sufficient to prevent invasion of biofilms by T7 phages.

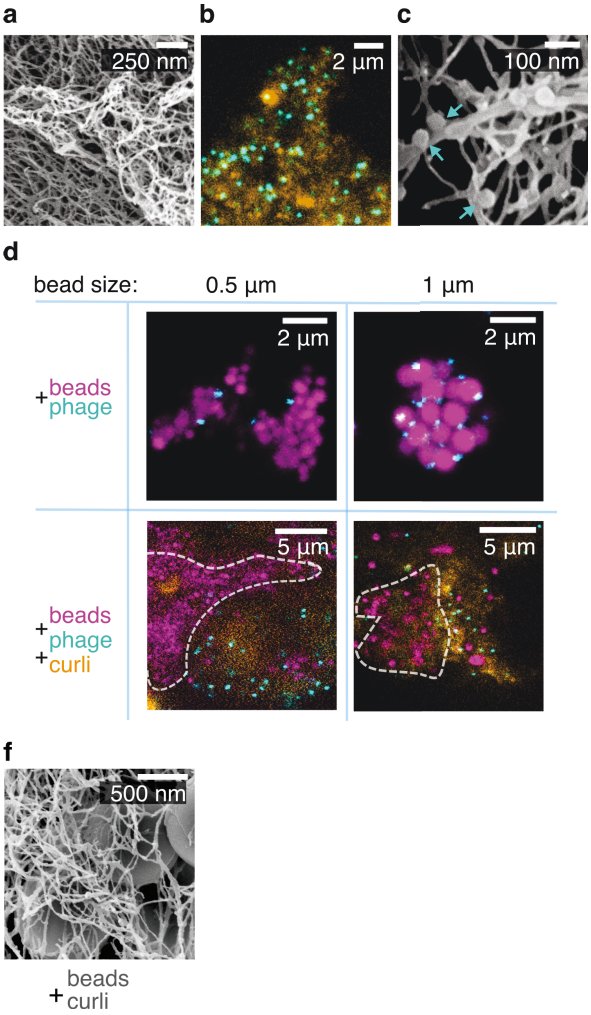

Figure 2.11: Construction of biofilms *in vitro* confirms cell spacing as a determinant for phage invasion of bacterial communities. (a) Scanning electron microscopy confirmed the successful polymerization of the purified curli monomer CsgA into curli fibers *in vitro*. (b) Fluorescently labelled phages (cyan) were able to penetrate the curli fiber network (orange, immunofluorescence staining). (c) T7 phages were trapped inside the fiber network (indicated by the arrows). (d)+(e) Construction of biofilms *in vitro* with curli fibers as the matrix component and fluorescent beads representing bacterial cells. Fluorescently labelled phages (cyan) were able to penetrate clusters made out of beads that are 1 µm in diameter, but not clusters made out of 0.5 µm sized beads. However, when beads were entangled in the curli fiber mesh, phages were not able to invade artificial biofilms.

Visualization of phage particles together with biofilm architecture analyses and biofilm reconstruction *in vitro* revealed the curli-mediated phage protection mechanism. The presence of a continuous curli fiber mesh in the upper region of biofilms limits diffusion of phages into the bacterial community. By preventing phage invasion, curli fibers provide collective protection against phage infection.

Visualization of fluorescently labelled T7 phages during co-incubation with biofilms formed by wild-type cells, Δ*csgB* and other matrix mutants established the requirement of curli fiber production against phage invasion (Figure 2.10 b-f). However, for flagella mutant biofilms (Δ*flhDC*, Δ*fliC*) inconsistent results were obtained regarding the spatial distribution of T7 phages. Biofilms lacking the flagella master regulator FlhDC prevented T7 phages from penetrating into the bacterial community (Figure 2.12 b). On the other hand, T7 phages were able to invade Δ*fliC* biofilms (Figure 2.12 c) and appeared in different layers of the bacterial community (Figure 2.12 d). To investigate the mechanism of how different flagella mutant biofilms either allow or prevent T7 phages from diffusing into the bacterial community, the biofilm architecture was analysed with respect to cell density. Single-cell analysis revealed that in 72 h old Δ*flhDC* and wild-type biofilms, the bacterial cell density was similar, with a tendency towards a tighter cell packing for Δ*flhDC* (Figure 2.12 a). In case of Δ*fliC* biofilms, local cell densities were more uniformly distributed.

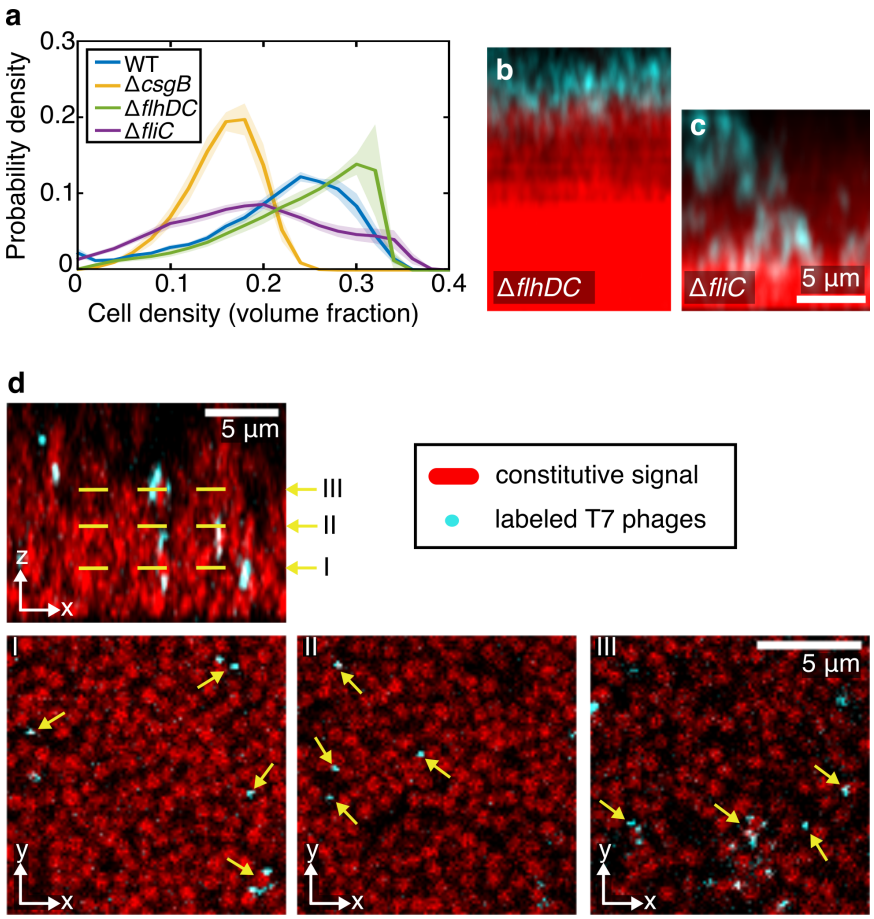

Figure 2.12: Biofilm architecture and phage mobility varies between flagella mutants (a) Single-cell analysis of the biofilm architecture revealed that cells in Δ*fliC* biofilms are less densely packed as compared to wild-type or Δ*flhDC* biofilms. (b)+(c) Spatial distribution of fluorescently labelled T7 phages varied after co-incubation with 72 h old Δ*fliC* or Δ*flhDC* biofilms for 8 h. (d) Fluorescently labelled phages were able to penetrate into different layers and localized in cell-free regions of Δ*fliC* biofilms as indicated by the yellow arrows (n=4).

Both mutants (Δ*fliC* and Δ*flhDC*) are deficient in flagella biogenesis, however only the deletion of *fliC* introduced architectural changes to the biofilms. These architectural differences were assumed to be associated with the inverse regulation of flagella and curli which results in the exclusive production of either flagella or curli by *E. coli* AR3110 [35]. Taking into account that FlhDC and FliC operate at different levels in the flagella regulatory network, it was hypothesized that the fraction of curli-producing cells in the bacterial population differs in Δ*flhDC* and Δ*fliC* biofilms. Specifically, loss of the flagella master regulator FlhDC was believed to disrupt the flagella regulatory network and shift the bacterial population towards curli production during biofilm development. To verify this, tran-

scriptional activity of the curli operon *csgBAC* was monitored with a fluorescent transcriptional reporter fusion (P_{csgBAC}-*mKate2*) and curli fibers were visualized by immunofluorescence staining. Confocal microscopy of Δ*flhDC* biofilms grown for 72 h confirmed that the bacterial community constituted curli-producing cells (Figure 2.13 a). Because FliC operates downstream of FlhDC [105], the flagella regulatory network was expected to be functional in Δ*fliC* cells, i.e., active transcription from the *fliC* promoter would still take place. Therefore, it was hypothesized that Δ*fliC* biofilms consist of a heterogeneous bacterial population (in respect to curli fiber production), similar to the wild type. Fluorescent transcriptional reporter fusions (P_{csgBAC}-*mKate2*, P_{fliC}-*sfgfp*) confirmed that Δ*fliC* biofilms are built up of P_{fliC}-ON as well as P_{csgBAC}-ON cells (Figure 2.13 b). However, due to the deletion of *fliC*, P_{fliC}-ON cells were deficient in flagella assembly. Curli production was exclusively seen in P_{csgBAC}-ON cells (Figure 2.13 c). Consequently, alterations in biofilm matrix composition allowed T7 phages to penetrate cell and matrix-free regions of Δ*fliC* biofilms (Figure 2.14). However, the extent of curli fiber production was sufficient to provide collective protection against phage infection.

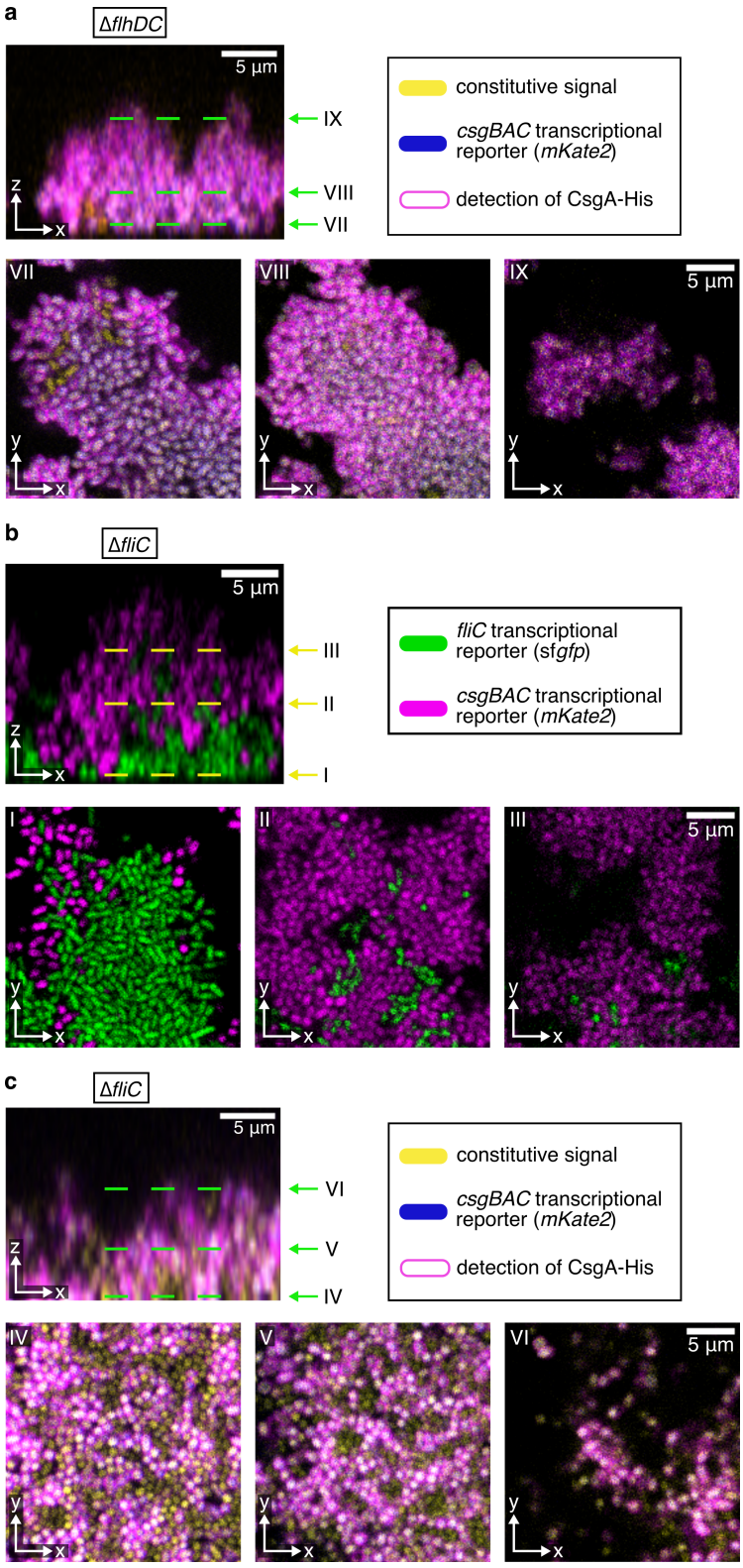

Figure 2.13: Biofilms formed by two flagella mutants differ in curli production (a) In 12 h old Δ*flhDC* biofilms, almost all cells produced curli fibers (magenta, immnunofluorescence staining), regardless of their spatial distribution within the community (n=3). (b)+(c) Δ*fliC* biofilms consisted of cells that were either transcribing flagella or curli. Bottom layers of the biofilm consisted of cells transcribing flagella whereas cells in the upper layers showed curli production (n=3).

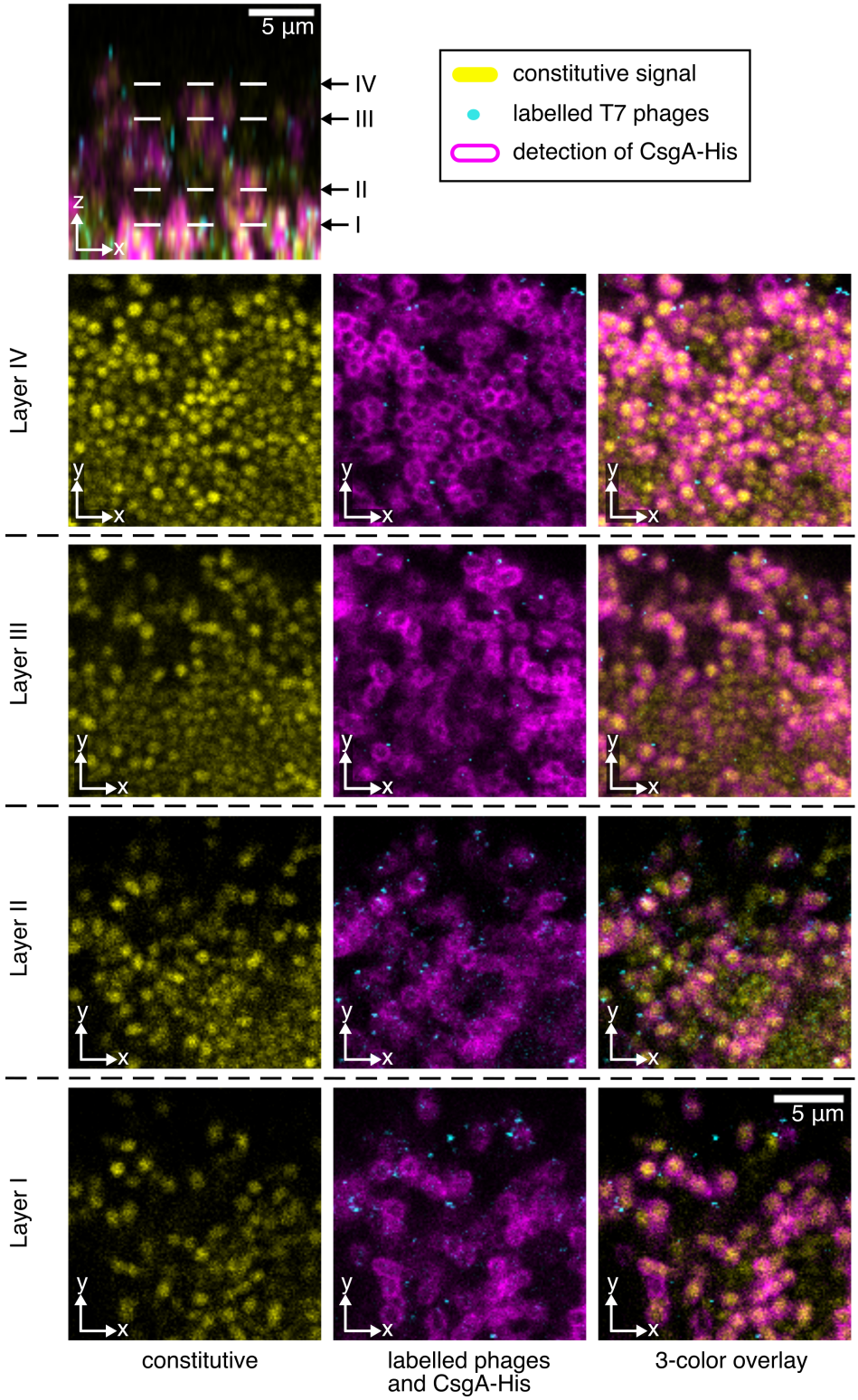

Figure 2.14: Visualization of curli fibers and fluorescently labelled T7 phages in Δ*fliC* biofilms. After co-incubation for 8 h, fluorescently labelled T7 phages (cyan) localized in close proximity to curli fibers (purple, immunofluorescence staining) in different layers (I-IV) of 72 h old Δ*fliC* biofilms (n=5).

2.2.6 Phage tolerance of individual cells depends on curli fibers

As the presence of a curli fiber mesh protected biofilms collectively, it suggested that individual bacteria, once encapsulated inside a curli fiber mesh, would be able to tolerate phages in their vicinity. To test if even single cells that are surrounded by curli fibers can survive phage predation, a heterogeneous bacterial population composed of curli-producing and non-producing cells was exposed to T7 phages (Figure 2.15 b). Curli non-producing cells were infected by T7 phages and subsequently, lysed. In contrast, cells embedded in a curli fiber mesh were able to survive in the presence of phages (Figure 2.15 a,b). Bacteria partially surrounded by curli fibers were not protected from T7 phage infection (Figure 2.15 c). In conclusion, curli fibers fully surrounding individual cells are sufficient to protect bacteria from phage infection.

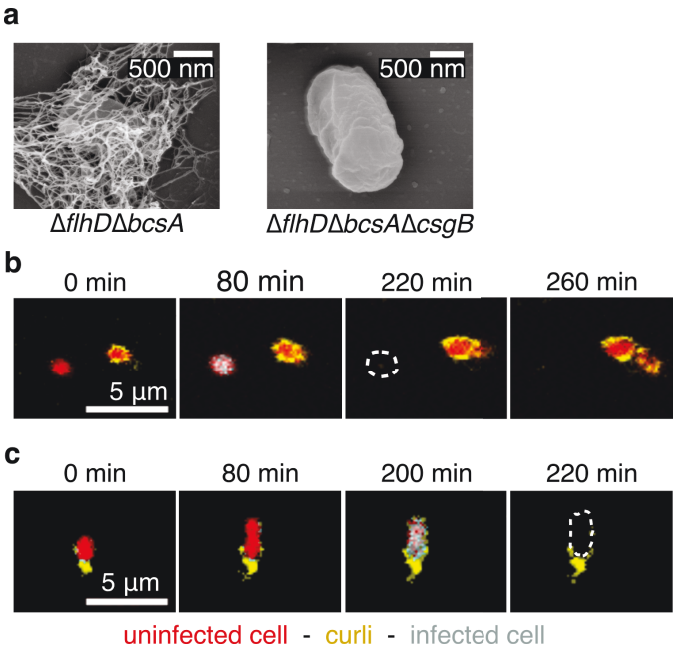

Figure 2.15: Curli fibers protect single cells from T7 phage infection. (a) Scanning electron microscopy revealed that bacteria producing curli fibers can be completely embedded in a mesh made out of curli fibers. (b)+(c) Bacteria (red) fully surrounded by curli fibers (yellow) were able to grow in the presence of T7 phages. Cells not producing curli fibers or ones that were partially covered were susceptible to phage-mediated killing.

2.3 Conclusion and Discussion

Interactions between biofilms and phages are likely common in the environment, since phages are the most abundant entities and biofilms constitute the predominant mode of life of bacterial cells [70, 71, 106]. Despite the numerous studies showing that biofilm formation and matrix production protect against phage infection, there is a lack of information on how biofilms gain protection [87, 91, 93, 107] In this study, the infection dynamics of *E. coli* biofilms by lytic T7 phages were investigated as one example, to understand the co-existence of phages and biofilms as well as the mechanism of phage-biofilm interactions.

Real-time visualization of phage-infected cells in a bacterial population by the use of genetically modified T7 phages together with fluorescence confocal microscopy reliably revealed a biofilm development-specific mechanism of phage protection (Figure 2.2). Survival of biofilms of a certain age coincides temporally with the production of curli fibers. Curli fibers are solely responsible for conferring collective protection against phage infection by preventing phage diffusion into bacterial communities formed by *E. coli* (Figure 2.5, Figure 2.10). In addition, production of a curli fiber mesh is sufficient to protect bacteria on the single-cell level (Figure 2.15).

Complete investigation of the infection dynamics of *E. coli* biofilms was performed in respect to T7 phages. However, biofilm age dependent phage protection could be discovered for lytic T5 phages as well (Figure 2.4). For both types of phages, the transition from being susceptible to protected occurred at the same biofilm age. This suggests that the mechanism, discovered for T7 phages, confers protection against T5 phages as well. Therefore, bacterial survival in the presence of T5 phages is potentially also associated with the production of curli fibers. Collective protection of *E. coli* biofilms emerges from the curli-mediated single cell protection and dense cell packing. In contrast, the survival of bacteria at the biofilm boundary depends on the protection of individual cells. There, bacteria are embedded in a curli fiber mesh, that obscures the bacterial cell surface and prevents phages from binding to their receptor located on the bacterial surface. At the same time, curli fibers ensure a dense cell packing by filling the space between cells, which limits phage diffusion. Due to the survival of the outer cell layer of the biofilm and prevention of phage invasion, biofilms can collectively withstand phage attack. Generation of a physical barrier and limiting the diffusivity of phages is indicated

to be an important determinant on the outcome of phage predation [93]. It suggests that curli fibers can protect *E. coli* biofilms from numerous phages; not only T7 and T5 phages.

Production of curli fibers favors co-existance of phages and *E. coli* biofilms. However, curli fibers are not only made by *E. coli*. In biofilms formed by *Salmonella*, curli fibers are part of the biofilm matrix as well [102]. Since both organisms exhibit similarities in their biofilm matrix composition, the curli fiber-mediated protection mechanism discovered for *E. coli* could potentially act in *Salmonella* biofilms and affect their susceptibility to phage infection. Curli fibers are also found in other members of the *Enterbacteriacae* [66]. In addition, bacteria from different phyla encode proteins showing homology to the curli formation system in *E. coli* [108]. Thus, curli-mediated phage protection could be a conserved mechanism, like variuos other anti-phage defense systems [85], present in different bacterial species. Owing to their high stability and resistance towards proteolysis [109], curli fibers are advantageous structures and can not be degraded by matrix-degrading enzymes. Thus, it is possible that phages can not overcome this protection mechanism by producing depolymerases.

The spatial organization of bacteria inside *E. coli* biofilms implicates a requirement for a certain community composition and structure to confer phage protection. *E. coli* biofilms are built up by flagella- and curli-producing cells (Figure 2.5, Figure 2.8). Limited phage diffusion and collective protection can only emerge because curli-producing cells shape the upper region of the biofilm and generate a curli fiber mesh. This mesh acts as a physical barrier in the upper region, that experiences constant exposure to phages. Flagella-producing cells benefit from the presence of a curli fiber mesh, spanning the outermost region of the biofilm, and survive. Therefore, curli fibers can be recognized as a public good. Since curli production by all bacteria is not a prerequisite for survival of a single species biofilm, it suggests that even multispecies biofilms could benefit from curli-producing cells. However, the amount of curli-producing cells and their spatial distribution could be the determining factors for collective protection.

Survival of *E. coli* biofilms is dependent on a sufficient production of curli fibers, which coincides with a certain biofilm age. Initially phages can propagate successfully in bacterial communities, which leads to an unstable co-existence between

phages and bacteria. However, curli-mediated phage protection turns the interaction into a stable co-existence. These dynamics suggest, that the process of biofilm formation and biofilm matrix production can determine the outcome of phage-biofilm interactions in natural environments. Immature biofilms could be the targets for phage replication.

This study comprehensively shows how the biofilm matrix composition at a certain biofilm age influences phage-biofilm interactions. Therefore, investigating such interactions with biofilms of one age only is not sufficient to make general conclusions about phage susceptibility of a given bacterial community. In future studies, the biofilm developmental stage and biofilm matrix composition should not be neglected. Understanding phage-biofilm interactions and biofilm protection mechanisms is not only important from the ecological point of view. The medical area requires new strategies to combat antibiotic-resistant bacteria and phage therapy is considered as one alternative. However, before phages can be applied to combat bacterial infections, the outcome of exposing biofilm to phages needs to be fully elucidated.

2.4 Materials and Methods

2.4.1 Microbiological Methods

2.4.1.1 Growth of *E. coli*

Bacteria were grown overnight in 5 mL lysogeny broth (LB) medium at 28 °C or 37 °C under shaking conditions (250 rpm). Whenever required, the growth medium was supplemented with antibiotics. Antibiotic concentrations were used according to Table 2.1. Bacterial strains used in this study are listed in Table S1 and Table S2.

Table 2.1: Antibiotic concentrations used for selection of *E. coli*

Antibiotic	Final concentration [µg mL^{-1}]
Ampicillin	100
Kanamycin	50
Chloramphenicol	10

2.4.1.2 Storage of *E. coli* cells

Bacterial cells grown overnight were mixed with glycerol (final concentration 20 %) and stored at −80 °C.

2.4.1.3 Monitoring bacterial growth and phage infection

Bacteria were grown in plastic 96-well plates and the growth was monitored using an automated plate reader (TECAN Spark 10M). For this, bacterial cells were grown overnight and back-diluted in LB medium to an $OD_{600\,nm}$ of 0.02. Individual wells were inoculated with 200 µL of the diluted bacterial suspension and the plate was placed in the plate reader. Optical density ($OD_{600\,nm}$) and fluorescence intensity was measured every 5 min for 5-12 h. Between measurements, the plate was shaking continuously (810 rpm). The temperature inside the plate reader was set to 37 °C. When bacteria reached exponential growth phase, T7 phages were added to a final concentration of 10^6 PFU mL^{-1}. For infection of slow-growing cells, T7 phages were added either at the beginning or 4 h after bacteria entered stationary phase.

2.4.1.4 Bacteriophage amplification and purification

For amplification of T7 phages, *E. coli* AR3110 was grown in LB medium supplemented with 5 mM $MgSO_4$ at 37 °C and 250 rpm shaking until an $OD_{600\,nm}$ of 0.5. Subsequently, 2 mL of a high-titer T7 phage lysate (10^8 PFU mL^{-1}) was added and bacterial cells were cultivated further at 37 °C and 250 rpm until the bacterial culture cleared as a result of phage propagation. The clear lysate was filtered-sterilized using a 0.22 µm filter and stored at 4 °C.

In order to amplify T5 phages, *E. coli* AR3110 was grown in LB medium supplemented with 0.1 mM $CaCl_2$ at 37 °C and 250 rpm shaking until an $OD_{600\,nm}$ of 0.5. T5 phages were added and incubation at 37 °C and 250 rpm followed. The clear lysate was stored at 4 °C.

For fluorescent labelling of T7 phages, further purification steps using a modified version of the protocol described by Boulanger [110] were applied. Briefly, 500 mL of a T7 phage lysate was treated with DNaseI (final concentration 1 µg mL^{-1}) for 30 min at 37 °C and 250 rpm. NaCl was added (final concentration 0.5 µg mL^{-1}) and the lysate was stored for one hour at 4 °C. After centrifugation for 10 min at 4 °C and 8000 rpm, the T7 phage-containing supernatant was filter-sterilized (0.22 µm pore size). Subsequently, PEG_{6000} was added to a final concentration of 10 % and dissolved by gentle stirring. The phage lysate was stored overnight at 4 °C. The next day, precipitated phages were collected by centrifugation for 15 min at 4 °C and 8000 rpm, resuspended in 5 mL PBS and stored at 4 °C, until they were further purified by CsCl density gradient centrifugation.

For CsCl density gradient centrifugation, a 62.5 % CsCl solution was prepared by dissolving 25 g CsCl in 15 mL H_2O. Afterwards, the 62.5 % CsCl solution was diluted in phosphate buffered saline (PBS) to generate CsCl solutions with lower densities (41.67 %, 31.25 %, 20.83 %). The CsCl density gradient was generated by layering solutions of decreasing density (2 mL of each). Finally, 2 mL of the T7 phage suspension was layered on top of the density gradient and ultracentrifugation (10^5 g, 20 h, 4 °C) followed. Phage particles were collected and CsCl was removed by dialysis against PBS at 4 °C. Prior to dialysis, a membrane with 12000-14000 MWCO was equlilibrated in H_2O and then PBS for 1 h each. Subsequently, the membrane was filled with 300 µL of the phage suspension and placed in 500 mL PBS for 2 h. Next, the membrane was transferred into 2 L PBS and

dialysis followed overnight. The next day, purified T7 phages were collected and stored at 4 °C until further use.

2.4.1.5 Determination of the phage titer

Whenever new phage lysates were generated, phages were purified or fluorescently labelled, phage titer measurements were carried out. Phages were serially diluted (up to 10^{-9}) in LB medium. Afterwards, 50 µL of the diluted phage suspension was mixed together with 200 µL of exponentially growing *E. coli* AR3110 cells and added to 5 mL 0.7 % LB agar. The LB agar was supplemented with 5 mM $MgSO_4$ or 0.1 mM $CaCl_2$ in case of T7 phages or T5 phages, respectively. Subsequently, the mixture was poured onto a 1.5 % LB agar plate and incubation at 37 °C for 6 h followed. Phage plaques were enumerated and the phage titer (PFU mL^{-1}) was calculated.

2.4.1.6 Labelling of bacteriophages with Alexa Fluor 488

Bacteriophages were labelled with Alexa Fluor 488 (Cat-No. A30005, Thermo Fisher Scientific) according to the protocol provided by the manufacturer and by Slootweg *et al.* [111]. Briefly, 100 µL of purified phages (concentration: 10^{12} PFU mL^{-1}) were mixed with 10 µL sodium bicarbonate (concentration: 1 M) before 0.1 mg Alexa Fluor 488 5-TFP (dissolved in 10 µL dimethylformamide) was added. After incubation for one hour at room temperature under continuous stirring, labelled phages were separated from unbound dye by dialysis against PBS at 4 °C. Prior to dialysis, a membrane with 12000-14000 MWCO was equlilibrated in H_2O and then PBS for 1 h each. Afterwards the membrane was filled with the phage-dye mixture and dialysis followed. First, the membrane was placed into 500 mL PBS for 3 h. Afterwards, the membrane was transferred into 2 L fresh PBS and dialysis occurred overnight. The next day, a third dialysis step for 4 h using 1 liter PBS took place before fluorescently labelled phages were collected and stored at 4 °C.

2.4.2 Molecular Cloning

2.4.2.1 Heat shock transformation of *E. coli* AR3110

For lambda red recombineering and removal of antibiotic resistance cassettes, plasmid pKD46 or pCP20 was brought into *E. coli* AR3110 via heat shock transformation. For this, bacterial cells grown overnight were back-diluted 1:25 in 25 mL

fresh LB medium supplemented with the appropriate antibiotic and re-grown at 37 °C and 250 rpm shaking. Once the bacterial culture reached an $OD_{600\ nm}$ of 0.5, cells were cooled down on ice for 10 min. After centrifugation for 3 min at 4 °C and 6000 g, bacteria were resuspended in 10 mL ice-cold 0.1 M $CaCl_2$ followed by incubation for 10 min on ice. Subsequently, cells were harvested for 3 min at 4 °C and 6000 g and resuspended in 500 µL of ice-cold 0.1 M $CaCl_2$/15 % glycerol. Immediately, chemically competent cells were used for heat shock transformation. Chemically competent cells (100 µL) were mixed with 100 ng plasmid DNA and incubated for 30 min on ice. Subsequently, heat shock was applied by transferring bacteria into a 42 °C waterbath for 45 s followed by incubation on ice for 2 min. Pre-warmed LB medium (500 µL) was added and cells were recovered for one hour at 37 °C and 550 rpm shaking. Afterwards, cells were plated on LB agar supplemented with ampicillin and grown overnight at 28 °C.

2.4.2.2 Lambda red recombineering in *E. coli* AR3110

Genetic modifications in *E. coli* AR3110 were carried out using two lambda red recombineering methods [112, 113].

All bacterial strains constitutively expressed a fluorescent protein constitutively under control of the *tac* promoter (P_{tac}) lacking the *lac* operator. Biofilm matrix mutants and wild-type *E. coli* AR3110 constitutively expressed mRuby2. Two *E. coli* codon-optimized *mRuby2* (with ribosomal binding sites) fused the tac promoter were introduced together with a kanamycin resistance cassette into the *E. coli* AR3110 genome at the *attB* site. When transcription was monitored using a fluorescent reporter protein or the cells produced CsgA with a C-terminal 6x His-Tag for immunofluorescence staining, bacteria expressed mKOkappa constitutively. For this, a single *mKOkappa* with a ribosomal binding site fused to the tac promoter and a kanamycin resistance cassette were inserted into the *E. coli* AR3110 genome at the *attB* site.

Lambda red recombineering for gene deletions

In case of gene deletions, the gene of interest was replaced either with a chloramphenicol or kanamycin resistance cassette, amplified from pKD3 or pKD4, respectively. In order to achieve successful genomic integration, oligonucleotides were designed so that the resulting PCR product harbours 45 bp long homology regions on both ends. After PCR purification, the DNA fragment was transformed

into *E. coli* AR3110 (expressing the phage λ Red recombinase) via electroporation. In order to generate *E. coli* expressing phage λ Red recombinase, *E. coli* transformed with plasmid pKD46 was grown overnight at 28 °C. The following day, 1 mL of overnight culture was back-diluted into 50 mL of fresh medium and re-grown at 28 °C. Once the bacterial culture reached an $OD_{600\,nm}$ of 0.1, arabinose was added (final concentration 0.4 %) and the cells were grown further until an $OD_{600\,nm}$ of 0.5. Afterwards, cells were incubated on ice for 5 min and then harvested by centrifugation for 5 min at 4 °C and 6000 g. Cells were resuspended in 25 mL of ice-cold H_2O, followed by centrifugation for 5 min at 4 °C and 6000 g. This step was repeated twice, and then the pellet was resuspended in a final volume of 500 µL H_2O, followed immediately by electroporation. Here, 50 µL of electrocompetent cells were mixed with 100 ng of purified PCR product and transferred into ice-cold electroporation cuvettes. Electroporation was performed using a Biorad Micropulser^{TM} (program Ec1, 1.8 kV). Immediately after electroporation, 500 µL of pre-warmed LB medium was added and the cells were incubated at 37 °C and 550 rpm shaking. After one hour, cells were plated on LB agar supplemented with the appropriate antibiotic. The next day, successful genetic modification was verified by colony PCR. The antibiotic resistance cassette was flipped out using FLP recombinase. Gene deletion as well as the subsequent flip-out of the antibiotic resistance cassette was confirmed by DNA sequencing.

Removal of antibiotic resistance cassettes by FLP recombinase

E. coli AR3110 containing either the kanamycin or chloramphenicol resistance cassette flanked by FRT sites was transformed with the plasmid pCP20 and grown at 28 °C. After growth in liquid culture at 28 °C in the presence of ampicillin bacteria were back-diluted 1:50 in LB medium and re-grown at 43 °C under non-selective conditions. Once the culture reached an $OD_{600\,nm}$ of 0.5, cells were back-diluted for a second time and re-grown until an $OD_{600\,nm}$ of 0.5. Finally, bacteria were diluted and plated on LB agar. Loss of the selectable marker was confirmed by plating clones on LB as well as on LB supplemented with chloramphenicol or kanamycin.

Scarless lambda red recombineering

Scarless lambda red recombineering was applied for gene insertions and gene replacements in *E. coli* AR3110. This method is based on two recombineering steps. First, a gene coding for a selectable marker is inserted into the locus to be modified,

which is then replaced with a DNA fragment containing the desired modification. In the first step, a kanamycin resistance cassette together with *ccdB* fused to a rhamnose-inducible promoter (amplified from pKD45) was inserted into the locus that was to be subjected to genetic modification. During the PCR, 45 bp long regions were added to both ends of the DNA fragment for genomic integration by homologous recombination. After PCR purification, the DNA fragment was transformed into *E. coli* AR3110 expressing the phage λ Red recombinase as described previously. In the second step, the whole cassette was exchanged with a DNA fragment containing the desired modification. Again, the DNA fragment was brought into *E. coli* AR3110 cells expressing phage λ Red recombinase via electroporation. Counter-selection was performed by plating the cells on M9 agar containing 0.2 % L-rhamnose and 0.1 % casamino acids. After three days of incubation at 37 °C, the exchange of DNA fragments was verified by colony PCR. Additionally, chromosomal modifications were confirmed by sequencing.

This method was utilized to generate *E. coli* strains expressing CsgA-6x-His-Tag. Here, the native *csgA* of *E. coli* was exchanged with *csgA* containing a C-terminal 6x-His-Tag. Similarly, a point mutation was introduced into the promoter of *csgD* to generate a curli overexpression strain [64]. For transcriptional reporter fusions, *mKate2*, encoding the fluorescent protein mKate2, was inserted into the native locus of the promoter of interest, thereby extending the native operon or creating an artificial operon. Ectopic expression of CsgB was achieved by inserting *csgB* fused to its native promoter into the *attB* site of Δ*csgB E. coli* AR3110.

2.4.2.3 Isolation of plasmid DNA

Plasmid DNA was isolated from an overnight grown bacterial culture using the NucleoSpin Plasmid EasyPure Kit according to the protocol provided by the manufacturer (Macherey-Nagel).

2.4.2.4 Isolation of genomic DNA

Genomic DNA was isolated from overnight grown bacterial cells in liquid culture using the NucleoSpin Tissue Kit (from Macherey-Nagel). The manufacturer's protocol was followed during the isolation procedure.

2.4.2.5 Polymerase chain reaction (PCR)

For lambda red recombineering, DNA fragments were amplified using Q5 DNA polymerase (M0491L, New England BioLabs). The composition of the reaction mixture and the PCR program are listed in Table 2.2 and Table 2.3.

Table 2.2: PCR reaction mixture using Q5 DNA polymerase

Reagent	
Q5 Reaction Buffer	1x
Q5 High GC Enhancer	1x
Oligonucleotide 1	10 µM
Oligonucleotide 2	10 µM
dNTP	0.2 mM
Q5 DNA polymerase	1 U
DNA template	50 ng genomic or plasmid DNA
Total volume	50 µL

Table 2.3: PCR program using Q5 DNA polymerase

Step	Temperature (°C)	Time (min)	Cycle
Initial Denaturation	98	5	1
Denaturation	98	0.5	30
Annealing	57-60	0.5	
Elongation	72	0.5/kbp	
Final Elongation	72	10	1

Overlap extension PCR was used to join individual DNA fragments for lambda red recombineering. For this, DNA fragments were amplified from plasmid or genomic DNA using the standard Q5 polymerase protocol (Table 2.2, Table 2.3). Oligonucleotides were designed so that each DNA fragment consisted of a 5' overhang that is complementary to the end of the other DNA fragment to be joined with. Complementary regions were 20-30 bp long with a melting temperature between 57 °C

and 60 °C. After PCR purification of the individual fragments to be joined, two consecutive PCRs followed. In the first PCR, the purified DNA fragments were joined together. In the second PCR, oligonucleotides were added, which facilitated fragment amplification. The composition of the reaction mixture for the first and second PCR are listed in Table 2.4. The PCR programs are listed in Table 2.5.

Table 2.4: Overlap extension PCR: PCR reaction mixture for the first and second PCR

Reagent	first PCR	second PCR
Q5 Reaction Buffer	1x	1x
Q5 High GC Enhancer	1x	1x
dNTP	0.16 mM	0.2 mM
Q5 DNA polymerase	1 U	1 U
DNA template	1 pmol/ DNA fragment	10 µL PCR product (first PCR)
Oligonucleotide 1		10 µM
Oligonucleotide 2		10 µM
Total volume	50 µL	50 µL

Table 2.5: Overlap extension PCR: PCR program for the first and second PCR

		first PCR		second PCR	
Step	Temperature (°C)	Time (min)	Cycle	Time (min)	Cycle
Initial Denaturation	98	2	1	2	1
Denaturation	98	0.5	13	0.5	30
Annealing	57-60	0.5		0.5	
Elongation	72	0.5/kbp		0.5/kbp	
Final Elongation	72	5	1	5	1

Colony PCR was performed to verify genetic modifications after lambda red recombineering. Here, a fraction of a grown colony after transformation was used as the source of DNA for PCR. DNA fragments were amplified from the *E. coli*

AR3110 genome using DreamTaq DNA polymerase (Cat-No. EP0702, Thermo Fisher Scientific). The composition of the reaction mixture as well as the PCR program are shown in Table 2.6 and Table 2.7.

Table 2.6: PCR reaction mixture using DreamTaq DNA polymerase

Reagent	
Reaction Buffer	1x
Oligonucleotide 1	10 µM
Oligonucleotide 2	10 µM
dNTP	0.2 mM
DreamTaq DNA polymerase	0.5 U
DNA template	bacterial cells
Total volume	10 µL

Table 2.7: PCR program using Dreamtaq DNA polymerase

Step	Temperature [°C]	Time [min]	Cycle
Initial Denaturation	95	10	1
Denaturation	95	0.5	30
Annealing	57-60	0.5	
Elongation	72	1/kbp	
Final Elongation	72	5	1

2.4.2.6 Agarose gel electrophoresis

Amplification of DNA fragments was verified by agarose gel electrophoresis on a 1 % agarose gel. For visualization of DNA, 5 µL of the PCR product was mixed with 1 µL of a fluorescent DNA binding dye (N313-Kit, VWR) prior to electrophoresis. As the DNA ladder, Gene Ruler DNA Ladder Mix from Thermo Fisher Scientific (Cat-No. SM0331) was used.

2.4.2.7 Treatment of PCR products with the restriction endonuclease DpnI

When plasmid DNA was used as the template in a PCR reaction, 20 Units of the restriction endonuclease DpnI (R0176L, New England Biolabs) were added to the completed PCR reaction mixture. After incubation for one hour at 37 °C, PCR products were purified.

2.4.2.8 Purification of DNA fragments

PCR products were purified using the NucleoSpin Gel and PCR Clean-up Kit according to the protocol provided by the manufacturer (Macherey-Nagel).

2.4.2.9 DNA sequencing

DNA sequencing was performed by Eurofins Genomics. Samples containing purified PCR products or isolated plasmid DNA were prepared according to the manufacturer's protocol. Sequencing results were analysed using the software SnapGene (GSL Biotech LLC, Chicago).

2.4.2.10 Construction of fluorescent reporter T7 phages

For construction of the fluorescent reporter T7 phage, the T7® 415-1 Cloning Kit from Merck was used. The native T7 *phi10* promoter, together with the Shine-Dalgarno (SD) sequence located downstream of the phi10 promoter and the T7 tag leader sequence from *gp10* were amplified by PCR from the T7 phage genome. A second DNA fragment was generated by PCR harbouring, two *E. coli* codon-optimized *sfgfp* separated by an SD sequence. Both DNA fragments were joined by overlap extension PCR and the resulting PCR product was purified. Afterwards, the DNA fragment was treated with the restriction endonucleases HindIII and EcoRI and purified again. Subsequently, ligation of the DNA fragment with the T7® vector arms took place using a molar ratio of 3:1 (insert:vector). For the composition of the ligation mixture see the manufacturer's manual. After ligatin for 5 h at 16 °C, *in vitro* packaging of the T7 phages took place (see manufacturer's protocol). The packaging reaction mixture was added to 200 µL of exponentially growing *E. coli* AR3110 together with 5 mL 0.7 % LB agar (supplemented with 5 mM $MgSO_4$) and poured onto a 1.5 % LB agar plate. Plates were incubated at 37 °C for plaque formation. T7 phages from individual plaques were collected and resuspended in 50 µL of LB medium. These T7 phages were then used for T7 phage

amplification in liquid culture. Successful modification of wild-type T7 phages was verified by PCR and DNA sequencing. For this, 10 µL of the T7 phage lysate was heated for 10 min at 95 °C and 1 µL was then used as the template for the PCR. Q5 DNA polymerase was used for DNA amplification. Oligonucleotides were designed to hybridize upstream and downstream of the DNA fragment inserted between both T7® vector arms. The design and construction of the fluorescent reporter T7 phage was done by P.K. Singh.

2.4.3 Biofilm-Phage Interaction Assay

2.4.3.1 Generation of microfluidic flow chambers

Microfluidic flow chambers, made from polydimethylsiloxane (PDMS), were 500 µm wide, 100 µm high and 7 mm long. PDMS pieces with five independent microfluidic flow channels were bonded to glass coverslips (0.17 mm thickness) using oxygen plasma. Each microfluidic channel was connected with PTFE tubing to a syringe. The syringes were placed on a syringe pump (pico Plus, Harvard Apparatus) which maintained a constant flow rate throughout the duration of the experiments.

2.4.3.2 Biofilm growth in microfluidic chambers

Bacterial cells grown overnight were washed with 0.9 % NaCl and diluted 1:80 in 0.9 % NaCl. Subsequently, microfluidic channels were inoculated and bacterial cells were incubated for one hour at room temperature to facilitate bacterial attachment to the glass surface. Afterwards, syringes filled with tryptone broth (10 $g\,L^{-1}$) were connected with PTFE tubing to the inlets of the microfluidic channels. During assembly, the flow rate was set to 5 $\mu L\,min^{-1}$. Non-attached bacterial cells were removed by flushing the microfluidic channel with tryptone broth using a flow rate of 50 $\mu L\,min^{-1}$ for 45 s. Biofilms were grown in the presence of tryptone broth under constant flow of 0.1 $\mu L\,min^{-1}$ for a defined time at room temperature.

2.4.3.3 Biofilm-phage interaction experiments using flow chambers

For biofilm-phage interaction studies, grown *E. coli* AR3110 biofilms were exposed to phages and the interaction was monitored by fluorescence confocal microscopy. After biofilm growth for a defined time, syringes filled with T7 phages diluted in tryptone broth supplemented with 5 mM $MgSO_4$ (final concentration of 10^7 PFU mL^{-1}) were connected with PTFE tubing to microfluidic channels containing grown biofilms.

During exchange of tubings, the flow rate was set to 1 µL min^{-1}. Immediately afterwards, the flow rate was decreased to 0.1 µL min^{-1}. Grown biofilms were exposed to a constant flow of phages for 12 h at room temperature. During phage exposure, fluorescence images were taken using a confocal microsocpe.

When T5 phages were used for biofilm interaction studies, syringes were filled with T5 phages diluted in tryptone broth (supplemented with 0.1 mM $CaCl_2$) to a final concentration of 10^9 PFU mL^{-1}.

2.4.3.4 Visualization of curli fibers in biofilms

The presence of curli fibers in biofilms was visualized by immnofluorescence staining. Grown biofilms, formed by *E. coli* AR3110 cells expressing CsgA with a C-terminal 6x-His-Tag, were incubated with anti-6x-His-Tag antibodies conjugated to Alexa Fluor for one hour prior, as well as during, confocal imaging. For this, syringes filled with antibodies diluted in tryptone broth (final concentration 0.4 µg mL^{-1}) were connected with PTFE tubing to the microfluidic channels containing grown biofilms. During insertion of the tubing the flow rate was set to 1 µL min^{-1}. Afterwards it was decreased to 0.1 µL min^{-1}.

2.4.3.5 Exposure of planktonic *E. coli* AR3110 cells to bacteriophages

E. coli AR3110 cells expressing CsgA-6x-His-Tag were grown in LB medium for 5 h at 37 °C and 250 rpm. Bacterial cells were back-diluted (1:100) in tryptone broth and re-grown overnight for curli fiber production at 28 °C and 250 rpm shaking. The next day, 50 µL of the bacterial suspension was incubated with anti-6x-His-Tag antibodies conjugated to Alexa Fluor (final concentration 0.8 µg mL^{-1}) for 1 h under constant shaking at room temperature. Afterwards, bacteria were introduced into microfluidic channels and allowed to attach to the poly-L-lysine coated glass surface for 30 min. Syringes filled with T7 phages (final concentration 10^8 PFU mL^{-1}) and 0.2 µg mL^{-1} anti-6x-His-Tag antibodies conjugated to Alexa Fluor (both diluted in tryptone broth) were connected with PTFE tubing to the mircrofluidic channels. The flow rate was set to 0.1 µL min^{-1}. Throughout the exposure of single cells to phages at room temperature, fluorescence images were taken using a confocal microscope.

2.4.3.6 Expression and purification of the curli monomer CsgA

The curli monomer CsgA was purified by affinity chromatography from an *E. coli* Rosetta DE3 lysate. For this, a plasmid was constructed based on the expression vector pET-24d (Novagen). The plasmid was designed such that *csgA* is located immediately upstream of the 6-His-Tag sequence. This ensured that *E. coli* produced CsgA with a C-terminal 6x-His-Tag. First, *csgA* from *E. coli* AR3110 (without the sequence coding for the N-terminal secretion signal and the stop codon) was amplified by PCR. In addition, the backbone of the plasmid pET-24d was amplified by an inverse PCR using oligonucleotides that hybridize upstream of the T7 Tag coding sequence and downstream of the multiple cloning site (located between the T7 Tag and His Tag coding sequence). Both DNA fragments were then joined by overlap extension PCR. The PCR product was purified and the ends of the DNA fragment were phosphorylated for the subsequent DNA ligation. For phosphorylation, 17 µL of the purified PCR product was mixed with 2 µL 10x T4 DNA Ligase buffer (Cat- No.B0202S, New England Biolabs) and 1 µL T4 Polynucleotide Kinase (Cat-No. M0201L, New England Biolabs). After 30 min of incubation at 37 °C, 1 µL T4 DNA Ligase (Cat-No. M0202L, New England Biolabs) was added to the reaction mixture and ligation followed for 1 h at room temperature. The ligation mixture was transformed into chemically competent *E. coli* Top10 by heat shock transformation. Transformants were screened by colony PCR and successful plasmid construction was verified by DNA sequencing. Finally, chemically competent *E. coli* Rosetta DE3 was transformed with pET-24d harbouring *csgA*.

For protein expression and purification of CsgA, the protocol published by Zhou *et al.* [114] was followed with minor exceptions. *E. coli* Rosetta DE3 cells harbouring the CsgA expression plasmid were grown overnight at 37 °C in 5 mL LB medium supplemented with antibiotics. The next day, the overnight culture was diluted 1:500 into 200 mL of fresh medium. Furthermore lactose was added to a final concentration of 0.05 % for induction of protein expression. Bacteria were grown overnight at 18 °C before they were harvested for 20 min at 5000 g. The pellet was resuspended in 20 mL of 8 M guanidine hydrochloride with continuous stirring for 1 h at room temperature. Centrifugation of the cell lysate for 20 min at 4 °C and 10,000 g as well as sonication of the supernatant followed. Proteins were purified from the bacterial lysate using a Protino Ni-TED 2000 Column (Macherey-Nagel). First, the column was equilibrated with 4 mL KPi buffer [114]. Next, the sonicated supernatant was loaded onto the column. The column was washed in four steps

- twice with 3 mL of KPi buffer and then twice with 3 mL of 10 mM imidazone in KPi buffer. Finally, CsgA with a C-terminal 6x-His-Tag was eluted in 7 mL of 125 mM imidazole in KPi. Eluates were collected in 1 mL fractions and stored on ice immediately. Successful protein purification was verified by Western Blotting. First, eluted proteins were separated by a discontinuous sodium dodecyl sulfate polyacrylamide gel electrophoresis (SDS-PAGE) according to Laemmli [115]. For this, a 4 % stacking gel and 12 % resolving gel were used. Afterwards, the proteins were transferred from the gel onto a nitrocellulose membrane by semi-dry blotting and detection of proteins was realized by immunofluorescence staining. The membrane was treated with 5 % non-fat dry milk in TBS-T to block unspecific binding before incubation with anti-6x-His-Tag antibodies conjugated to Alexa Fluor 488 and their detection followed.

Purified CsgA was stored at 4 °C. After one week of incubation at 4 °C, elution fractions appeared to contain *in vitro* polymerized fibers (visible by eye).

2.4.3.7 Interaction of phages with artificial biofilms

For biofilm construction *in vitro*, bacterial cells were represented by fluorescent microspheres of 0.5 µm or 1 µm in diameter and curli fibers were used as the exclusive biofilm matrix component. First, colloidal particles together with *in vitro* polymerized curli fibers were co-incubated under constant shaking for 1 h at room temperature in order to embed microspheres in the curli fiber network. Simultaneously, curli fibers were stained with congo red (final concentration 40 µg mL^{-1}) in the presence of 1 % BSA for fluorescence imaging. Subsequently, a syringe was loaded with the bead-curli fiber mixture and connected with PTFE tubing to microfluidic channels. The mixture was introduced into the channels with a flow rate of 1 µL min^{-1} for 1.5 h. Numerous pillars regularly arranged in decreasing distances from each other were present inside the channels. Additionally, the glass surface of microfluidic channels was coated with poly-L-lysine to facilitate surface attachment of the artificial biofilms. The surface treatment and presence of pillars ensured that the biofilms were not washed out of the microfluidic channel. Artificial biofilms were exposed to T7 phages labelled with Alexa FLuor 488 (final concentration 10^8 PFU mL^{-1}) under constant flow (1 µL min^{-1}) for one hour before fluorescence images were acquired with a confocal microscope.

As a control, clusters made of fluorescent microspheres alone (matrix-free biofilms)

were exposed to fluorescently labelled T7 phages. Here, microspheres suspended in PBS with 1 % BSA were pelleted at 8000 rpm for 5 min. Subsequently, fractions of the pellet were introduced into microfluidic channels and the clusters were allowed to attach to the poly-L-lysine coated glass surface for 30 min. Afterwards, microfluidic channles were connected to syringes filled with fluorescently labelled T7 phages (final concentration 10^8 PFU mL^{-1}). Phages passed through the channels under a constant flow of 1 µL min^{-1} for one hour, before fluorescence imaging with a confocal microscope took place.

In a second control experiment, *in vitro* polymerized curli fibers were exposed to fluorescently labelled T7 phages. For this, curli fibers were stained with congo red (final concentration 40 µg mL^{-1}) for one hour at room temperature under constant shaking. Afterwards, a syringe was filled with the stained curli fibers and connected with PTFE tubing to microfluidic channels containing a poly-L-lysine coated glass surfaces. Numerous pillars arranged in decreasing distances were present inside the microfluidic channels to ensure that the polymerized curli fibers were not washed out during constant flow. Curli fibers were introduced into the microfluidic channels for 1.5 h with a flow rate of 1 µL min^{-1}. Subsequently, these microfluidic channels were connected to fresh syringes filled with fluorescently labelled T7 phages (final concentration 10^8 PFU mL^{-1}). Phages were introduced into the channels for one hour under constant flow (1 µL min^{-1}) before fluorescence images were taken using a confocal microscope.

2.4.3.8 Fixation and staining of *E. coli* AR3110 biofilms

To analyze the architecture of *E. coli* AR3110 biofilms, it was necessary to fix and stain the biofilms. For fixation, syringes filled with 4 % paraformaldehyde (in PBS) were connected with PTFE tubing to microfluidic channels containing grown biofilms. Under constant flow (0.5 µL min^{-1}) biofilms were fixed for 5 h at room temperature before staining with 10 µM Syto9 (Cat-No. S34854, Thermo Fischer Scientific) in PBS followed. During staining for 5 h at room temperature, syringes filled with the fluorescent dye as well as the microfluidic channels were protected from light.

2.4.4 Microscopy and Image Analysis

2.4.4.1 Confocal laser scanning microscopy

Fluorescence images to study the susceptibility of wild type as well as matrix mutant biofilms to phages were acquired with a Yokogawa CSU confocal spinning disk unit mounted on a Nikon Ti-E inverted microscope using a Nikon 100x oil objective with 1.45 NA. Fluorescent proteins (sfGFP and mRuby2) were excited with 488 nm and 552 nm lasers, respectively, and emission was detected with an Andor iXon electron-multiplying charge-coupled device (EMCCD) camera. During confocal imaging a 488/552/594 nm dichroic filter as well as 525/50 and 650/150 emission filters were used. For biofilms up to an age of 48 h, images were acquired every 30 min for 12 h with a step size of 0.4 µm in the z-direction. In case of older biofilms, the time intervall was set to 1 h. During single-cell resolution imaging for biofilm architecture analyses, an additional 2x lens was placed between the spinning disk unit and the Nikon Ti-E side port. Furthermore, the step size in the z-direction was changed to 0.2 µm.

When curli fibers and fluorescently labelled phages were visualized together with biofilms or transcriptional activity of genes was monitored during biofilm growth, fluorescent images were acquired with an inverted Zeiss Axio Observer Laser Scanning Microscope (LSM) 880 using a Plan-Apochromat 63x oil objective with 1.4 NA. Images were acquired every 30 min or 60 min according to the biofilm age, as described above. The step-size in z-direction was 0.4 µm.

2.4.4.2 Scanning electron microscopy

Scanning electron microsocopy was applied to visualize curli fiber networks around bacterial cells or as part of the biofilm matrix in artifical biofilms. Additionally,co-localization of T7 phages with curli fibers was imaged with an scanning electron microscope.

In order to visualize bacterial cells naturally surrounded by a curli fiber network, *E. coli* AR3110 was grown for 5 h at 37 °C and 250 rpm shaking. Afterwards, bacteria were back-diluted 1:100 in tryptone broth and grown overnight at 28 °C and 250 rpm shaking. The next day, 50 µL of the bacterial culture was spotted onto a poly-L-lysine coated glass slide (thickness 0.17 mm). Cells were allowed to attach to the glass surface for 1 h at room temperature, fixed by placing the glass slide

into a 4 % paraformaldehyde solution for 5 min and washed three times in H_2O (5 min each). Subsequently, samples were dehydrated in a graded ethanol series. Here, glass slides were placed in solutions with an increasing ethanol concentration (30 %, 50 %, 70 %, 90 %, 100 %) for 5 min each. Samples were dried by critical point drying, sputter coated with platinum for 90 s followed by imaging with a JEOL JSM-7500F scanning electron microscope. The microscope was operated at 10 kV. Images were analysed using ImageJ.

For scanning electron microscopy of artifical biofilms, biofilms were constructed as described previously (Chapter 2.4.3.7). Afterwards, they were deposited onto a poly-L-lysine coated glass slide and processed further.

Visualization of T7 phages bound to curli fibers involved incubation of phages together with *in vitro* polymerized fibers for 1 h under constant shaking. Afterwards, unbound phages were removed by centrifugation for 3 min at 13,000 rpm. In addition, curli fibers were washed once with PBS, prior to transferring them onto a poly-L-lysine coated glass slide and preparing for electron microscopy.

2.4.4.3 Data analysis

Initially, floating cells, that were not associated with a biofilm, were discarded from the z-stack using median filtering. After denoising by 3D-convolution with an averaging kernel and Top-hat filtering of out-of-focus fluorescence, bacterial cells were detected three-dimensionally by a 3D Laplacian-of-Gaussian edge detection algorithm. Subsequently, k-means clustering and/or watershedding was used to separate clumped structures into individual cells. Temporal differences in bacterial biomass were quantified using the volume fraction of bacterial cells, normalized to the biomass at the time, t_0, of phage addition.

Spatiotemporal transcription dynamics during biofilm growth were analyzed by tracking both the projected biofilm height and mKate2 fluorescence intensity along z-direction for different biofilm ages.

The cell density inside grown biofilms was analyzed by placing a sphere with 3 µm in diameter around each individual biofilm-associated bacterial cell. Afterwards the fraction of the occupied area inside the sphere by neighbouring cells was calculated. The analysis code was written in MATLAB (MathWorks) by R. Hartmann

and is described in more detail in [103].

3 Interaction dynamics of *Vibrio cholerae* with macrophages

3.1 Introduction

3.1.1 *Vibrio cholerae* surface colonization

Vibrio cholerae is a facultative pathogenic Gram-negative bacterium that lives in aquatic environments [116]. There, *V. cholerae* forms biofilms on zooplankton and phytoplankton [117, 118]. Chitin, found in the exoskeleton of zooplankton, can be utilized by *V. cholerae* as a carbon source. In addition, growth on chitin has been shown to induce natural competence [119, 120]. Pathogenic strains of *V. cholerae* can invade the human host through oral ingestion of contaminated water, form biofilms on epithelial cells in the intestine and cause the diarrheal cholera disease [121]. The virulence factors required for the cholera disease are encoded by the CTX prophage [122].

Studying *V. cholerae* biofilm formation on a glass surface *in vitro* revealed that the bacterium uses the polar flagellum together with mannose-sensitive hemagglutinin (MSHA) pili to scan the surface, before attachment occurs [15]. Following attachment, bacteria form a three-dimensional structure. Biofilm formation is controlled by quorum sensing, a bacterial system for cell-cell-communication that enables collective behaviour [123, 124]. The *V. cholerae* biofilm matrix constituents are vibrio polysaccharide (VPS) and three proteins (RbmA, RbmC, Bap1). Bap1 is responsible for surface adhesion of the growing biofilm. In contrast, RbmA localizes throughout the biofilm and connects cells to each other. A mix of RbmC, Bap1 and VPS forms an envelope that surrounds cell clusters inside the biofilms. Production of matrix is essential for biofilm formation on a glass surface. Bacteria impaired in VPS or matrix protein production are not able to establish a three-dimensional structure [13, 125]. Dispersal, the last step in biofilm development, is triggered by a combination of the general stress response (RpoS) and local bacte-

rial cell densities (via quorum sensing) [11].

Microscopic analysis of intestines after infection with *V. cholerae* and the investigation of stool samples of patients confirms *V. cholerae* biofilm formation inside the human host [126, 127]. Once *V. cholerae* penetrates the mucus layer and reaches the epithelium, the bacterium attaches to the epithelial cells via adhesins present on the bacterial surface and forms biofilms [126, 128]. Colonization seems to be dependent on the production of the biofilm matrix components RbmA and VPS [129]. Furthermore, biofilm formation requires the production of toxin-coregulated pili (TCP) [130, 131]. The exact mechanism of biofilm formation in the human intestine and the composition of the biofilm matrix are still unclear.

3.1.2 Mannose-sensitive hemagglutinin and toxin-coregulated pili

Mannose-sensitive hemagglutinin (MSHA) pili are produced by *V. cholerae* strains of the El Tor biotype [132, 133]. The structural subunit of those type IV pili is the protein MshA [134]. MSHA pili facilitate attachment of *V. cholerae* not only to zooplankton but also to glass surfaces [15, 135]. For glass surfaces it has been show, that MSHA pili together with the polar flagellum promote surface scanning, before attachment occurs [15]. Colonization of the intestine is however independent of MSHA pili [136, 137].

In contrast, toxin-coregulated pili (TCP) facilitate attachment of *V. cholerae* to epithelial cells in the intestine and mediate interactions between bacterial cells. Furthermore, in biofilms formed on epithelial cells, the bacteria are encapsulated in a matrix made out of toxin-coregulated pili [131, 138]. Toxin-coregulated pili are encoded by the *tcp* operon and TcpA is the major subunit of the pilus [139]. Expression of TCP but also cholera toxin is modulated by quorum sensing. At low cell densities, TcpPH together with ToxRS activate the transcription of *toxT*. And ToxT in turn is the transcriptional activator for the expression of virulence factors including TCP and cholera toxin [140–142].

3.1.3 Macrophages - immune cells with phagocytic activity

The innate immune system includes phagocytic cells such as neutrophils and macrophages in order to eliminate invading bacteria [143]. The human body is

comprised of tissue-resident macrophages as well as moncyte-derived macropages [144]. Tissue-resident macrophages can recognize invading microoragnisms by different types of receptors and induce an inflammatory response. As a result, neutrophils and monocytes are recruited from the blood to the site of inflammation. Upon recruitment into tissues, monocytes can differentiate into macrophages [145–149].

After recognition by macrophages, the invading organism is internalized by macrophages and a phagosome is formed which matures into a phagolysosome. Phagolysosomes are characterized by low pH, the presence of reactive oxygen species as well as peptidases and hydrolases, all of which contribute to degradation of the invading mircoorganism [150]. In order to survive in the presence of macrophages, bacteria have developed different strategies. Those can include survival in the presence of low pH, interference with phagosome maturation or counteracting macrophage-derived degrading enzymes [151–154]. In addition to single cell protection mechanisms, bacteria can evade phagocytosis by the formation of biofilms [155, 156].

3.2 Results

Invasion by pathogenic bacteria can be a threat to the human body. Bacteria are able to colonize human tissues and cause serious diseases. To protect the human body from invading organisms, the immune system is comprised of phagocytes, such as neutrophils or macrophages. However, bacteria can develop mechanisms to evade destruction by phagocytes [143, 151–154]. To uncover the mechanism of how pathogenic bacteria accomplish a stable co-existence with immune cells, the interaction between macrophages and the biofilm-forming bacterial species *Vibrio cholerae* was investigated.

The results described in this chapter have not been published. Bacterial strain construction and the experimentation was carried out by myself. K. Raveendran was involved in strain construction. H. Jeckel created custom scripts for image analysis in MATLAB. K. Drescher initiated the project.

3.2.1 Interaction dynamics of *V. cholerae* with human macrophages

In order to study bacterial interactions with immune cells, *V. cholerae* cells were incubated with human macrophages (derived from THP-1 monocytes) and the interaction was monitored by fluorescence confocal mircoscopy. *V. cholerae* constitutively expressed sfGFP and macrophages were visualized by staining with CellTracker Red CMPTX (Cat-No. C34552, Thermo Fisher Scientific). As macrophages are recognized by their ability to phagocytize bacterial cells, ingestion of bacteria by the immune cells was expected to be observed during the *V. cholerae*-macrophage interaction. However, during co-incubation for 7 h, phagocytosis of bacteria by the macrophages could not be detected. Instead, *V. cholerae* encircled the macrophages, exhibiting biofilm dynamics on the macrophage surface (Figure 3.1). The progression of *V. cholerae* propagation on the surface of macrophages was comprised of three stages, as generally seen during the formation of biofilms. In the first stage, *V. cholerae* cells attached to the surface of human macrophages. The second stage included the development of a biofilm on the macrophage surface. Termination of the interaction by biofilm dispersal represented the third stage. This time period was accompanied by cell death of the macrophages. Identification of these stages occurred by visual examination of the acquired microscopy images. For further characterization, the amount of bacteria

surrounding the macrophages was quantified by image analysis. For every imaged time point, the accumulation of bacterial biomass in direct vicinity of the macrophage surface was measured. The attached biomass was normalized by the amount of non-attached bacterial biomass. Quantification of this phenotype showed initially an increase in bacterial biomass attached to the bacterial surface. When biofilm dispersal occurred, a reduction in attached biomass could be observed (Figure 3.1).

V. cholerae also showed biofilm formation on the surface of macrophages that evolved from human blood monocytes (Figure 3.1, Figure S1). The formation of biofilms on the surface of macrophages derived from different origins reflects the versatility of this interaction between bacteria and immune cells.

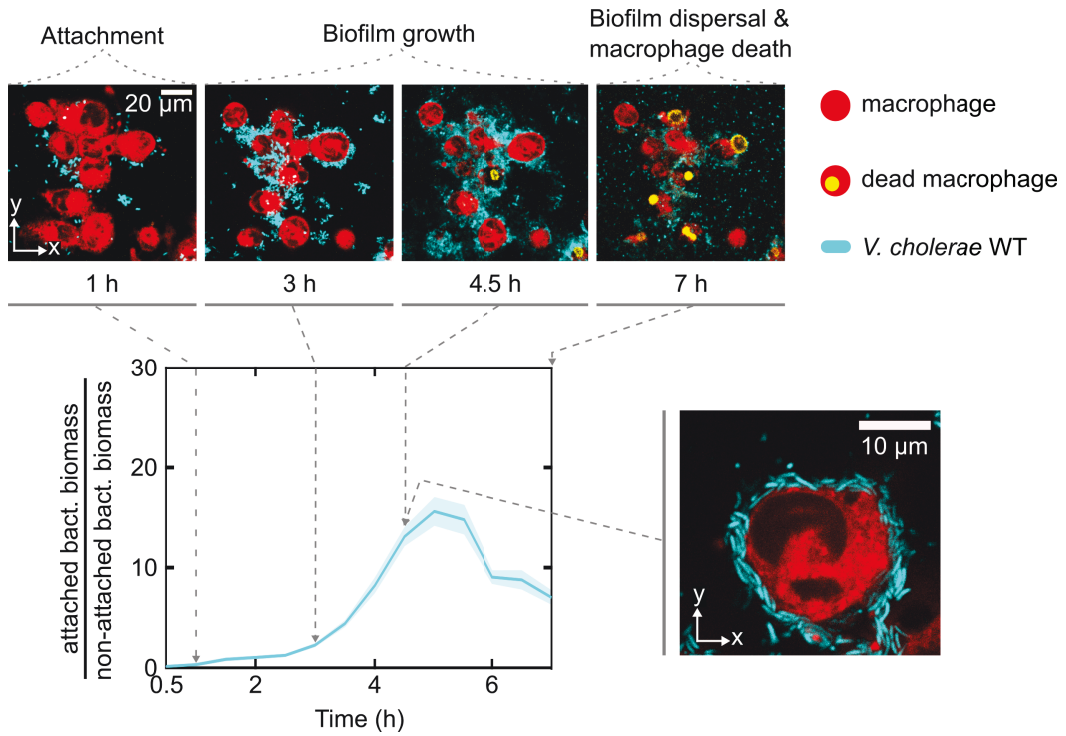

Figure 3.1: Temporal dynamics of the interaction between *V. cholerae* and human macrophages. After initial attachment, *V. cholerae* formed a few cell layers thick biofilm on the surface of human macrophages (derived from THP-1 monocytes). Termination of the interaction process by the dispersal of biofilms was accompanied by macrophage cell death. Representative images in xy-plane show the progression of the *V. cholerae*-macrophage interaction. The plotted line represents the mean bacterial biomass attached to macrophages normalized by the biomass of non-attached bacteria. The shaded area denotes the standard error of the mean (n=31).

The attachment of *V. cholerae* was examined with respect to its surface specificity.

It was tested if bacterial attachment is limited to the surface of macrophages or if it can also occur in the presence of macrophage-precursor cells (monocytes). When *V. cholerae* was co-incubated with THP-1 monocytes for 1 h, bacterial attachment to the monocytes was attenuated (Figure 3.2 a). Thus, the difference in attachment between macrophages and their precursor cells indicates selectivity in the bacterial interaction with immune cells.

Next, it was tested if bacterial biofilm formation depends on the number of macrophages or the initial bacterial cell count. Varying the total number of both cell types revealed that the initial bacterial cell count, but not the the number of macrophages, plays a crucial role in the establishment of a bacteria-macrophage interaction. By lowering the bacterial count, accumulation of bacterial biomass around macrophages and subsequently, biofilm dispersal, was delayed in time or did not occur at all during co-incubation for 7 h (Figure 3.2 b). Conversely, increasing the bacterial count resulted in faster progression of biofilm formation. Changing the number of macrophages in the interaction assay did not affect the *V. cholerae*-macrophage interaction process.

In conclusion, the interaction between *V. cholerae* and macrophages involves the development of bacterial biofilms on a biotic surface. The interaction is characterized by three stages: bacterial attachment, biofilm formation and dispersal of biofilms. The final stage was also accompanied by macrophage cell death. Bacterial attachment to immune cells is specific to macrophages, regardless of their origin. The pace of the interaction process is determined only by the initial bacterial count introduced into the system. In this study, the first two stages of the interaction were investigated to uncover how *V. cholerae* attaches to and forms biofilms on the surface of macrophages.

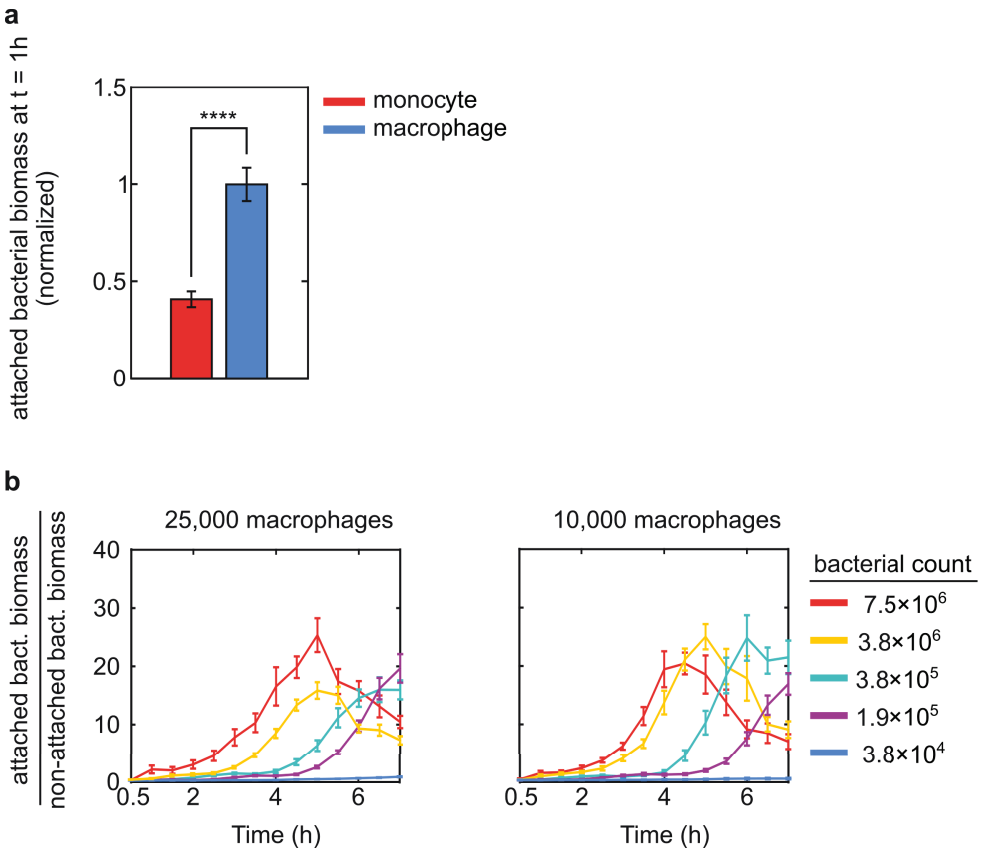

Figure 3.2: *V. cholerae* selectively attaches to human macrophages and temporal dynamics of biofilm formation depend on the initial bacterial cell count. (a) During co-incubation, *V. cholerae* attached to macrophages (derived from THP-1 monocytes). In contrast, attachment was significantly decreased in the presence of THP-1 monocytes. Bars represent the mean bacterial biomass attached to immune cells after one hour of co-incubation, normalized to the macrophage interaction. Errorbars represent the standard error of the mean ($n_{macrophage}$=31; $n_{monocyte}$=8). Statistical significance was calculated using an unpaired t-test (**** p<0.0001). (b) By reducing the bacterial cell count for a given number of macrophages, the formation and dispersal of biofilms around macrophages was delayed or did not occur at all, regardless of the total number of macrophages present. Plotted lines represent the mean bacterial biomass attached to macrophages normalized by the biomass of non-attached cells. Error bars represent the standard error of the mean (n>3).

3.2.2 Flagella and MSHA pili initiate attachment of *V. cholerae* to human macrophages

Initiation of the *V. cholerae*-macrophage interaction requires bacterial attachment to the macrophage surface. Various structures and proteins present in *V. cholerae* have been described to facilitate bacterial attachment to mammalian cells [128]. To test their involvement in the attachment to macrophages, deletion mutants

were constructed, thereby removing one of these components from the bacterial surface: toxin-coregulated pilus (TCP, Δ*tcpA*), mannose-sensitive hemagglutinin (MSHA) pilus (Δ*mshA*), flagellum-regulated hemagglutinin (Δ*frhC*), GbpA (Δ*gbpA*), Mam7 (Δ*mam7*) or the polar flagellum (Δ*flaA*). After one hour of coincubation with macrophages (derived from THP-1 monocytes), *V. cholerae* cells lacking flagellum-regulated hemagglutinin, GbpA, Mam7 or TCP were able to attach to the macrophage surface, similar to the wild type (Figure 3.3). Only bacteria deficient in flagellum (Δ*flaA*) or MSHA pili (Δ*mshA*) biogenesis were impaired in macrophage attachment (Figure 3.3). Ectopic expression of *flaA* or *mshA*, under control of the native promoter, in the corresponding deletion mutant successfully restored the ability for attachment, as seen for wild-type bacteria (Figure 3.3). Similar results were obtained in interaction studies using macrophages derived from human blood monocytes (Figure S2). In conclusion, the polar flagellum, together with MSHA pili, is required for attachment of *V. cholerae* to the macrophage surface.

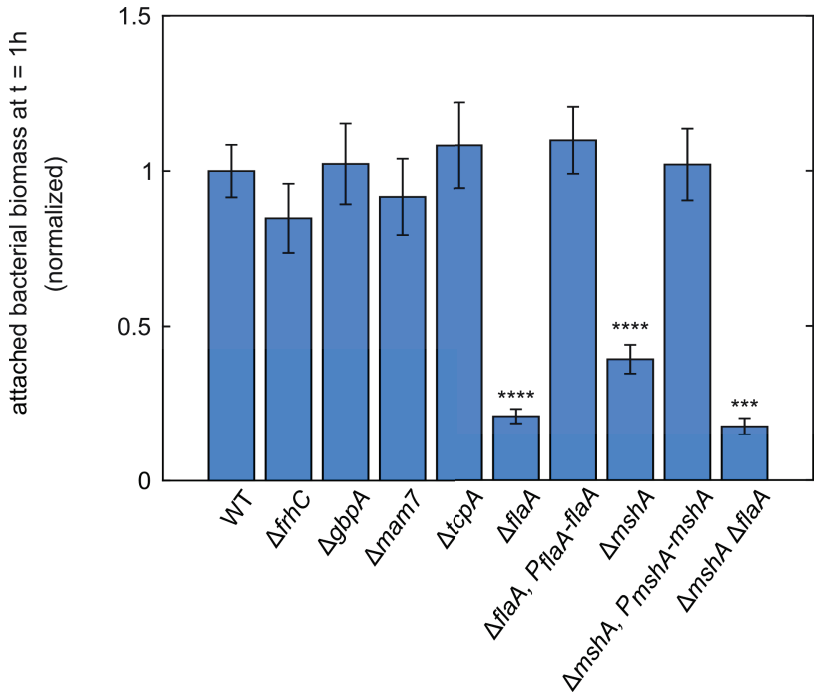

Figure 3.3: Flagella and MSHA pili facilitate attachment of *V. cholerae* to macrophages. Macrophages (derived from THP-1 monocytes) were exposed to *V. cholerae* lacking components known to facilitate surface attachment. After co-incubation for one hour, mutants lacking flagellum-regulated hemagglutinin (Δ*frhC*), GbpA (Δ*gbpA*), Mam7 (Δ*mam7*) or TCP (Δ*tcpA*) showed attachment similar to wild-type bacteria. *V. cholerae* deficient in assembly of the polar flagellum (Δ*flaA*) or MSHA pili (Δ*mshA*) showed impaired attachment to the macrophage surface. Ectopic expression of *flaA* or *mshA*, under control of the native promoter, successfully restored attachment to macrophages. Bars represent the mean bacterial biomass attached to the macrophage surface after one hour of co-incubation, normalized to the wild type. Error bars denote the standard error of the mean (n_{WT}=31; $n_{\Delta frhC}$=6; $n_{\Delta gbpA}$=6; $n_{\Delta mam7}$=6; $n_{\Delta tcpA}$=12; $n_{\Delta flaA}$=5; $n_{\Delta flaA,\ P_{flaA}\text{-}flaA}$=3; $n_{\Delta mshA}$=11; $n_{\Delta mshA,\ P_{mshA}\text{-}mshA}$=7; $n_{\Delta mshA\ \Delta flaA}$=4). Statistical analysis using a one-way ANOVA, with Bonferroni's correction for multiple comparisons, confirmed significant differences in attachment between the wild type and Δ*flaA*, Δ*mshA* as well as Δ*mshA*Δ*flaA* (**** p<0.0001; *** p<0.01; ns, not significant).

3.2.3 Production of toxin-coregulated pili by *V. cholerae* facilitates late attachment to macrophages

V. cholerae lacking MSHA pili or the polar flagellum was impaired in attachment to macrophages during the first hour of co-incubation. However, approximately 4 h after the initial exposure, accumulation of Δ*mshA* cells could be observed (Figure 3.4 a, b). This suggested a delayed production of additional surface components, that could compensate for the loss of MSHA pili and restore

the ability for macrophage attachment. Flagella appeared to be crucial for surface attachment, as Δ*flaA* did not show delayed attachment (Figure 3.4 a). To understand how *V. cholerae* accomplished attachment in the absence of MSHA pili, previously tested bacterial surface components were examined once more for their engagement in delayed attachment. For this, deletion mutants were constructed using Δ*mshA* as the background strain. During exposure to macrophages, Δ*mshA*Δ*frhC*Δ*gbpA*Δ*mam7* cells showed the same attachment pattern, as seen for the single deletion mutant Δ*mshA* (Figure 3.4 a). Thus, flagellum-regulated hemagglutinin, GbpA as well as Mam7 do not contribute to attachment in the absence of MSHA pili. In contrast, the removal of TCP in Δ*mshA* cells was sufficient to prevent attachment of *V. cholerae* (Figure 3.4 a,b). This suggests that in the absence of MSHA pili, *V. cholerae* uses TCP, together with the flagellum, to facilitate attachment to human macrophages. Similar results could be observed with macrophages that were derived from human blood monocytes (Figure S4 a).

TCP-mediated delayed attachment suggests that *V. cholerae* does not produce TCP from the beginning of co-incubation with macrophages. To test if the production of TCP temporally coincides with bacterial attachment to macrophages, a strain with inducible TCP production was constructed. This was indirectly achieved by overexpression of ToxT, which is required for the transcription of *tcpA* and adequate pilus assembly [157]. Here, *toxT* was fused to the arabinose inducible promoter P_{BAD}. When bacteria were grown in the presence of 0.2 % arabinose, *V. cholerae* lacking MSHA pili was able to attach to macrophages during the first hour of co-incubation (Figure 3.4 c). In the absence of arabinose, bacteria showed impaired attachment which is in agreement with the result obtained for Δ*mshA* cells (Figure 3.3). Overexpression of ToxT in Δ*mshA*Δ*tcpA* did not lead to bacterial attachment. Similar results were obtained with macrophages that were derived from human blood monocytes (Figure S4 b). Thus, overproduction of TCP shifted the TCP-mediated bacterial attachment to an earlier time point during exposure to macrophages.

Together, the results reveal dynamics in pili formation on the bacterial surface. In the absence of MSHA pili, the production of TCP restores the capability of bacteria to attach to the macrophage.

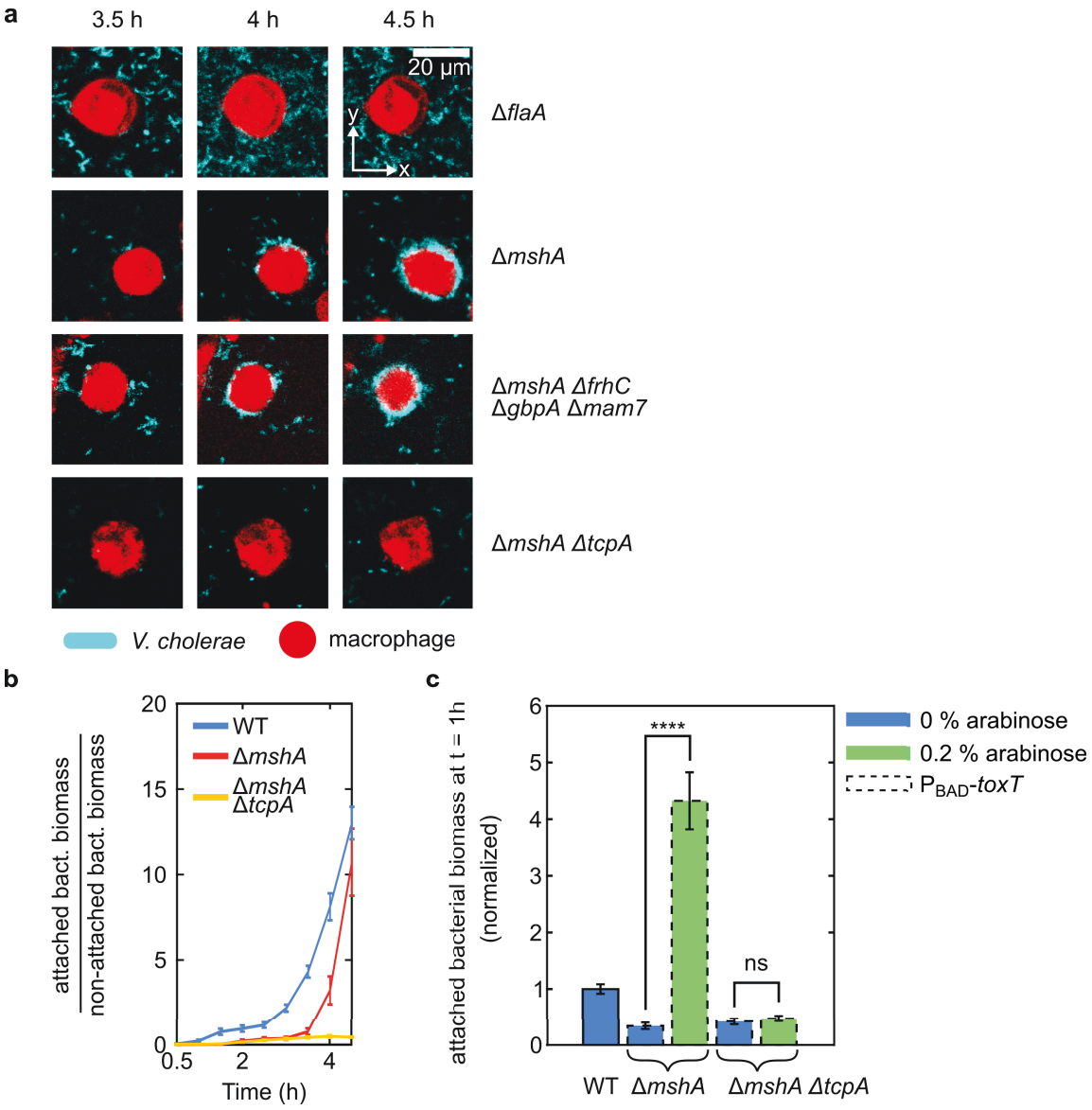

Figure 3.4: Production of toxin-coregulated pili facilitates bacterial attachment in the absence of MSHA pili. (a)+(b) *V. cholerae* impaired in MSHA pili biogenesis (Δ*mshA*) adhered to human macrophages (derived from THP-1 monocytes) approximately 4 h after the start of the co-incubation. Attachment required the polar flagellum, as Δ*flaA* cells did not adhere. Furthermore, attachment was independent of flagellum-regulated hemagglutinin (Δ*frhC*) , GbpA (Δ*gbpA*) and Mam7 (Δ*mam7*). In contrast, removal of TCP (Δ*tcpA*) together with MSHA pili (Δ*mshA*) impaired attachment to the macrophage surface. Representative images in xy-direction show bacterial accumulation around macrophages. Plotted lines represent the mean attached bacterial biomass normalized by non-attached biomass. Errorbars denote the standard error of the mean (n_{WT}=31; $n_{\Delta mshA}$=11; $n_{\Delta mshA\ \Delta tcpA}$=4). (c) Overexpression of *toxT* under control of the arabinose inducible promoter pBAD enabled bacteria for TCP-mediated attachment during the first hour of co-incubation. Bars represent the mean bacterial biomass attached to macrophages after one hour of co-incubation, normalized to the interaction with wild-type bacteria. Error bars denote the standard error of the mean ($n_{\Delta mshA,\ 0\,\%}$=4; $n_{\Delta mshA,\ 0.2\,\%}$=5; $n_{\Delta mshA\ \Delta tcpA,\ 0\,\%}$ =5; $n_{\Delta mshA\ \Delta tcpA,\ 0.2\,\%}$ =5). Statistical significance was calculated using an unpaired t-test (**** $p<0.0001$; ns, not significant).

3.2.4 Bacterial biofilm formation on the surface of human macrophages

The second stage of the interaction process involves the formation of biofilms on the surface of macrophages. Biofilms are identified by the presence of a self-produced matrix, that encapsulates the bacterial cells [8]. In order to characterize the biofilms formed on the macrophage surface, the composition of the matrix was investigated.

The role of the major matrix components and their local distribution has been largely described for *V. cholerae* biofilms grown on a glass surface [13, 125]. The *V. cholerae* biofilm matrix constitutes three proteins (RbmA, RbmC and Bap1) and vibrio polysaccharide (VPS). To determine if these components are important for biofilm growth on the macrophage surface, a deletion mutant impaired in production of all four components (Δ*rbmA* Δ*rbmC* Δ*bap1* Δ*vpsL*) was constructed. Upon exposure to macrophages (derived from THP-1 monocytes), *V. cholerae* was still able to form biofilms on the surface of macrophages (Figure 3.5). Surprisingly, the biofilms appeared thicker and were comprised of 2.5 times more biomass as the ones formed by wild-type bacteria (Figure S3 a). To explain the enhanced biofilm formation phenotype of Δ*rbmA* Δ*rbmC* Δ*bap1* Δ*vpsL* cells, bacterial colonization of the 96-well glass bottom plate, used for interaction studies, was investigated, since these components are crucial for colonization of abiotic surfaces. Specifically, areas not occupied by resident macrophages were analysed for colonization and biofilm formation by *V. cholerae*. As compared to wild-type bacteria, approximately three times less bacterial biomass was present in macrophage-free areas when Δ*rbmA* Δ*rbmC* Δ*bap1* Δ*vpsL* bacteria were used in the interaction studies (Figure S3 b). This suggests that *V. cholerae* deficient in production of RbmA, RbmC, Bap1 and VPS is impaired in colonization of the glass surface. Thus, these bacteria are more likely to encounter macrophages, which results in attachment and enhanced bacterial biomass accumulation around the immune cells. On the other hand, wild-type bacteria are able to colonize both surfaces: macrophages, as well as, the glass surface of the 96-well plate. Accordingly, less bacterial biomass accumulates on the macrophage surface.

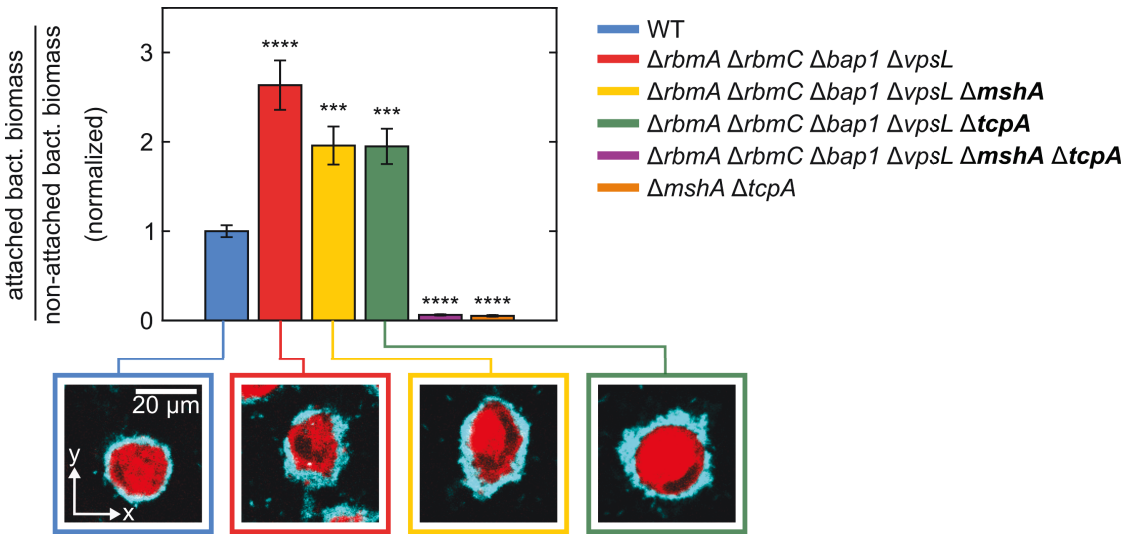

Figure 3.5: Biofilm formation on the macrophage surface depends on the production of type IV pili. *V. cholerae* cells deficient in the production of the major biofilm matrix components RbmA, RbmC, Bap1 and VPS were able to form biofilms on the surface of macrophages (THP-1 monocyte derived). Removal of only MSHA pili or TCP did not impair biofilm growth, for a strain that lacks all major biofilm matrix components. However, *V. cholerae* lacking MSHA pili and TCP was not able to form biofilms on macrophages. Loss of biofilm formation was exclusively dependent on the absence of pili and not related to the major matrix components of *V. cholerae* biofilms. Representative images in xy-planes show biofilms formed by the wild type and three biofilm matrix mutants on the surface of macrophages. Bars represent the mean ratio between bacterial biomass attached to the macrophages surface and biomass present in macrophage-free areas. Error bars denote the standard error of the mean (n_{WT}=31; $n_{\Delta rbmA\ \Delta rbmC\ \Delta bap1\ \Delta vpsL}$=5; $n_{\Delta rbmA\ \Delta rbmC\ \Delta bap1\ \Delta vpsL\ \Delta mshA}$=3; $n_{\Delta rbmA\ \Delta rbmC\ \Delta bap1\ \Delta vpsL\ \Delta tcpA}$=3; $n_{\Delta rbmA\ \Delta rbmC\ \Delta bap1\ \Delta vpsL\ \Delta mshA\ \Delta tcpA}$=5; $n_{\Delta mshA\ \Delta tcpA}$=4). Statistical significance was calculated using an one-way ANOVA with Bonferroni's correction for multiple comparisons (**** $p<0.0001$; *** $p<0.0002$).

Even though the lack of the major matrix components did not impede biofilm formation, wild-type biofilms formed on the macrophage surface still consisted of the matrix component RbmA (Figure 3.6). RbmA was visualized by immunofluorescence staining during co-incubation of macrophages (THP-1 monocyte derived) with *V. cholerae* expressing RbmA with a C-terminal 6x-His-Tag. The presence of secreted RbmA was mostly limited to regions in the outer boundary area of the biofilms. This indicates that matrix proteins are redundant in biofilms formed on macrophage surfaces.

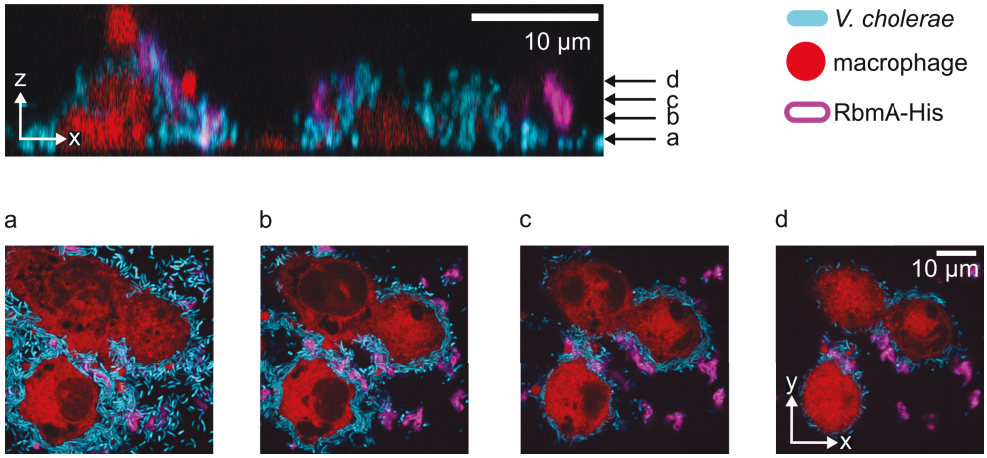

Figure 3.6: Biofilms formed on the surface of macrophages contain RbmA as part of the matrix. (a)-(d) Secreted RbmA was visualized by immunofluorescence staining during co-incubation of human macrophages (derived from THP-1 monocytes) with *V. cholerae* expressing RbmA with a C-terminal 6x-His-Tag. After 4 h of co-incubation, secreted RbmA was detected in different layers (a-d) of the biofilm. RbmA mostly localized at the outer boundary of the bacterial community.

To determine how bacteria are held together in macrophage-attached biofilms, other deletion mutants were analysed for their biofilm formation capability. As MSHA pili and TCP are present on the bacterial surface and facilitate bacterial attachment to macrophages (Figure 3.3, Figure 3.4), both pili were examined as potential components of the biofilm matrix. Bacteria deficient in MSHA pili ($\Delta mshA$) or TCP ($\Delta tcpA$) biogenesis successfully formed biofilms on the macrophage surface, regardless of the additional removal of RbmA, RbmC, Bap1 and VPS (Figure 3.5). In contrast, *V. cholerae* lacking MSHA as well as TCP in the $\Delta rbmA$ $\Delta rbmC$ $\Delta bap1$ $\Delta vpsL$ background strain were impaired in bacterial attachment and the establishment of biofilms. Identical results were obtained with bacteria lacking TCP and MSHA pili only ($\Delta mshA$ $\Delta tcpA$) (Figure 3.5). Thus, production of one type of pili - MSHA or TCP - by motile cells of *V. cholerae* is necessary and sufficient for attachment and biofilm formation on the macrophage surface during bacteria-macrophage interactions.

Investigation of biofilm dispersal further supported the hypothesis that TCP are part of the biofilm matrix and hold bacteria together. Biofilms formed by wild-type bacteria did not completely disperse; approximately 30 % of the bacterial biomass remained attached to the macrophage surface. However, when bacteria were deficient in TCP production, biofilms dispersed entirely from the macrophage

surface (Figure 3.7 a). Complete biofilm dispersal could be observed for Δ*rbmA* Δ*rbmC* Δ*bap1* Δ*vpsL* Δ*tcpA*,as well as, the Δ*tcpA* single deletion mutant. When bacteria overproduced TCP, biofilm dispersal from the bacterial surface could not be observed (Figure 3.7 b). This suggests that TCP is an integral part of the biofilm matrix of *V. cholerae* biofilms formed on the surface of macrophages.

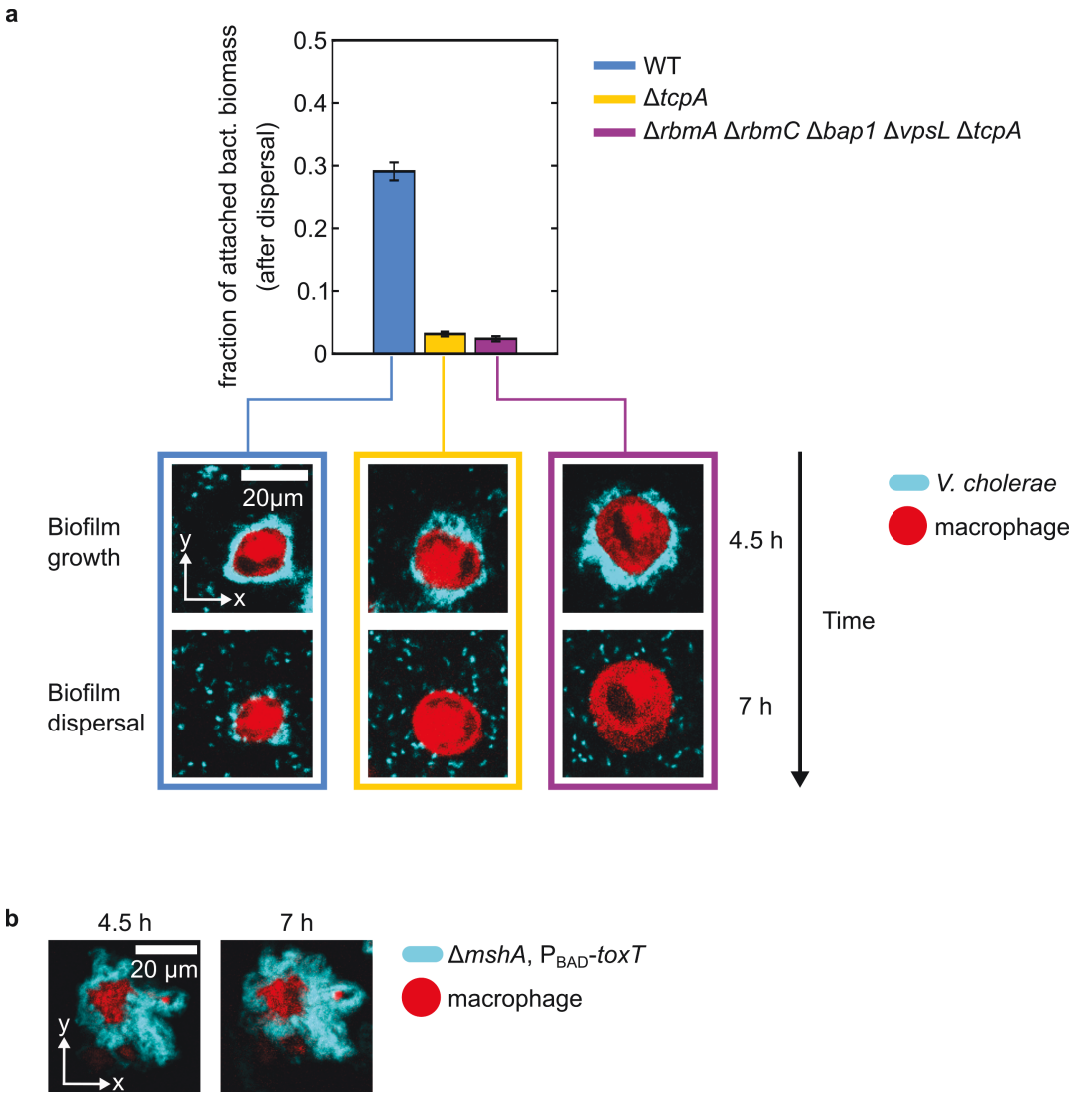

Figure 3.7: Toxin-coregulated pili are part of the biofilm matrix and prevent complete biofilm dispersal.(a) Biofilms formed by wild-type bacteria on the surface of macrophages (THP-1 derived) did not show complete dispersal: approximately 30 % of the bacterial biomass remained attached after 7 h of co-incubation. When bacteria were deficient in TCP production (Δ*tcpA*), biofilms dispersed completely. The extent of biofilm dispersal was independent of the major matrix components of *V. cholerae* biofilms (RbmA, RbmC, Bap1, VPS). Representative images in xy-plane show *V. cholerae* wild-type and mutant biofilms formed on the macrophage surface. Furthermore, the same macrophage is shown after 7 h of co-incubation, when biofilm dispersal occurred. Bars represent the mean fraction of attached bacterial biomass at 7 h after start of the co-incubation. Error bars denote the standard error of the mean (n_{WT}=31;$n_{\Delta tcpA}$=12; $n_{\Delta rbmA\ \Delta rbmC\ \Delta bap1\ \Delta vpsL\ \Delta tcpA}$=3). (b) When bacteria overproduced TCP, dispersal of biofilms from the macrophage surface was not observed. Images in the xy-plane show the accumulation of *V. cholerae* at the time points 1 h and 7 h after the initiation of the co-incubation with macrophages (THP-1 monocyte derived).

3.3 Discussion and Outlook

The innate immune system includes macrophages with phagocytic activity. Macrophages are tissue-resident cells, that confer the first line of defense and recruit neutrophils and monocytes from the blood in order to resolve inflammation [143, 144]. Within this study, the interaction between the human biofilm-forming pathogen *V. cholerae* and human macrophages was investigated.

Studying the interaction between *V. cholerae* and macrophages using fluorescence microscopy revealed the capability of *V. cholerae* to attach to and initiate biofilm formation on the surface of human macrophages (Figure 3.1). Phagocytosis of *V. cholerae* could not be observed. The ability of *V. cholerae* to form biofilms on the surface of immune cells did not extend to macrophage-precursor cells, i.e. monocytes (Figure 3.2). Propagation on the macrophage surface displayed the characteristic stages of traditional biofilm formation - attachment, growth and dispersal. The formation of biofilms on the macrophage surface was facilitated by the combined action of the polar flagellum and the bacterial type IV pili - MSHA pili or TCP (Figure 3.3, Figure 3.4). Flagella and MSHA pili were crucial for the initial attachment of bacteria to macrophages. This interaction was strengthened by TCP, whose presence prevented complete dispersal of bacteria from the macrophage surface (Figure 3.7). Other matrix components, traditionally found in *V. cholerae* biofilms formed on an abiotic surface (RbmA, RbmC, Bap1 and VPS), were dispensable for biofilm growth on the macrophage surface (Figure 3.5).

Attachment of *V. cholerae* seems to be specific to macrophages and does not occur during exposure to monocytes. A prerequisite for detection and phagocytosis of invading bacteria is their recognition by receptors that are present on the macrophage surface [158]. This suggests that upon differentiation, *V. cholerae* is able to bind those receptors on the macrophage surface. Since attachment of *V. cholerae* is facilitated by the presence of a polar flagellum, binding to the marophage surface could occur via the toll-like receptor 5 (TLR5) that recognizes bacterial flagalla [159, 160]. In addition to the polar flagellum, *V. cholerae* requires MSHA pili for macrophage attachment. MSHA pili are able to bind sugars [161]. This suggests, that attachment of *V. cholerae* could be facilitated by binding to glycoproteins present on the macrophage surface. In addition to MSHA pili, toxin-coregulated pili facilitated attachment of motile to macrophages. This is in accordance to previous studies where bacterial colonization by toxin-coregulated pili has been

established already [157]. In order to fully understand the attachment mechanism, motility of bacterial cells should be considered. Here, it should be further investigated whether the flagellum is only required for motility or actually interacts with macrophages and mediates bacterial binding.

V. cholerae biofilm formation on the macrophage surface requires type IV pili as well. Again, production of MSHA pili or TCP by motile bacteria was sufficient for surface colonization (Figure 3.5). This suggests, that pili constitute the matrix of *V. cholerae* biofilms grown on the surface of macrophages. Toxin-coregulated pili have been already shown to form a fibrious mesh with encapsulated *V. cholerae* cells [157]. Traditional matrix components observed in biofilms formed on a glass surface (RbmA, RbmC, Bap1 and VPS) are not required for colonization of macrophages. This suggests that *V. cholerae* can adapt to different environments and form biofilms with different types of matrix components. Since *V. cholerae* lives in marine environment and the human intestine, it is not surprising, that this bacterium evolved different modes of biofilm formation.

The last step in biofilm formation is dispersal. Dispersal of *V. cholerae* biofilms from the macrophage surface is accompanied by cell death of macrophages. Biofilm dispersal and macrophage death need to be investigated in future experiments. Preliminary data suggests, that biofilm dispersal is independent of quorum sensing. Time-resolved dual-RNA sequencing could be applied to elucidate the mechanisms that trigger biofilm dispersal and macrophage cell death. Furthermore, the data could help to uncover, why *V. cholerae* is not phagocytized by macrophages. Studies with neutrophils showed that those immune cells can not phagocytize *V. cholerae*. Impaired phagocytosis was linked to production of toxins by *V. cholerae* [162]. This suggests, that *V. cholerae* could actively evade phagocytosis by immune cells for efficient colonization of the human intestine.

3.4 Material and Methods

3.4.1 Microbiological Methods

3.4.1.1 Growth of *V. cholerae* and *E. coli*

Bacteria were grown overnight in 5 mL LB (Lysogeny Broth) medium at 37 °C under shaking conditions (250 rpm). Where necessary, the bacterial culture was supplemented with antibiotics. Antibiotic concentrations used for liquid cultures are listed in Table 3.1. Bacterial strains used in this study are listed in Table S3.

Table 3.1: Antibiotic concentrations used for selection of *E. coli* and *V. cholerae*

Antibiotic	Final concentration [µg mL^{-1}]
Gentamicin	30
Kanamycin	50 (*E. coli*), 100 (*V. cholerae*)
Chloramphenicol	10
Streptomycin	5000

3.4.1.2 Storage of *V. cholerae* and *E. coli*

Overnight grown bacteria stored as described previously (Chapter 2.4.1.2).

3.4.2 Molecular Cloning

3.4.2.1 Genetic modifications in *V. cholerae* C6706

Chromosomal modifications in *V. cholerae* O1 biovar El Tor strain C6706 were carried out by homologous recombination using the suicide vector pKAS32 [163, 164]. For successful chromosomal integration of the suicide vector into the *V. cholerae* genome, two 1000 base pair long DNA fragments flanking the genomic region of interest were inserted into the pKAS32 vector as described in section 3.4.2.2. Afterwards, the suicide vector was transformed into *V. cholerae* C6706 by bacterial conjugation. For this, overnight grown *E. coli* S17-1 λ pir harboring pKAS32 were washed once and concentrated ten times in LB medium. Afterwards 100 µL of overnight grown *V. cholerae* were mixed with 50 µL concentrated *E. coli* cells and spotted onto an LB agar plate. Following incubation for 6 h at

37 °C, bacteria were streaked on an LB agar plate supplemented with Polymyxin B (50 U/mL) and Kanamycin, in order to select for *V. cholerae* with the pKAS 32 plasmid integrated into the genome. Plates were incubated overnight at 37 °C. The next day, bacteria from two colonies were re-grown for 4 h at 37 °C in 1 mL LB medium supplemented with Streptomycin. Afterwards, cells were back-diluted 1:20 and grown for a second time under the same conditions before being finally diluted $1{:}10^7$ in LB medium and plated on LB agar supplemented with Streptomycin. Growth in the presence of Streptomycin selects for *V. cholerea* cells that underwent a second homologous recombination step and do not harbor the pKAS 32 plasmid in their genome. Clones obtained after overnight growth at 37 °C were screened by colony PCR for the correct genomic modifications. Positive transformants were re-streaked on LB agar and plates were incubated overnight at 37 °C. Bacteria from one colony were re-grown in liquid culture and stored afterwards.

Chromosomal modifications were verified by DNA sequencing. In order to generate the DNA fragment for sequencing, the genomic region of interest was amplified by PCR using PrimeSTAR GXL polymerase (see reaction mixture Table 3.2 and PCR program Table 3.3) with 0.5 µL of overnight grown bacterial cells as the source of DNA.

All *V. cholerae* strains used for bacteria-macrophage interaction studies were transformed with the plasmid pNUT542 (for constitutive production of sfGFP) by bacterial conjugation. Overnight grown *E. coli* Top 10 harboring pNUT542 as well as *E. coli* carrying the helper plasmid pRK600 were washed once and concentrated ten times in LB medium. Afterwards, 50 µL of both concentrated *E. coli* strains were mixed with 100 µL of overnight grown *V. cholerae*. The cell suspension was spotted onto an LB agar plate incubated for 6 h at 37 °C. Bacteria were streaked on an LB agar plate supplemented with Polymyxin (50 U/mL) and Gentamicin. Bacteria were grown overnight at 37 °C. The next day, bacteria from one colony were grown in LB medium supplemented with Gentamicin overnight at 37 °C and stored afterwards.

3.4.2.2 Plasmid construction by Gibson assembly

Gibson assembly was applied to construct suicide plasmids based on pKAS32 for genetic modifications in *V. cholerae*. Individual DNA fragments, with 20-30 bp long overlap regions for fusion by Gibson assembly, were first generated in a PCR

and purified. Subsequently, the Gibson assembly reaction mixture was prepared on ice as described in [165] for one-step isothermal DNA assembly. Here, 200 ng of the pKAS vector and equimolar amounts of the inserts (DNA fragments to be joined with pKAS32 vector) were added to 7.5 µL of the assembly master mixture in a total volume of 10 µL. The reaction mixture was placed for 20 min at 50 °C and 350 rpm shaking. Afterwards, the reaction mixture was cooled on ice for 5 min and the assembled plasmid was transformed into *E. coli* S17-1 λ pir by heat shock. Bacteria harboring the assembled plasmid (as verified by colony PCR) were grown in liquid culture and stored afterwards. In addition, the plasmid was isolated (see chapter 2.4.2.3) and sent for DNA sequencing (see chapter 2.4.2.9).

3.4.2.3 Polymerase chain reaction (PCR)

For Gibson assembly or generation of DNA fragments for subsequent DNA sequencing, DNA fragments were amplified using PrimeSTAR GXL polymerase (Cat-No. R050A, Takara). The composition of the reaction mixture and the PCR program are listed in Table 3.2 and Table 3.3. Amplification of DNA fragments was verified by agarose gel electrophoresis (see chapter 2.4.2.6). When plasmid DNA was used as the template in the PCR, the resulting PCR product was treated with the restriction endonuclease DpnI (see chapter 2.4.2.7).

Table 3.2: PCR reaction mixture using PrimeSTAR GXL DNA polymerase

Reagent	
Reaction Buffer	1x
Oligonucleotide 1	10 µM
Oligonucleotide 2	10 µM
dNTP	0.2 mM
PrimeSTAR GXL DNA polymerase	0.63 U
DNA template	50 ng genomic or plasmid DNA
Total volume	50 µL

Table 3.3: PCR program using PrimeSTAR GXL DNA polymerase

Step	Temperature [°C]	Time [min]	Cycle
Initial Denaturation	98	5	1
Denaturation	98	0.5	30
Annealing	57-60	0.5	
Elongation	68	0.5/kbp	
Final Elongation	68	10	1

Genetic modifications in *V. cholerae* were verified by colony PCR. For this, transformants were re-grown in 100 µL LB medium (supplemented with 5 mg mL^{-1} Streptomycin) in plastic 96-well plates for 30 min at 37 °C and 250 rpm shaking. Subsequently, 1 µL of the grown bacterial culture was used as the source of DNA within the PCR reaction. The composition of the PCR reaction mixture and the PCR program are listed in Table 2.6 and Table 2.7.

3.4.2.4 Heat shock transformtion of *E. coli* S17-1 λ pir

Chemically competent *E. coli* S17-1 λ pir were mixed with 10 µL of the Gibson assembly reaction mixture and incubated for 30 min on ice. Afterwards, heat shock was applied by transferring bacteria to a 42 °C waterbath for 1 min followed by incubation on ice for 2 min. Cells were recovered in LB medium (500 µL) and grown for 2 h at 37 °C and 550 rpm shaking. Finally, cells were plated on LB agar supplemented with the appropriate antibiotic and grown overnight at 37 °C. The next day, transformants were verified by colony PCR (see Table 2.6 and Table 2.7).

3.4.3 Mammalian Cell Culture Techniques

3.4.3.1 Cultivation of the human monocytic cell line THP-1

THP-1 cells were grown at 37 °C and 5 % CO_2 in Dulbecco's Modified Eagle Medium (DMEM, Cat-No. 11880-028, Thermo Fisher Scientific) supplemented with GlutaMAX^{TM} (Cat-No. 35050-038, Thermo Fisher Scientific), 10 % heat-inactivated fetal calf serum (FCS, Cat-No. 10500064, Thermo Fisher Scientific) and Gentamicin (30 µg mL^{-1}). Monocytes were subcultured every 2-4 days and maintained at density of approximately 2.5×10^5 cells mL^{-1}. Before every subcul-

ture, the cell density was determined using a hemocytometer. Cells were subcultured until passage number 12 was reached, before fresh cells were thawed.

3.4.3.2 Cryopreservation of mammalian cells

At a low passage number and when cells reached a density of approximately 2.5×10^5 cells mL^{-1}, cells were harvested by centrifugation for 5 min at 200 g. Afterwards, the cell pellet was resuspended in FCS+10 % DMSO at a cell density of 1.5×10^6 cells mL^{-1} and cryogenic tubes were filled with 1 mL of the cell suspension. Subsequently, the vials were placed in a freezing container (Mr. Frosty, Cat-No. 5100-0001, Thermo Fisher Scientific) and cooled down at a low freezing rate overnight at −80 °C. Finally, frozen cells were transferred into a liquid nitrogen filled storage tank.

3.4.3.3 Thawing mammalian cells

Frozen cells were thawed for 3 min at room temperature. Afterwards 5 mL of prewarmed growth medium was added and the cells were pelleted at 200 g for 5 min. Subsequently, THP-1 cells were resuspended in 10 mL growth medium, transferred into a culture flask and grown at 37 °C and 5 % CO_2.

3.4.3.4 Isolation of monocytes from buffy coat

Isolation of monocytes from buffy coat was performed by Marina Aznaourova (Institute for Lung Research, Philipps-University Marburg). Monocytes were isolated using CD14 MicroBeads (Cat-No. 130-050-201, Miltenyi Biotec).

3.4.3.5 Differentiation of human monocytic THP-1 cells into macrophages

THP-1 cells were differentiated in 96-well glass bottom plates (Cat-No. 655892, Greiner Bio-One) in the presence of Phorbol 12-myristate 13-acetate (PMA, Cat-No. P1585-1MG, Sigma Aldrich). First, monocytes were harvested for 5 min at 200 g and resuspended in fresh growth medium to a cell concentration of 10^5 monocytes/mL. Next, PMA was added (final concentration: 20 nM) and 200 µL of the cell suspension (25,000 cells) was transferred into individual wells of the 96-well plate. Monocytes were differentiated for 72 h at 37 °C and 5 % CO_2.

3.4.3.6 Differentiation of monocytes derived from human blood into macrophages

After isolation of monocytes from buffy coat, the cells were differentiated into macrophages using X-VIVO-15 serum-free hematopoietic cell medium supplemented with 5 % FBS Superior (Biochrom GmbH), Gentamicin (25 ng mL^{-1}) and 15 ng mL^{-1} recombinant human GM-CSF (Cat-No. 300-03, PeproTech). For differentiation, primary monocytes were resuspended in differentiation medium to a cell concentration of 4×10^5 cells/mL. Afterwards 200 µL of the cell suspension (80,000 cells) were transferred into individual wells of a 96-well glass bottom well plate where cell differentiation occurred for eight days at 37 °C and 5 % CO_2. After four days, 50 µL of fresh differentiation medium was added to each well.

3.4.4 Bacteria-Macrophage Interaction Assay

3.4.4.1 Staining of mammalian cells

After differentiation of THP-1 cells or primary monocytes, the medium was removed and 100 µL of 3 mM CellTracker Red CMTPX (Cat-No. C34552, Thermo Fisher Scientific) staining solution (in Hanks Balanced Salt Solution, HBSS) was added to the macrophages. Following incubation for 15 min at 37 °C and 5 % CO_2, the staining solution was removed and the cells were washed once with 100 µL HBSS. Subsequently, bacteria were added to the wells.

For staining of monocytes, cells were harvested for 5 min at 200 g and resuspended in 500 µL staining solution. After incubation for 15 min at 37 °C and 5 % CO_2, the staining solution was removed by centrifugation for 5 min at 200 g and monocytes were resuspended in fresh growth medium to a cell concentration of 10^5 cells/mL.

3.4.4.2 Exposure of mammalian cells to bacteria

For bacteria-macrophage interaction studies, bacterial cells were grown in 500 µL LB medium at 37 °C for 2 h. Afterwards, 20 µL of the bacterial culture was transferred into 5 mL DMEM (supplemented with GlutaMax, FCS and Gentamicin) and the cells were re-grown for 12 h at 37 °C. Bacteria from 100 µL of the grown culture were harvested for 1 min at 11,000 rpm, resuspended in equal volume using fresh DMEM (supplemented) and diluted to an $OD_{600\ nm}$ of 0.01. Finally, 200 µL of the diluted bacterial suspension was added to stained macrophages residing in 96-well plates and co-incubation for 6 h at 37 °C and 5 % CO_2 followed.

During co-incubation, fluorescence images were taken using a confocal microscope.

As a control, monocytes were exposed to *V. cholerae*. For this, bacteria were grown and prepared for the interaction study as described above with one exception. Bacteria were diluted to an $OD_{600\,nm}$ of 0.1 (instead of 0.01). Afterwards, 200 µL of stained monocytes (corresponding to 25,000 cells) and 1 µL of the bacterial suspension was added to individual wells of a 96-well glass bottom plate. Subsequently, fluorescence images were taken with a confocal microscope.

3.4.4.3 Visualization of dead macrophages

In order to visualize dead macrophages during bacteria-macrophage interaction studies, the growth medium was supplemented with NucRed Dead 647 (Cat-No. R37113, Thermo Fisher Scientific). For this, the dye was diluted 1:70 in growth medium.

3.4.4.4 Visualization of RbmA inside biofilms

The presence of secreted RbmA within biofilms was confirmed by immunofluorescence staining. Macrophages were exposed to *V. cholerae* expressing RbmA with a C-terminal 6x-His-Tag during bacteria-macrophage interaction studies. After 4 h of co-incubation, anti-6x-His-Tag antibodies conjugated to Alexa Fluor 647 (0.2 µg mL^{-1}, Cat-No. 35370, Qiagen) and bovine serum albumin (1 mg mL^{-1}) were added to the well. Subsequently, fluorescence images were taken with a confocal microscope.

3.4.5 Microscopy and Image Analysis

3.4.5.1 Confocal laser scanning microscopy

To study the interaction between *V. cholerae* and macrophages, fluorescence images were acquired with a Yokogawa CSU confocal spinning disk unit mounted on a Nikon Ti-E inverted microscope using a Nikon 40x Plan Fluor oil objective with 1.3 NA. Fluorescent proteins sfGFP and mRuby3 were excited with 488 nm and 552 nm lasers, respectively. Dyes, CellTracker Red CMTPX and NucRed Dead 647, were excited with 552 nm and 640 nm lasers. Emission was detected with an Andor iXon electron-multiplying charge-coupled device (EMCCD) camera. During confocal imaging a 405/488/552/640 nm dichroic filter, as well as a 525/50,

650/150 and 731/137 emission filter, were used. The hardware was controlled using µManager [166]. Images were acquired every 30 min with a step size of 3 µm in z-direction.

3.4.5.2 Data analysis

Z-stacks of bacterial biofilms, obtained by fluorescent confocal microscopy, were analyzed slice-by-slice by dynamic thresholding. Out of the five slices of the z-stack, only the 3 upper most xy-planes were analyzed. Threshold values for the identification of bacterial cells from intensity images were determined by Otsu's method [167], assuming three classes, of which two are assumed to correspond to the background. Identified cells smaller than 10 pixels were discarded, under the assumption that those are most likely artefacts of salt-and-pepper noise.

Macrophages were identified by applying the same Otsu-thresholding as described above. A subsequent series of morphological operations was applied to smoothen the shape of identified macrophages with objects smaller than 500 pixels discarded, as they are most likely noise. As observations showed that bacteria attach to, but do not enter, macrophages, bacterial cells that were not within a distance of 15 pixel to the identified macrophage surface were discarded resulting in a binary image of the sole attached bacterial cells. Macrophages at the image boundary were discarded.

Based upon those images, attachment was determined as the areal fraction of macrophage-attached cells and macrophages. Biofilm formation was quantified using the areal fraction of bacterial cells within a distance of 20 pixel around the macrophages and bacterial cells in the space between macrophages. The analysis code was written in MATLAB (MathWorks) by H. Jeckel.

4 Bibliography

1. Whitman, W. B., Coleman, D. C. & Wiebe, W. J. Prokaryotes: the unseen majority. *Proceedings of the National Academy of Sciences of the United States of America* **95,** 6578–83 (1998).
2. Kallmeyer, J., Pockalny, R., Adhikari, R. R., Smith, D. C. & D'Hondt, S. Global distribution of microbial abundance and biomass in subseafloor sediment. *Proceedings of the National Academy of Sciences* **109,** 16213–16216. doi:10.1073/pnas.1203849109 (2012).
3. Arnosti, C. Microbial Extracellular Enzymes and the Marine Carbon Cycle. *Annual Review of Marine Science* **3,** 401–425. doi:10.1146/annurev-marine-120709-142731 (2010).
4. Fuhrman, J. A. *Marine viruses and their biogeochemical and ecological effects* 1999. doi:10.1038/21119.
5. Hooper, L. V. *Bacterial contributions to mammalian gut development* 2004. doi:10.1016/j.tim.2004.01.001.
6. Bäckhed, F., Ley, R. E., Sonnenburg, J. L., Peterson, D. A. & Gordon, J. I. *Host-bacterial mutualism in the human intestine* 2005. doi:10.1126/science.1104816.
7. Flemming, H.-C. *et al.* Biofilms: an emergent form of bacterial life. *Nature Reviews Microbiology* **14,** 563–575. doi:10.1038/nrmicro.2016.94 (2016).
8. Flemming, H.-C. & Wingender, J. The biofilm matrix. *Nature reviews. Microbiology* **8,** 623–633. doi:10.1080/0892701031000072190 (2010).
9. O'Toole, G., Kaplan, H. B. & Kolter, R. Biofilm formation as microbial development. *Annu Rev Microbiol* **54,** 49–79. doi:10.1146/annurev.micro.54.1.49 (2000).
10. McDougald, D., Rice, S. a., Barraud, N., Steinberg, P. D. & Kjelleberg, S. Should we stay or should we go: mechanisms and ecological consequences for biofilm dispersal. *Nature Reviews Microbiology* **10,** 39–50. doi:10.1038/nrmicro2695 (2011).

11. Singh, P. K. *et al.* Vibrio cholerae Combines Individual and Collective Sensing to Trigger Biofilm Dispersal. *Current Biology* **27,** 3359–3366.e7. doi:10.1016/j.cub.2017.09.041 (2017).

12. Hobley, L., Harkins, C., MacPhee, C. E. & Stanley-Wall, N. R. Giving structure to the biofilm matrix: an overview of individual strategies and emerging common themes. *FEMS Microbiology Reviews,* fuv015. doi:10.1093/femsre/fuv015 (2015).

13. Berk, V. *et al.* Molecular architecture and assembly principles of Vibrio cholerae biofilms. *Science* **337,** 236–239. doi:10.1126/science.1222981 (2012).

14. Drescher, K. *et al.* Architectural transitions in Vibrio cholerae biofilms at single-cell resolution. *Proceedings of the National Academy of Sciences* **113,** E2066–E2072. doi:10.1073/pnas.1601702113 (2016).

15. Utada, A. S. *et al.* Vibrio cholerae use pili and flagella synergistically to effect motility switching and conditional surface attachment. *Nature Communications* **5.** doi:10.1038/ncomms5913 (2014).

16. Stewart, P. S. & Franklin, M. J. Physiological heterogeneity in biofilms. *Nature Reviews Microbiology* **6,** 199–210. doi:10.1038/nrmicro1838 (2008).

17. Besharova, O., Suchanek, V. M., Hartmann, R., Drescher, K. & Sourjik, V. Diversification of gene expression during formation of static submerged biofilms by Escherichia coli. *Frontiers in Microbiology* **7,** 1–17. doi:10.3389/fmicb.2016.01568 (2016).

18. Balaban, N. Q., Merrin, J., Chait, R., Kowalik, L. & Leibler, S. Bacterial persistence as a phenotypic switch. *Science* **305,** 1622–1625. doi:10.1126/science.1099390 (2004).

19. Nadell, C. D., Xavier, J. B. & Foster, K. R. The sociobiology of biofilms. *FEMS Microbiology Reviews* **33,** 206–224. doi:10.1111/j.1574-6976.2008.00150.x (2009).

20. Nadell, C. D., Drescher, K. & Foster, K. R. *Spatial structure, cooperation and competition in biofilms* 2016. doi:10.1038/nrmicro.2016.84.

21. Hausner, M. & Wuertz, S. High rates of conjugation in bacterial biofilms as determined by quantitative in situ analysis. *Applied and Environmental Microbiology* **65,** 3710–3713 (1999).

22. Høiby, N., Bjarnsholt, T., Givskov, M., Molin, S. & Ciofu, O. Antibiotic resistance of bacterial biofilms. *International Journal of Antimicrobial Agents* **35,** 322–332. doi:10.1016/j.ijantimicag.2009.12.011 (2010).

23. Tseng, B. S. *et al.* The extracellular matrix protects Pseudomonas aeruginosa biofilms by limiting the penetration of tobramycin. *Environmental Microbiology* **15,** 2865–2878. doi:10.1111/1462-2920.12155 (2013).

24. Lewis, K. Persister cells, dormancy and infectious disease. *Nature Reviews Microbiology* **5,** 48–56. doi:10.1038/nrmicro1557 (2007).

25. Parsek, M. R. & Singh, P. K. Bacterial biofilms: an emerging link to disease pathogenesis. *Annu.Rev.Microbiol.* **57,** 677–701. doi:10.1146/annurev.micro.57.030502.090720 (2003).

26. Moreno, A. M. *et al.* Biofilm formation and phenotypic variation enhance predation-driven persistence of Vibrio cholerae. *Proceedings of the National Academy of Sciences* **102,** 16819–16824. doi:10.1073/pnas.0505350102 (2005).

27. Matz, C., Bergfeld, T., Rice, S. A. & Kjelleberg, S. Microcolonies, quorum sensing and cytotoxicity determine the survival of Pseudomonas aeruginosa biofilms exposed to protozoan grazing. *Environmental Microbiology* **6,** 218–226. doi:10.1111/j.1462-2920.2004.00556.x (2004).

28. Clements, A., Young, J. C., Constantinou, N. & Frankel, G. *Infection strategies of enteric pathogenic Escherichia coli* 2012. doi:10.4161/gmic.19182.

29. Tenaillon, O., Skurnik, D., Picard, B. & Denamur, E. *The population genetics of commensal Escherichia coli* 2010. doi:10.1038/nrmicro2298.

30. Pratt, L. a. & Kolter, R. Genetic analysis of Escherichia coli biofilm formation: Roles of flagella, motility, chemotaxis and type I pili. *Molecular Microbiology* **30,** 285–293. doi:10.1046/j.1365-2958.1998.01061.x (1998).

31. Müller, C. M. *et al.* Type 1 fimbriae, a colonization factor of uropathogenic Escherichia coli, are controlled by the metabolic sensor CRP-cAMP. *PLoS Pathogens* **5.** doi:10.1371/journal.ppat.1000303 (2009).

32. Serra, D. O., Richter, A. M., Klauck, G., Mika, F. & Hengge, R. Microanatomy at cellular resolution and spatial order of physiological differentiation in a bacterial biofilm. *MBio* **4,** e00103–13. doi:10.1128/mBio.00103-13 (2013).

33. Serra, D. O., Richter, A. M. & Hengge, R. Cellulose as an architectural element in spatially structured Escherichia coli biofilms. *Journal of Bacteriology* **195,** 5540–5554. doi:10.1128/JB.00946-13 (2013).

34. Grantcharova, N., Peters, V., Monteiro, C., Zakikhany, K. & Römling, U. Bistable expression of CsgD in biofilm development of Salmonella enterica serovar typhimurium. *Journal of Bacteriology* **192,** 456–466. doi:10.1128/JB.01826-08 (2010).

35. Pesavento, C. *et al.* Inverse regulatory coordination of motility and curli-mediated adhesion in Escherichia coli. *Genes and Development* **22,** 2434–2446. doi:10.1101/gad.475808 (2008).

36. Chilcott, G. S. & Hughes, K. T. Coupling of Flagellar Gene Expression to Flagellar Assembly in Salmonella enterica Serovar Typhimurium and Escherichia coli. *Microbiology and Molecular Biology Reviews* **64,** 694–708. doi:10.1128/mmbr.64.4.694-708.2000 (2000).

37. Soutourina, O. A. & Bertin, P. N. Regulation cascade of flagellar expression in Gram-negative bacteria. *FEMS Microbiology Reviews* **27,** 505–523. doi:10.1016/S0168-6445(03)00064-0 (2003).

38. Kalir, S. *et al.* Ordering genes in a flagella pathway by analysis of expression kinetics from living bacteria. *Science* **292,** 2080–2083. doi:10.1126/science.1058758 (2001).

39. Liu, X. & Matsumura, P. The FlhD/FlhC complex, a transcriptional activator of the Escherichia coli flagellar class II operons. *Journal of Bacteriology* **176,** 7345–7351. doi:10.1128/jb.176.23.7345-7351.1994 (1994).

40. Ohnishi, K., Kutsukake, K., Suzuki, H. & Iino, T. Gene fliA encodes an alternative sigma factor specific for flagellar operons in Salmonella typhimurium. *MGG Molecular & General Genetics* **221,** 139–147. doi:10.1007/BF00261713 (1990).

41. Karlinsey, J. E. *et al.* Completion of the hook-basal body complex of the Salmonella typhimurium flagellum is coupled to FlgM secretion and fliC transcription. *Molecular Microbiology* **37,** 1220–1231. doi:10.1046/j.1365-2958.2000.02081.x (2000).

42. Barembruch, C. & Hengge, R. Cellular levels and activity of the flagellar sigma factor FliA of Escherichia coli are controlled by FlgM-modulated proteolysis. *Molecular Microbiology* **65,** 76–89. doi:10.1111/j.1365-2958.2007.05770.x (2007).

43. Hammar, M., Arnqvist, A., Bian, Z., Olsén, A. & Normark, S. Expression of two csg operons is required for production of fibronectin- and congo red-binding curli polymers in Escherichia coli K-12. *Molecular microbiology* **18,** 661–670. doi:10.1111/j.1365-2958.1995.mmi_18040661.x (1995).

44. Ogasawara, H., Yamada, K., Kori, A., Yamamoto, K. & Ishihama, A. Regulation of the Escherichia coli csgD promoter: Interplay between five transcription factors. *Microbiology* **156,** 2470–2483. doi:10.1099/mic.0.039131-0 (2010).

45. Römling, U., Bian, Z., Hammar, M., Sierralta, W. D. & Normark, S. Curli fibers are highly conserved between Salmonella typhimurium and Escherichia coli with respect to operon structure and regulation. *Journal of Bacteriology* **180,** 722–731 (1998).

46. Brombacher, E., Dorel, C., Zehnder, A. J. B. & Landini, P. The curli biosynthesis regulator CsgD co-ordinates the expression of both positive and negative determinants for biofilm formation in Eschericia coli. *Microbiology* **149,** 2847–2857. doi:10.1099/mic.0.26306-0 (2003).

47. Weber, H., Pesavento, C., Possling, A., Tischendorf, G. & Hengge, R. Cyclic-di-GMP-mediated signalling within the σS network of Escherichia coli. *Molecular Microbiology* **62,** 1014–1034. doi:10.1111/j.1365-2958.2006.05440.x (2006).

48. Dudin, O., Geiselmann, J., Ogasawara, H., Ishihama, A. & Lacour, S. Repression of Flagellar Genes in Exponential Phase by CsgD and CpxR, Two Crucial Modulators of Escherichia coli Biofilm Formation. *Journal of Bacteriology* **196,** 707–715. doi:10.1128/jb.00938-13 (2013).

49. Pesavento, C. & Hengge, R. The global repressor FliZ antagonizes gene expression by σ s-containing RNA polymerase due to overlapping DNA binding specificity. *Nucleic Acids Research* **40,** 4783–4793. doi:10.1093/nar/gks055 (2012).

50. Povolotsky, T. L. & Hengge, R. 'Life-style' control networks in Escherichia coli: Signaling by the second messenger c-di-GMP. *Journal of Biotechnology* **160,** 10–16. doi:10.1016/j.jbiotec.2011.12.024 (2012).

51. Chapman, M. R. M. *et al.* Role of Escherichia coli curli operons in directing amyloid fiber formation. *Science (New York, N.Y.)* **295,** 851–855. doi:10.1126/science.1067484 (2002).

52. Sunde, M. & Blake, C. The Structure of Amyloid Fibrils by Electron Microscopy and X-Ray Diffraction. *Advances in Protein Chrmistry* **50,** 123–159. doi:10.1016/S0065-3233(08)60320-4 (1997).

53. Sunde, M. *et al.* Common core structure of amyloid fibrils by synchrotron X-ray diffraction. *Journal of Molecular Biology* **273,** 729–739. doi:10.1006/jmbi.1997.1348. arXiv: 9910064v1 [arXiv:nucl-th] (1997).

54. Knowles, T. P., Vendruscolo, M. & Dobson, C. M. *The amyloid state and its association with protein misfolding diseases* 2014. doi:10.1038/nrm3810. arXiv: NIHMS150003.

55. Prigent-Combaret, C. *et al.* Developmental pathway for biofilm formation in curli-producing Escherichia coli strains: Role of flagella, curli and colanic acid. *Environmental Microbiology* **2,** 450–464. doi:10.1046/j.1462-2920.2000.00128.x (2000).

56. Shu, Q. *et al.* The E. coli CsgB nucleator of curli assembles to β-sheet oligomers that alter the CsgA fibrillization mechanism. *Proceedings of the National Academy of Sciences* **109,** 6502–6507. doi:10.1073/pnas.1204161109 (2012).

57. Hammer, N. D., Schmidt, J. C. & Chapman, M. R. The curli nucleator protein, CsgB, contains an amyloidogenic domain that directs CsgA polymerization. *Proceedings of the National Academy of Sciences* **104,** 12494–12499. doi:10.1073/pnas.0703310104 (2007).

58. Evans, M. L. *et al.* The bacterial curli system possesses a potent and selective inhibitor of amyloid formation. *Molecular Cell* **57,** 445–455. doi:10.1016/j.molcel.2014.12.025 (2015).

59. Robinson, L. S., Ashman, E. M., Hultgren, S. J. & Chapman, M. R. Secretion of curli fibre subunits is mediated by the outer membrane-localized CsgG protein. *Molecular Microbiology* **59,** 870–881. doi:10.1111/j.1365-2958.2005.04997.x (2006).

60. Goyal, P. *et al.* Structural and mechanistic insights into the bacterial amyloid secretion channel CsgG. *Nature* **516,** 250–253. doi:10.1038/nature13768 (2014).

61. Nenninger, A. A. *et al.* CsgE is a curli secretion specificity factor that prevents amyloid fibre aggregation. *Molecular Microbiology* **81,** 486–499. doi:10.1111/j.1365-2958.2011.07706.x (2011).

62. Nenninger, A. A., Robinson, L. S. & Hultgren, S. J. Localized and efficient curli nucleation requires the chaperone-like amyloid assembly protein CsgF. *Proceedings of the National Academy of Sciences* **106,** 900–905. doi:10.1073/pnas.0812143106. arXiv: arXiv:1408.1149 (2009).

63. Kikuchi, T., Mizunoe, Y., Takade, A., Naito, S. & Yoshida, S.-i. Curli fibers are required for development of biofilm architecture in Escherichia coli K-12 and enhance bacterial adherence to human uroepithelial cells. *Microbiology and immunology* **49,** 875–884. doi:10.1111/j.1348-0421.2005.tb03678.x (2005).

64. Römling, U., Sierralta, W. D., Eriksson, K. & Normark, S. Multicellular and aggregative behaviour of Salmonella typhimurium strains is controlled by mutations in the agfD promoter. *Molecular Microbiology* **28,** 249–264. doi:10.1046/j.1365-2958.1998.00791.x (1998).

65. Hung, C., Marschall, J., Burnham, C. A. D., Byun, A. S. & Henderson, J. P. The bacterial amyloid curli is associated with urinary source bloodstream infection. *PLoS ONE* **9.** doi:10.1371/journal.pone.0086009 (2014).

66. Zogaj, X., Bokranz, W., Nimtz, M. & Römling, U. Production of cellulose and curli fimbriae by members of the family Enterobacteriaceae isolated from the human gastrointestinal tract. *Infection and Immunity* **71,** 4151–4158. doi:10.1128/IAI.71.7.4151-4158.2003 (2003).

67. Blanco, L. P., Evans, M. L., Smith, D. R., Badtke, M. P. & Chapman, M. R. *Diversity, biogenesis and function of microbial amyloids* 2012. doi:10.1016/j.tim.2011.11.005.

68. Taglialegna, A., Lasa, I. & Valle, J. Amyloid Structures as Biofilm Matrix Scaffolds. *JOURNAL OF BACTERIOLOGY* **198,** 2579–2588. doi:10.1128/JB.00122-16 (Oct. 2016).

69. DePas, W. H. & Chapman, M. R. Microbial manipulation of the amyloid fold. *Research in Microbiology* **163,** 592–606. doi:10.1016/j.resmic.2012.10.009. arXiv: NIHMS150003 (2012).

70. Brüssow, H. & Hendrix, R. W. *Phage Genomics: Small is beautiful* 2002. doi:10.1016/S0092-8674(01)00637-7.

71. Clokie, M. R., Millard, A. D., Letarov, A. V. & Heaphy, S. Phages in nature. *Bacteriophage* **1,** 31–45. doi:10.4161/bact.1.1.14942 (2011).

72. Salmond, G. P. C. & Fineran, P. C. A century of the phage: past, present and future. *Nature reviews. Microbiology* **13,** 777–86. doi:10.1038/nrmicro3564 (2015).

73. Howard-Varona, C., Hargreaves, K. R., Abedon, S. T. & Sullivan, M. B. *Lysogeny in nature: Mechanisms, impact and ecology of temperate phages* 2017. doi:10.1038/ismej.2017.16.

74. Dunn, J. J., Studier, F. W. & Gottesman, M. Complete nucleotide sequence of bacteriophage T7 DNA and the locations of T7 genetic elements. *Journal of Molecular Biology* **166,** 477–535. doi:10.1016/S0022-2836(83)80282-4 (1983).

75. Ionel, A. *et al.* Molecular rearrangements involved in the capsid shell maturation of bacteriophage T7. *Journal of Biological Chemistry* **286,** 234–242. doi:10.1074/jbc.M110.187211 (2011).

76. Studier, F. W. Bacteriophage T7. *Science* **176,** 367–376. doi:10.1126/science.176.4033.367 (1972).

77. Kemp, P., Garcia, L. R. & Molineux, I. J. Changes in bacteriophage T7 virion structure at the initiation of infection. *Virology* **340,** 307–317. doi:10.1016/j.virol.2005.06.039 (2005).

78. Krüger, D. H. & Schroeder, C. Bacteriophage T3 and bacteriophage T7 virus-host cell interactions. *Microbiological reviews* **45,** 9–51 (1981).

79. González-García, V. A. *et al.* Conformational changes leading to T7 DNA delivery upon interaction with the bacterial receptor. *Journal of Biological Chemistry* **290,** 10038–10044. doi:10.1074/jbc.M114.614222 (2015).

80. Koskella, B. & Brockhurst, M. A. Bacteria-phage coevolution as a driver of ecological and evolutionary processes in microbial communities. *FEMS Microbiology Reviews* **38,** 916–931. doi:10.1111/1574-6976.12072 (2014).

81. Moineau, S. *et al.* CRISPR Provides Acquired Resistance Against Viruses in Prokaryotes. *Science* **315,** 1709–1712 (2007).

82. Samson, J. E., Magadán, A. H., Sabri, M. & Moineau, S. Revenge of the phages: defeating bacterial defences. *Nature reviews. Microbiology* **11,** 675–87. doi:10.1038/nrmicro3096 (2013).

83. Tock, M. R. & Dryden, D. T. *The biology of restriction and anti-restriction* 2005. doi:10.1016/j.mib.2005.06.003.

84. Molineux, I. J. Host-parasite interactions: recent developments in the genetics of abortive phage infections. *The New Biologist* **3,** 230–6 (1991).

85. Rostøl, J. T. & Marraffini, L. (Ph)ighting Phages: How Bacteria Resist Their Parasites. *Cell Host and Microbe* **25,** 184–194. doi:10.1016/j.chom.2019.01.009 (2019).

86. Labrie, S. J., Samson, J. E. & Moineau, S. Bacteriophage resistance mechanisms. *Nature reviews. Microbiology* **8,** 317–327. doi:10.1038/nrmicro2315 (2010).

87. Heilmann, S., Sneppen, K. & Krishna, S. Coexistence of phage and bacteria on the boundary of self-organized refuges. *Proceedings of the National Academy of Sciences of the United States of America* **109,** 12828–33. doi:10.1073/pnas.1200771109 (2012).

88. Schrag, S. J. & Mittler, J. E. Host-Parasite Coexistence: The Role of Spatial Refuges in Stabilizing Bacteria-Phage Interactions. *The American Naturalist* **148,** 348–377. doi:10.1086/285929 (2002).

89. Brockhurst, M. A., Buckling, A. & Rainey, P. B. Spatial heterogeneity and the stability of host-parasite coexistence. *Journal of Evolutionary Biology* **19,** 374–379. doi:10.1111/j.1420-9101.2005.01026.x (2006).

90. Cerca, N., Oliveira, R. & Azeredo, J. Susceptibility of Staphylococcus epidermidis planktonic cells and biofilms to the lytic action of staphylococcus bacteriophage K. *Letters in Applied Microbiology* **45,** 313–317. doi:10.1111/j.1472-765X.2007.02190.x (2007).

91. May, T., Tsuruta, K. & Okabe, S. Exposure of conjugative plasmid carrying Escherichia coli biofilms to male-specific bacteriophages. *The ISME journal* **5,** 771–5. doi:10.1038/ismej.2010.158 (2011).

92. Doolittle, M. M., Cooney, J. J. & Caldwell, D. E. Tracing the interaction of bacteriophage with bacterial biofilms using fluorescent and chromogenic probes. *Journal of industrial microbiology* **16,** 331–41. doi:10.1007/BF01570111 (1996).

93. Simmons, M., Drescher, K., Nadell, C. D. & Bucci, V. Phage mobility is a core determinant of phage-bacteria coexistence in biofilms. *ISME Journal* **12,** 532–543. doi:10.1038/ismej.2017.190 (2018).

94. Sutherland, I. W., Hughes, K. A., Skillman, L. C. & Tait, K. The interaction of phage and biofilms. *FEMS Microbiology Letters* **232,** 1–6. doi:10.1016/S0378-1097(04)00041-2 (2004).

95. Hughes, K. A., Sutherland, I. W., Jones, M. V. & Rutherford, D. Biof ilm susceptibility to bacteriophage attack : the role of phage-borne polysaccharide depol yrnerase. *Microbiology* **144,** 3039–3047 (1996).

96. Lu, T. K. & Collins, J. J. Dispersing biofilms with engineered enzymatic bacteriophage. *Proceedings of the National Academy of Sciences of the United States of America* **104,** 11197–202. doi:10.1073/pnas.0704624104 (2007).

97. Kim, M. S. *et al.* phage-encoded colanic acid-degrading enzyme permits lytic phage: Infection of a capsule-forming resistant mutant Escherichia coli strain. *Applied and Environmental Microbiology* **81,** 900–909. doi:10.1128/AEM.02606-14 (2015).

98. Hall-Stoodley, L., Costerton, J. W. & Stoodley, P. Bacterial biofilms: from the natural environment to infectious diseases. *Nat Rev Microbiol.* **2,** 95–108. doi:10.1038/nrmicro821 (2004).

99. Ito, A., May, T., Kawata, K. & Okabe, S. Significance of rpoS during maturation of Escherichia coli biofilms. *Biotechnology and Bioengineering* **99,** 1462–1471. doi:10.1002/bit.21695 (2008).

100. Hentzer, M., Eberl, L. & Givskov, M. Transcriptome analysis of Pseudomonas aeruginosa biofilm development: Anaerobic respiration and iron limitation. *Biofilms* **2,** 37–61. doi:10.1017/S1479050505001699 (2005).

101. Zivanovic, Y. *et al.* Insights into Bacteriophage T5 Structure from Analysis of Its Morphogenesis Genes and Protein Components. *Journal of Virology* **88,** 1162–1174. doi:10.1128/jvi.02262-13 (2014).

102. Römling, U., Sierralta, W. D., Eriksson, K. & Normark, S. Multicellular and aggregative behaviour of Salmonella typhimurium strains is controlled by mutations in the agfD promoter. *Molecular Microbiology* **28,** 249–264 (1998).

103. Hartmann, R. *et al. Emergence of three-dimensional order and structure in growing biofilms* 2019. doi:10.1038/s41567-018-0356-9.

104. Barnhart, M. M. & Chapman, M. R. Curli biogenesis and function. *Annual review of microbiology* **60,** 131–47. doi:10.1146/annurev.micro.60.080805.142106 (2006).

105. Soutourina, O. A. & Bertin, P. N. *Regulation cascade of flagellar expression in Gram-negative bacteria* 2003. doi:10.1016/S0168-6445(03)00064-0.

106. Flemming, H. C. & Wuertz, S. Bacteria and archaea on Earth and their abundance in biofilms. *Nature Reviews Microbiology* **17,** 247–260. doi:10.1038/s41579-019-0158-9 (2019).

107. Scholl, D., Adhya, S. & Merril, C. Escherichia coli K1 ' s Capsule Is a Barrier to Bacteriophage T7. *Applied and environmental microbiology* **71,** 4872–4874. doi:10.1128/AEM.71.8.4872 (2005).

108. Dueholm, M. S., Albertsen, M., Otzen, D. & Nielsen, P. H. Curli Functional Amyloid Systems Are Phylogenetically Widespread and Display Large Diversity in Operon and Protein Structure. *PLoS ONE* **7.** doi:10.1371/journal.pone.0051274 (2012).

109. Collinson, S. K., Emody, L., Muller, K. H., Trust, T. J. & Kay, W. W. Purification and characterization of thin, aggregative fimbriae from Salmonella enteritidis. *Journal of Bacteriology* **173,** 4773–4781. doi:10.1128/jb.173.15.4773-4781.1991 (1991).

110. Boulanger, P. Purification of bacteriophages and SDS-PAGE analysis of phage structural proteins from ghost particles. *Methods in molecular biology* **502,** 227–238. doi:10.1007/978-1-60327-565-1_13 (2009).

111. Slootweg, E. J. *et al.* Fluorescent T7 display phages obtained by translational frameshift. *Nucleic Acids Research* **34.** doi:10.1093/nar/gkl600 (2006).

112. Datsenko, K. A. & Wanner, B. L. One-step inactivation of chromosomal genes in Escherichia coli K-12 using PCR products. *Proceedings of the National Academy of Sciences* **97,** 6640–6645. doi:10.1073/pnas.120163297 (2002).

113. Boehm, A. *et al.* Second messenger signalling governs Escherichia coli biofilm induction upon ribosomal stress. *Molecular Microbiology* **72,** 1500–1516. doi:10.1111/j.1365-2958.2009.06739.x (2009).

114. Zhou, Y., Smith, D. R., Hufnagel, D. A. & Chapman, M. R. Experimental manipulation of the microbial functional amyloid called curli. *Methods in Molecular Biology* **966,** 53–75. doi:10.1007/978-1-62703-245-2-4 (2013).

115. U K Laemmli. Cleavage of structural proteins during the assembly of the head of bacteriophage T4. *nature* **227,** 680–685 (1970).

116. Charles, R. C. & Ryan, E. T. *Cholera in the 21st century* 2011. doi:10.1097/QCO.0b013e32834a88af.

117. Tamplin, M. L., Gauzens, A. L., Huq, A., Sack, D. A. & Colwell, R. R. Attachment of Vibrio cholerae serogroup O1 to zooplankton and phytoplankton of Bangladesh waters. *Applied and Environmental Microbiology* **56,** 1977–1980 (1990).

118. Rawlings, T. K., Ruiz, G. M. & Colwell, R. R. Association of Vibrio cholerae O1 El Tor and O139 Bengal with the copepods Acartia tonsa and Eurytemora affinis. *Applied and Environmental Microbiology* **73,** 7926–7933. doi:10.1128/AEM.01238-07 (2007).

119. Meibom, K. L. *et al.* The Vibrio cholerae chitin utilization program. *Proceedings of the National Academy of Sciences* **101,** 2524–2529. doi:10.1073/pnas.0308707101 (2004).

120. Meibom, K. L., Blokesch, M., Dolganov, N. A., Wu, C. Y. & Schoolnik, G. K. Microbiology: Chitin induces natural competence in vibrio cholerae. *Science* **310,** 1824–1827. doi:10.1126/science.1120096 (2005).

121. Reidi, J. & Klose, K. E. Vibrio cholerae and cholera:out of the water and into the host. *Microbiology Reviews* **26,** 125–139 (2002).

122. Waldor, M. K. & Mekalanos, J. J. Lysogenic conversion by a filamentous phage encoding cholera toxin. *Science* **272,** 1910–4 (1996).

123. Hammer, B. K. & Bassler, B. L. Quorum sensing controls biofilm formation in Vibrio cholerae. *Molecular Microbiology* **50,** 101–114. doi:10.1046/j.1365-2958.2003.03688.x (2003).

124. Ng, W.-L. & Bassler, B. L. Bacterial Quorum-Sensing Network Architectures. *Annual Review of Genetics* **43,** 197–222. doi:10.1146/annurev-genet-102108-134304 (2009).

125. Hartmann, R. *et al.* Emergence of three-dimensional order and structure in growing biofilms. *Nature Physics.* doi:10.1038/s41567-018-0356-9 (2018).

126. Millet, Y. A. *et al.* Insights into Vibrio cholerae Intestinal Colonization from Monitoring Fluorescently Labeled Bacteria. *PLoS Pathogens* **10.** doi:10.1371/journal.ppat.1004405 (2014).

127. Faruque, S. M. *et al.* Transmissibility of cholera: In vivo-formed biofilms and their relationship to infectivity and persistence in the environment. *Proceedings of the National Academy of Sciences* **103,** 6350–6355. doi:10.1073/pnas.0601277103 (2006).

128. Almagro-Moreno, S., Pruss, K. & Taylor, R. K. Intestinal Colonization Dynamics of Vibrio cholerae. *PLoS Pathogens* **11,** 1–11. doi:10.1371/journal.ppat.1004787 (2015).

129. Fong, J. C. N., Syed, K. A., Klose, K. E. & Yildiz, F. H. Role of Vibrio polysaccharide (vps) genes in VPS production, biofilm formation and Vibrio cholerae pathogenesis. *Microbiology* **156,** 2757–2769. doi:10.1099/mic.0.040196-0 (2010).

130. Chiang, S. L., Taylor, R. K., Koomey, M. & Mekalanos, J. J. Single amino acid substitutions in the N-terminus of Vibrio cholerae TcpA affect colonization, autoagglutination, and serum resistance. *Molecular Microbiology* **17,** 1133–1142. doi:10.1111/j.1365-2958.1995.mmi_17061133.x (1995).

131. Krebs, S. J. & Taylor, R. K. Protection and attachment of Vibrio cholerae mediated by the toxin-coregulated pilus in the infant mouse model. *Journal of Bacteriology* **193,** 5260–5270. doi:10.1128/JB.00378-11 (2011).

132. Hanne, L. F. & Finkelstein, R. A. Characterization and distribution of the hemagglutinins produced by Vibrio cholerae. *Infection and Immunity* **36,** 209–214 (1982).

133. Jonson, G., Holmgren, J. & Svennerholm, A. M. Identification of a mannose-binding pilus on Vibrio cholerae El Tor. *Microbial Pathogenesis* **11,** 433–441. doi:10.1016/0882-4010(91)90039-D (1991).

134. Jonson, G., Lebens, M. & Holmgren, J. Cloning and sequencing of Vibrio cholerae mannose-sensitive haemagglutinin pilin gene: localization of mshA within a cluster of type 4 pilin genes. *Molecular Microbiology* **13,** 109–118. doi:10.1111/j.1365-2958.1994.tb00406.x (1994).

135. Chiavelli, D. A., Marsh, J. W. & Taylor, R. K. The Mannose-Sensitive Hemagglutinin of Vibrio cholerae Promotes Adherence to Zooplankton. *Applied and Environmental Microbiology* **67,** 3220–3225. doi:10.1128/AEM.67.7.3220-3225.2001 (2001).

136. Helene Thelin, K. & Taylor, R. K. Toxin-coregulated pilus, but not mannose-sensitive hemagglutinin, is required for colonization by Vibrio cholerae O1 El Tor biotype and O139 strains. *Infection and Immunity* **64,** 2853–2856 (1996).

137. Attridge, S. R., Manning, P. A., Holmgren, J. & Jonson, G. Relative significance of mannose-sensitive hemagglutinin and toxin- coregulated pili in colonization of infant mice by Vibrio cholerae El Tor. *Infection and Immunity* **64,** 3369–3373 (1996).

138. Kirn, T. J., Lafferty, M. J., Sandoe, C. M. & Taylor, R. K. Delineation of pilin domains required for bacterial association into microcolonies and intestinal colonization by Vibrio cholerae. *Molecular Microbiology* **35,** 896–910. doi:10.1046/j.1365-2958.2000.01764.x (2000).

139. Manning, P. A. *The tcp gene cluster of Vibrio cholerae* in *Gene* **192** (1997), 63–70. doi:10.1016/S0378-1119(97)00036-X.

140. Zhu, J. *et al.* Quorum-sensing regulators control virulence gene expression in Vibrio cholerae. *Proceedings of the National Academy of Sciences* **99,** 3129–3134. doi:10.1073/pnas.052694299 (2002).

141. Higgins, D. E. & DiRita, V. J. Transcriptional control of toxT, a regulatory gene in the ToxR regulon of Vibrio cholerae. *Molecular Microbiology* **14,** 17–29. doi:10.1111/j.1365-2958.1994.tb01263.x (1994).

142. Yu, R. R. & Dirita, V. J. Analysis of an autoregulatory loop controlling ToxT, cholera toxin, and toxin-coregulated pilus production in Vibrio cholerae. *Journal of Bacteriology* **181,** 2584–2592 (1999).

143. Flannagan, R. S., Cosío, G. & Grinstein, S. *Antimicrobial mechanisms of phagocytes and bacterial evasion strategies* 2009. doi:10.1038/nrmicro2128.

144. Davies, L. C. *et al.* Distinct bone marrow-derived and tissue-resident macrophage lineages proliferate at key stages during inflammation. *Nature Communications* **4.** doi:10.1038/ncomms2877 (2013).

145. Furth, B. Y. R. V. A. N. & Colin, Z. A. The origin and kinetics of mononuclear phagocytes. *The Journal of Experimental Medicine,* 415–435 (1968).

146. Warren, M. K. & Vogel, S. N. Bone marrow-derived macrophages: development and regulation of differentiation markers by colony-stimulating factor and interferons. *Journal of immunology (Baltimore, Md. : 1950)* **134,** 982–9 (1985).

147. Taylor, P. *et al.* MACROPHAGE RECEPTORS AND IMMUNE RECOGNITION. *Annual Review of Immunology* **23,** 901–944. doi:10.1146/annurev.immunol.23.021704.115816 (2005).

148. Cailhier, J. F. *et al.* Conditional Macrophage Ablation Demonstrates That Resident Macrophages Initiate Acute Peritoneal Inflammation. *The Journal of Immunology* **174,** 2336–2342. doi:10.4049/jimmunol.174.4.2336 (2014).

149. Maus, U. a. *et al.* Role of resident alveolar macrophages in leukocyte traffic into the alveolar air space of intact mice. *American Journal of Physiology-Lung Cellular and Molecular Physiology* **282,** L1245–L1252. doi:10.1152/ajplung.00453.2001 (2015).

150. Flannagan, R. S., Cosío, G. & Grinstein, S. *Antimicrobial mechanisms of phagocytes and bacterial evasion strategies* 2009. doi:10.1038/nrmicro2128.

151. Park, Y. K., Bearson, B., Bang, S. H., Bang, I. S. & Foster, J. W. Internal pH crisis, lysine decarboxylase and the acid tolerance response of Salmonella typhimurium. *Molecular Microbiology* **20,** 605–611. doi:10.1046/j.1365-2958.1996.5441070.x (1996).

152. Vandal, O. H., Pierini, L. M., Schnappinger, D., Nathan, C. F. & Ehrt, S. A membrane protein preserves intrabacterial pH in intraphagosomal Mycobacterium tuberculosis. *Nature Medicine* **14,** 849–854. doi:10.1038/nm.1795 (2008).

153. Schmidtchen, A., Frick, I. M., Andersson, E., Tapper, H. & Björck, L. Proteinases of common pathogenic bacteria degrade and inactivate the antibacterial peptide LL-37. *Molecular Microbiology* **46,** 157–168. doi:10.1046/j.1365-2958.2002.03146.x (2002).

154. Van der Wel, N. *et al.* M. tuberculosis and M. leprae Translocate from the Phagolysosome to the Cytosol in Myeloid Cells. *Cell* **129,** 1287–1298. doi:10.1016/j.cell.2007.05.059 (2007).

155. Schommer, N. N. *et al.* Staphylococcus epidermidis Uses Distinct Mechanisms of Biofilm Formation To Interfere with Phagocytosis and Activation of Mouse Macrophage-Like Cells 774A.1. *INFECTION AND IMMUNITY* **79,** 2267–2276. doi:10.1128/IAI.01142-10 (June 2011).

156. Leid, J. G. *et al.* The exopolysaccharide alginate protects Pseudomonas aeruginosa biofilm bacteria from IFN-gamma-mediated macrophage killing. *JOURNAL OF IMMUNOLOGY* **175,** 7512–7518 (2005).

157. Krebs, S. J. & Taylor, R. K. Protection and attachment of Vibrio cholerae mediated by the toxin-coregulated pilus in the infant mouse model. *Journal of Bacteriology* **193,** 5260–5270. doi:10.1128/JB.00378-11 (2011).

158. Akira S, Uematsu S & Takeuchi O. Pathogen recognition and innate immunity. *Cell* **124,** 783–801. arXiv: arXiv:1011.1669v3 (2006).

159. Feuillet, V. *et al.* Involvement of Toll-like receptor 5 in the recognition of flagellated bacteria. *Proceedings of the National Academy of Sciences* **103,** 12487–12492. doi:10.1073/pnas.0605200103 (2006).

160. Feuillet, V. *et al.* Involvement of Toll-like receptor 5 in the recognition of flagellated bacteria. *Proceedings of the National Academy of Sciences* **103,** 12487–12492. doi:10.1073/pnas.0605200103 (2006).

161. Finkelstein, R. A. & Mukerjee, S. Hemagglutination: A Rapid Method for Differentiating Vibrio cholerae and El Tor Vibrios. *Experimental Biology and Medicine* **112,** 355–359. doi:10.3181/00379727-112-28043 (2013).

162. Queen, J. & Fullner Satchell, K. J. Neutrophils are essential for containment of Vibrio cholerae to the intestine during the proinflammatory phase of infection. *Infection and Immunity* **80,** 2905–2913. doi:10.1128/IAI.00356-12 (2012).

163. Skorupski, K. & Taylor, R. K. Positive selection vectors for allelic exchange. *Gene* **169,** 47–52. doi:10.1016/0378-1119(95)00793-8 (1996).

164. Drescher, K., Nadell, C. D., Stone, H. A., Wingreen, N. S. & Bassler, B. L. Solutions to the public goods dilemma in bacterial biofilms. *Current Biology* **24,** 50–55. doi:10.1016/j.cub.2013.10.030 (2014).

165. Smith, H. O. *et al.* Enzymatic assembly of DNA molecules up to several hundred kilobases. *Nature Methods* **6,** 343–345. doi:10.1038/nmeth.1318 (2009).

166. Edelstein, A. D. *et al.* Advanced methods of microscope control using μManager software. *Journal of Biological Methods* **1,** 10. doi:10.14440/jbm.2014.36 (Nov. 2014).

167. Otsu, N. A Threshold Selection Method from Gray-Level Histograms. *IEEE Transactions on Systems, Man, and Cybernetics* **9,** 62–66. doi:10.1109/tsmc.1979.4310076 (2008).

5 List of Figures

6 List of Tables

Acknowledgements

First of all, I would like to thank Prof. Dr. Knut Drescher for giving me this opportunity to do my PhD Thesis in his lab and work on two exciting projects.

Additionally, I would like to thank the members of my Thesis Advisory Committee; Prof. Dr. Victor Sourjik and Dr. Hannes Link.

I would like to thank Praveen Singh and Carey Nadell for fruitfull discussions and every help I could get in the start.

Special thanks to Sanika Vaidya for being such a great friend and colleague. Thank you for reading and re-reading my PhD thesis!

I would like to thank former and current members of the Drescher lab; especially those who were and still are involved in the two projects of my PhD Thesis.

Last but not least. Pascal, thank you for listening to me when experiments failed and frustration was quite high, even if I repeated myself over and over again. Thank you for your advice, patience and support!

A Appendix 1 Supplementary Figures

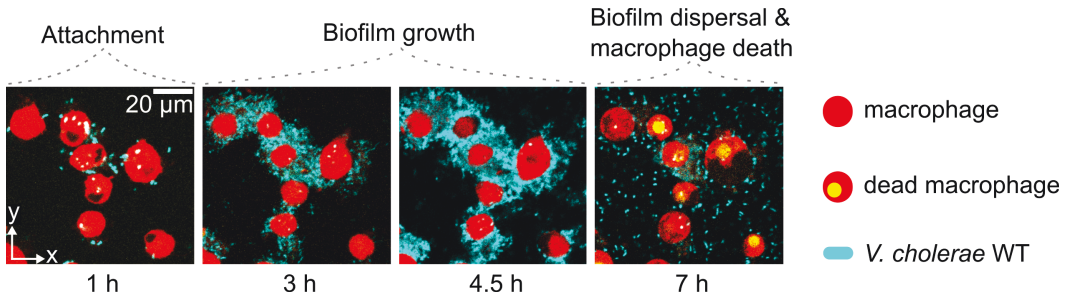

Figure S1: Interaction dynamics between *V. cholerae* and macrophages derived from human blood monocytes. *V. cholerae* attached to the surface of human macrophages. Attachment was accompanied by bacterial biofilm formation and subsequent dispersal of the biofilms. The interaction process was further characterized by death of the macrophages.

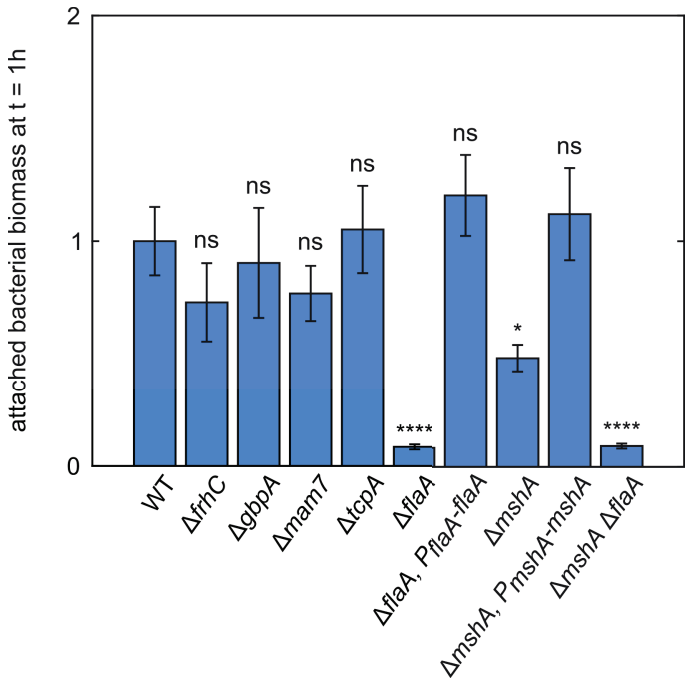

Figure S2: *V. cholerae* uses the polar flagellum and MSHA pili for attachment to the surface of macrophages derived from human blood monocytes. Deletion mutants, impaired in the production of cell surface components known to facilitate surface attachment, were tested for colonization of the macrophage surface. Bacteria lacking flagellum-regulated hemagglutinin (Δ*frhC*), GbpA (Δ*gbpA*), Mam7 (Δ*mam7*) and TCP (Δ*tcpA*) were able to attach to the macrophage surface, similar to the wild type. By the removal of the polar flagellum (Δ*flaA*) or MSHA pili (Δ*mshA*), the ability for macrophage attachment by *V. cholerae* was significantly attenuated. Ectopic expression of *flaA* or *mshA*, under control of the native promoter, could restore macrophage attachment. Bacteria were able to adhere efficiently, as observed for wild-type cells. Bars represent the mean bacterial biomass attached to the macrophage surface after one hour of co-incubation, normalized to the wild type. Errorbars denote the standard error of the mean (n_{WT}=8; $n_{\Delta frhC}$=3; $n_{\Delta gbpA}$=3; $n_{\Delta mam7}$=3; $n_{\Delta tcpA}$=5; $n_{\Delta flaA}$=5; $n_{\Delta flaA,\ P_{flaA}\text{-}flaA}$=4; $n_{\Delta mshA}$=6; $n_{\Delta mshA,\ P_{mshA}\text{-}mshA}$=4; $n_{\Delta mshA\ \Delta flaA}$=3). P values were calculated using one-way ANOVA (**** p<0.0001; *** p<0.02; ns, not significant).

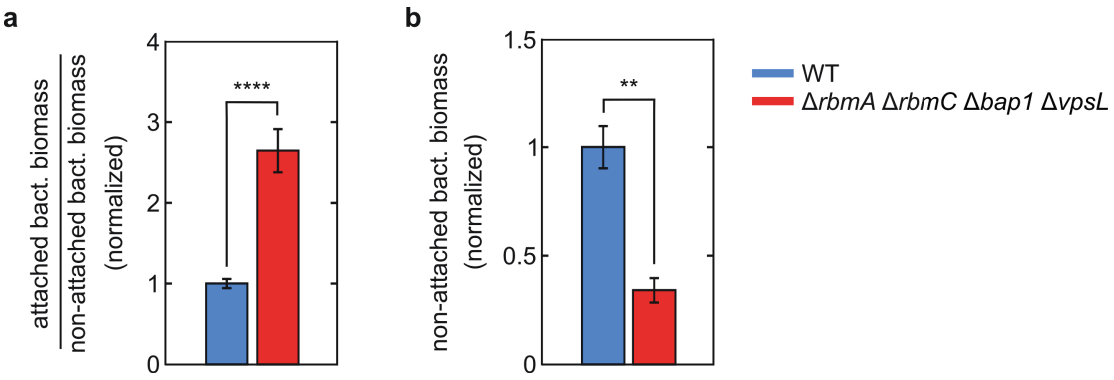

Figure S3: Biofilm formation on the macrophage surface does not depend on the matrix components RbmA, RbmC, Bap1 and VPS. (a) *V. cholerae* impaired in RbmA, RbmC, Bap1 and VPS production was able to form biofilms on the surface of macrophages (derived from THP-1 monocytes). Bars represent the mean ratio between bacterial biomass attached to macrophages and biomass present in macrophage-free areas. Errorbars denote the standard error of the mean (n_{WT}=31; $n_{\Delta rbmA\ \Delta rbmC\ \Delta bap1\ \Delta vpsL}$=5). The p value was calculated using a two-tailed unpaired t-test (**** p<0.0001). (a)+(b) Differences with respect to biomass accumulation could be observed between wild-type bacteria and the matrix mutant. As compared to the wild type, the matrix mutant primarily localized on the surface of macrophages, than in macrophage-free areas. Bars represent the mean bacterial biomass present in the macrophage-free area. Errorbars denote the standard error of the mean (n_{WT}=31; $n_{\Delta rbmA\ \Delta rbmC\ \Delta bap1\ \Delta vpsL}$=5). The p value was calculated using a two-tailed unpaired t-test (**** p<0.002).

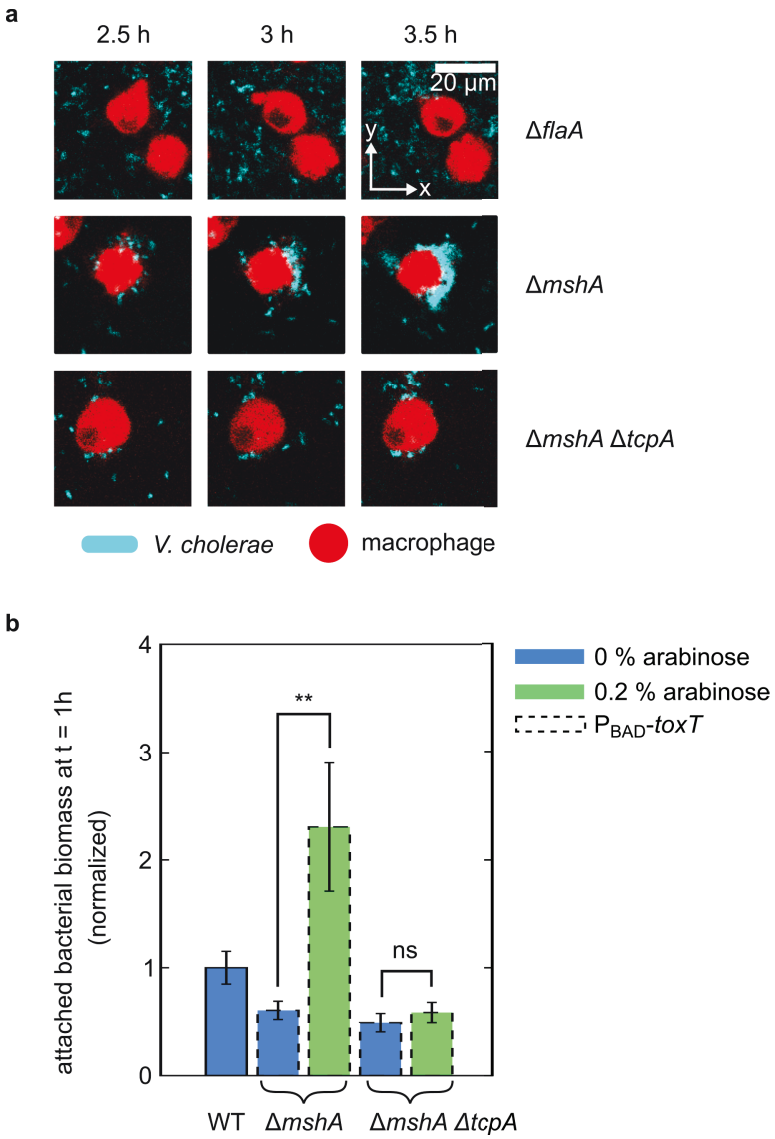

Figure S4: Production of TCP enables bacterial attachment, in the absence of MSHA pili. (a) *V. cholerae* deficient in MSHA pili biogenesis (Δ*mshA*) showed attenuated attachment during the first hour of co-incubation with macrophages that evolved from human blood monocytes. However, approximately after 3 h, cells initiated attachment and formed biofilms on the macrophage surface. Attachment was achieved by TCP, as biofilm formation could not be observed for Δ*mshA* Δ*tcpA* cells. (b) With the overproduction of TCP, bacterial attachment was shifted to an ealier time point during co-incubation. For overproduction of TCP by *V. cholerae*, *toxT* was fused to the arabinose inducible promoter P_{BAD} and bacteria were grown in the presence of 0.2 % arabinose. Overproduction could compensate for the loss of MSHA pili and resulted in bacterial attachment to macrophages that derived from human blood monocytes. Attachment was dependent on TCP production, as Δ*mshA* Δ*tcpA* cells were attenuated in colonization of the macrophage surface. Bars represent the mean bacterial biomass attached to the macrophage surface after one hour of co-incubation, normalized to the interaction with wild-type bacteria. Errorbars denote the standard error of the mean (n_{WT}=8; $n_{\Delta mshA,\,0\,\%}$=5; $n_{\Delta mshA,\,0.2\,\%}$=4; $n_{\Delta mshA\ \Delta tcpA,\,0\,\%}$=3; $n_{\Delta mshA\ \Delta tcpA,\,0.2\,\%}$=5). The p value was calculated using a two-tailed unpaired t-test (** $p<0.002$; ns, not significant).

B Appendix 2 Supplementary Tables

Table S1: Bacterial strains and bacteriophages used for phage-biofilm interaction studies.

Strain	Relevant markers & genotype	Source
KDE474	E. coli AR3110 WT	Serra et al.
KDE679	AR3110, with P_{tac}_*mRuby2* and Kan^R inserted at *attB* site (P_{tac} without operator).	This study
KDE702	AR3110, with Δ*csgB*::scar, P_{tac}_*mRuby2* and Kan^R inserted at *attB* site (P_{tac} without operator).	This study
KDE722	AR3110, with Δ*fliC*::scar, P_{tac}_*mRuby2* and Kan^R inserted at *attB* site (P_{tac} without operator).	This study
KDE726	AR3110, with Δ*bcsA*::scar, P_{tac}_*mRuby2* and Kan^R inserted at *attB* site (P_{tac} without operator).	This study
KDE956	AR3110, with Δ*pgaC*::scar, P_{tac}_*mRuby2* and Kan^R inserted at *attB* site (P_{tac} without operator).	This study
KDE965	AR3110, with Δ*wcaE*::Cm^R, P_{tac}_*mRuby2* and Kan^R inserted at *attB* site (P_{tac} without operator).	This study
KDE729	AR3110, with Δ*flhDC*::scar, P_{tac}_*mRuby2* and Kan^R inserted at *attB* site (P_{tac} without operator).	This study
KDE755	AR3110, with Δ*csgA*::scar, P_{tac}_*mRuby2* and Kan^R inserted at *attB* site (P_{tac} without operator).	This study
KDE757	AR3110, with Δ*csgBA*::scar, P_{tac}_*mRuby2* and Kan^R inserted at *attB* site (P_{tac} without operator).	This study
KDE1309	AR3110, with Δ*fimA*::scar, P_{tac}_*mRuby2* and Kan^R inserted at *attB* site (P_{tac} without operator).	This study
KDE813	AR3110, with point mutation inside *csgD* promoter according to ref (24), P_{tac}_*mRuby2* and Kan^R inserted at *attB* site (P_{tac} without operator).	This study*
KDE780	AR3110, with Δ*csgB*::scar, complementation, csgB with native promoter inserted at *attB* site P_{tac}_*mRuby2* and Kan^R inserted at *attB* site (P_{tac} without operator).	This study
KDE771	AR3110, with *csgBAC*-mKate2 transcriptional fusion, P_{tac}_*mKOk* and Kan^R inserted at *attB* site (P_{tac} without operator).	This study
KDE782	AR3110, with *fliC*-mKate2 transcriptional fusion, P_{tac}_*mKOk* and Kan^R, inserted at *attB* site (P_{tac} without operator).	This study
KDE1005	AR3110, with *dgcC*-mKate2 transcriptional fusion, P_{tac}_*mKOk* and Kan^R inserted at *attB* site (P_{tac} without operator).	This study

*: Promoter mutation from Grantcharova et al.

Table S2: Bacterial strains and bacteriophages used for phage-biofilm interaction studies (continued).

Strain	Relevant markers & genotype	Source
KDE1062	AR3110, with *pgaC*-mKate2 transcriptional fusion, P_{tac}_mKOk and Kan^R inserted at *attB* site (P_{tac} without operator).	This study
KDE1020	AR3110, with *wcaE*-mKate2 transcriptional fusion, P_{tac}_mKOk and Kan^R inserted at *attB* site (P_{tac} without operator).	This study
KDE1330	AR3110, with *fimA*-mKate2 transcriptional fusion, P_{tac}_mKOk and Kan^R inserted at *attB* site (P_{tac} without operator).	This study
KDE923	AR3110, with *CsgA* with C-terminal 6x His Tag (from chromosome, native site), *csgBAC*-mKate2 transcriptional fusion, P_{tac}_mKOk and Kan^R inserted at *attB* site.	This study
KDE931	E. coli Rosetta DE3 transformed with plasmid pNUT915, which is a pET plasmid with *csgA*-C-terminal 6x His Tag in front of the T7 promoter.	This study
KDE1128	AR3110, Δ*fliC*::scar, *csgA* with C-terminal 6x His Tag (from chromosome, native site), *csgBAC*-mKate2 transcriptional fusion, P_{tac}_mKOk and Kan^R inserted at *attB* site	This study
KDE1130	AR3110, Δ*flhDC*::scar, *csgA* with C-terminal 6x His Tag (from chromosome, native site), *csgBAC*-mKate2 transcriptional fusion, P_{tac}_mKOk and Kan^R inserted at *attB* site	This study
KDE1215	AR3110, Δ*fliC*::scar, *csgA* with C-terminal 6x His Tag (from chromosome, native site), *fliC-sfgfp* transcriptional fusion, csgBAC-mKate2 transcriptional fusion, P_{tac}_mKOk and Kan^R inserted at *attB* site	This study
KDH35	WT phage T7	DSMZ (DSM-4623)
KDH37	T7 with *sfgfp* under control of the phi 10 promoter.	This study
KDH52	WT phage T5	DSMZ (DSM-16353)

Table S3: Bacterial strains used for *V. cholerae*-macrophage interaction studies.

Strain	Relevant markers & genotype	Source
S17	*E. coli* Δ*lacU*169 (ΦlacZΔM15), *recA1*, *endA1*, *hsdR17*, *thi*-1, *gyrA96*, *relA1*, λ *pir*	
TOP10	*E. coli mcrA*Δ(mrr-hsdRMS-mcrBC) Φ *80lacZΔM15ΔlacX74deoRrecA1 araD*139Δ(ara-leu)7697 *galU galK rpsL endA1 nupG*	
KV201	*V. cholerae* C6706 (O1 El Tor, Sm^R)/ Wild type	
KDV296	*V. cholerae* C6706 contains plasmid pNUT542	[11]
KDV1301	*V. cholerae* C6706 Δ*frhC* contains plasmid pNUT542	This study
KDV1323	*V. cholerae* C6706 Δ*gbpA* contains plasmid pNUT542	This study
KDV1307	*V. cholerae* C6706 Δ*mam7* contains plasmid pNUT542	This study
KDV1305	*V. cholerae* C6706 Δ*tcpA* contains plasmid pNUT542	This study
KDV956	*V. cholerae* C6706 Δ*flaA* contains plasmid pNUT542	This study
KDV1987	*V. cholerae* C6706 Δ*flaA*, P_{flaA}-*flaA* contains plasmid pNUT542	This study
KDV1303	*V. cholerae* C6706 Δ*mshA* contains plasmid pNUT542	This study
KDV1916	*V. cholerae* C6706 Δ*mshA*, P_{mshA}-*mshA* contains plasmid pNUT542	This study
KDV1775	*V. cholerae* C6706 Δ*mshA* Δ*flaA* contains plasmid pNUT542	This study
KDV1360	*V. cholerae* C6706 Δ*mshA* Δ*frhC* Δ*gbpA* Δ*mam7* contains plasmid pNUT542	This study
KDV1776	*V. cholerae* C6706 Δ*mshA* Δ*tcpA* contains plasmid pNUT542	This study
KDV1733	*V. cholerae* C6706 Δ*rbmA* Δ*rbmC* Δ*bap1* Δ*vspL* contains plasmid pNUT542	This study
KDV1752	*V. cholerae* C6706 Δ*rbmA* Δ*rbmC* Δ*bap1* Δ*vspL* Δ*mshA* contains plasmid pNUT542	This study
KDV1753	*V. cholerae* C6706 Δ*rbmA* Δ*rbmC* Δ*bap1* Δ*vspL* Δ*tcpA* contains plasmid pNUT542	This study
KDV1770	*V. cholerae* C6706 Δ*rbmA* Δ*rbmC* Δ*bap1* Δ*vspL* Δ*mshA* Δ*tcpA* contains plasmid pNUT542	This study
KDV1730	*V. cholerae* C6706 expressing RmbA with a C-terminal 6x-His-Tag contains plasmid pNUT542	This study
KDV1959	*V. cholerae* C6706 Δ*mshA*, P_{BAD}-*toxT* contains plasmid pNUT542	This study
KDV1960	*V. cholerae* C6706 Δ*mshA* Δ*tcpA*, P_{BAD}-*toxT* contains plasmid pNUT542	This study

Table S4: Chemicals used.

Chemical	**Cat-No. and Supplier**
EZ-Vision Three	N313-Kit VWR
LB-Medium	X968.3 Carl Roth
LB-Agar	X969.3 Carl Roth
Polyethylene glycol 6000	0158.4 Carl Roth
Bacto Tryptone	211705 Becton Dickinson
Glycerol	3783.2 Carl Roth
Agarose NEEO ultra-quality	2267.3 Carl Roth
Calcium chloride	C5670-100G
Caesium chloride	7878.1 Carl Roth
Sodium chloride	HN00.2 Carl Roth
Poly-L-Lysine Solution	P8920-100ML Sigma Aldrich
Streptomycin sulphate	HP66.3 Carl Roth
l(+)-Rhamnose monohydrate	4655.1 Carl Roth
Dimethyl sulphoxide	4720.4 Carl Roth
Guanidin hydrochloride	0035.1 Carl Roth
Bovine Serum Albumin	A3059-10G Sigma Aldrich
Chloramphenicol	3886.1 Carl Roth
Ampicillin sodium salt	K029.2 Carl Roth
Kanamycin sulphate	T832.3 Carl Roth
Gentamycin sulphate	0233.3 Carl Roth
Sylgard 184 silicone elastomer	Dow Corning
FluoSpheres^{TM} Size Kit #1	F8887 Thermo Fischer Scientific